Association for Information and Image Management

1100 Wayne Avenue, Suite 1100
Silver Spring, Maryland 20910
301/587-8202

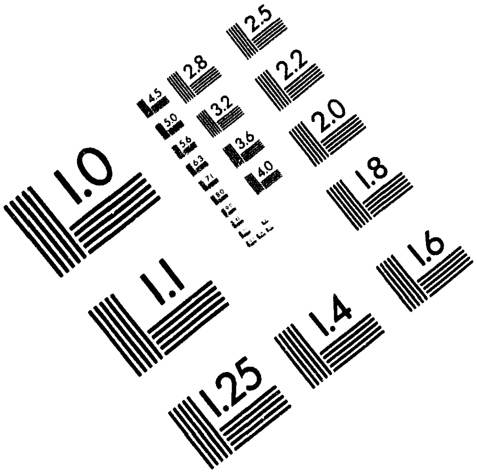

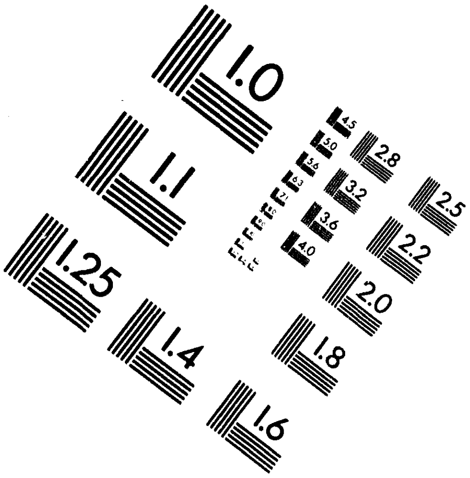

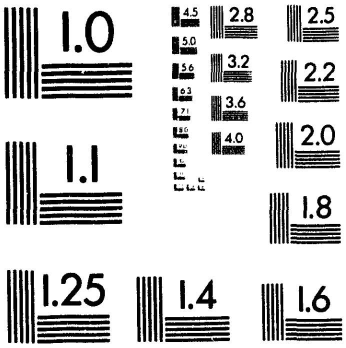

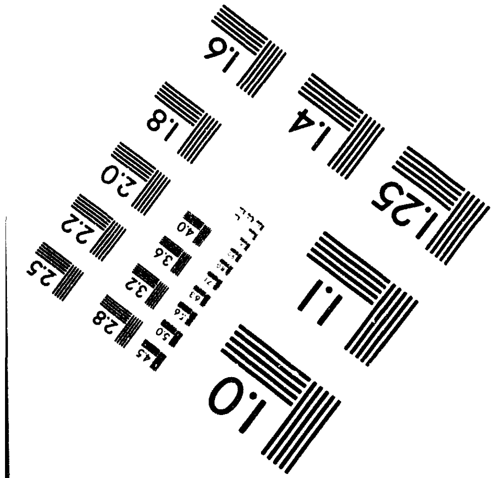

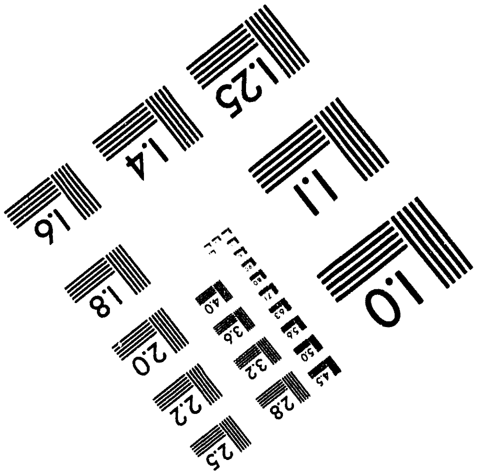

MANUFACTURED TO AIIM STANDARDS
BY APPLIED IMAGE, INC.

1 of 2

NOTICE

DOE/ER/10629--T4

6.13.83) -6-14.84
Ref

G-1

A STUDY OF THE DECAY $D^\circ \to K^-\pi^+\pi^\circ$ IN HIGH ENERGY PHOTOPRODUCTION

D.J. Summers, V.K. Bharadwaj,(a) C.H. Denby, A.M. Eisner,(b) R.G. Kennett,(c)
A. Lu, R.J. Morrison, M.S. Witherell, S.J. Yellin
University of California, Santa Barbara
Santa Barbara, California 93106

P. Estabrooks, J. Pinfold
Carleton University, Ottawa K1S 5B6, Canada

D.F. Bartlett, S. Bhadra, A.L. Duncan,(d) J.R. Elliott, U. Nauenberg
University of Colorado, Boulder, Colorado 80309

J.A. Appel, J. Biel,(e) D. Bintinger,(f) J. Bronstein,(e) C. Daum,(g)
P.M. Mantsch, T. Nash, W. Schmidke(h) K. Sliwa, M.D. Sokoloff,
K.C. Stanfield, M. Streetman, S.E. Willis(i)
Fermi National Accelerator Laboratory
Batavia, Illinois 60510

M.J. Losty
National Research Council of Canada
Ottawa, Ontario K1A 0R6, Canada

G.R. Kalbfleisch, M. Robertson(j)
University of Oklahoma, Norman, Oklahoma 73019

D.E. Blodgett, S.B. Bracker, G.F. Hartner, B.R. Kumar, G.J. Luste
J.F. Martin, K.K. Shahbazian, R.A. Sheperd, W.J. Spalding,(k) C.J. Zorn
University of Toronto, Toronto M5S 1A7, Canada

MASTER

ABSTRACT

Results are presented from an experiment observing photoproduction of the D^* at an average energy of 103 GeV. Clean signals are seen for the decay $D^{*\pm} \rightarrow \pi^{\pm}D^{\circ}$ with the D° decaying into both $K^{\mp}\pi^{\pm}$ and $K^{\mp}\pi^{\pm}\pi^{\circ}$. Analysis of the Dalitz plot for the $K\pi\pi$ mode gives branching fractions for $K^-\rho^+$, $K^{*-}\pi^+$, and $\overline{K}^{*\circ}\pi^{\circ}$ final states. The observed branching fraction for $D^{\circ} \rightarrow K^-\rho^+$, which is much lower than a previous result, is in approximate agreement with the value expected for an $I = 1/2$ final state.

The nonleptonic weak decays of the charmed mesons have been the subject of much experimental and theoretical effort. One important question is whether the branching ratios for the various two-body and quasi-two-body states ($K\pi$, $K\rho$, and $K^*\pi$) are consistent with an $I = 1/2$ final state, which is expected if the $D°$ decay is dominated by W exchange.[1] We report the results of an experiment using the Tagged Photon Spectrometer at Fermilab which observed the decay $D^{*+} \rightarrow \pi^+ D°$ with the $D°$ decaying into both $K^-\pi^+$ and $K^-\pi^+\pi°$. (The charge conjugate states are implicitly included in all decay modes.) The $K^-\pi^+\pi°$ sample represents the largest reported to date, and it was used to measure the branching ratio for the $K\rho$ and $K^*\pi$ modes, as well as that for non-resonant $K^-\pi^+\pi°$ decay.

The D^* events were produced by tagged photons of energy between 60 and 160 GeV, generated by a 170 GeV electron beam in a 0.2 radiation length copper radiator. The tagged photons impinged on a 1.5 meter liquid hydrogen target, which was placed at the front end of the spectrometer shown in Figure 1.[2] The low-level trigger required the detection of at least 30% of the tagged photon energy in the downstream calorimeters. Recoil protons were measured and identified by three layers of MWPC and four layers of scintillation counters in the recoil detector,[3] and the missing mass of the forward state was computed by a very fast data driven processor.[4] The high-level trigger demanded that the recoil system detect either a single proton at the primary vertex with a high missing mass or at least three charged tracks. The forward charged particles were analyzed with drift chambers and two magnets of large aperture, with a momentum resolution for fast tracks of $\frac{\Delta P}{P} = .004 + .0005xP$ (GeV/c). Two multi-cell Cherenkov counters identified charged tracks separating pions from kaons in the momentum range 6-36 GeV/c. Photons were detected either in the forward Segmented Liquid Ionization Calorimeter (SLIC)[5] or in smaller counters placed above and below the aperture of the second magnet (Outriggers). Almost all the π°'s from detected D° decays were seen in the SLIC, in which the energy resolution was about $15\%/E^{1/2}$ for photons, and the spatial resolution was a few millimeters. The spectrometer also included a hadronic calorimeter which was used in the trigger and to separate neutral hadrons from photons, and an iron muon filter.

To measure the ratio $B(D^\circ \to K^-\pi^+\pi^\circ)/B(D^\circ \to K^-\pi^+)$ the desired final states are $K^-\pi^+\pi^+$ and $K^-\pi^+\pi^+\pi^\circ$. In each case a cut was applied on the probability that the three charged particles satisfy the $K^-\pi^+\pi^+$ hypothesis. This cut was chosen to minimize the relative systematic error between the two decay modes, although it reduced the number of events used in this analysis. In addition, for the π° sample, a cut was applied on a π° probability calculated from the mass of the two gammas and the background underneath the π° peak. To observe the decay cascade $D^{*+} \to D^\circ\pi^+$, $D^\circ \to K^-\pi^+$, we chose $K^-\pi^+\pi^+$ combinations with $M_{K^-\pi^+}$ less than 60 MeV/c^2 from the D° mass. For such combinations the spectrum of the mass difference, $\Delta M = M_{K\pi\pi} - M_{K\pi}$ has a clear peak at the $D^{*+} - D^\circ$ mass difference. This spectrum gives a good fit to background of the form $aQ^{1/2}(1-bQ)$ (where $Q = \Delta M - M_{\pi^+}$, a and b are constants) plus a Gaussian centered at $\Delta M = 0.1454$ GeV/c^2 and $\sigma = 1.2$ MeV/c^2, with 39 ± 8 events in the peak. A similar analysis was carried out for the $K^-\pi^+\pi^+\pi^\circ$ sample, and the fit to the ΔM plot using the same peak parameters as above yields 41 ± 9 events in the peak.

To determine the branching ratio $B(D^\circ \to K^-\pi^+\pi^\circ)/B(D^\circ \to K^-\pi^+)$, the ratio of the efficiencies for the two modes is needed. Many factors, including the beam flux and spectrum, trigger efficiencies, target size, etc., are common to both modes. The reconstruction efficiency and identification efficiency are the only factors which need to be calculated from Monte Carlo studies.

The only strong difference between the two cases is the probability of reconstructing the π°, which varies with the energy of the π° from a threshold at 4 GeV to a value of approximately 40% at 30 GeV and above. This efficiency was determined by adding to real events photon showers generated by a Monte Carlo program, and processing these events by the usual π°-finding programs. To check this determination we also studied the π° efficiency using the various charge states of the decay $K^* \to K\pi$. A Monte Carlo which used this π° efficiency gave for the ratio of efficiencies $\varepsilon(K^-\pi^+\pi^\circ)/\varepsilon(K^-\pi^+) = 0.25 \pm 0.04$. Using this number and the relative number of events in the two D^* peaks we calculate $B(D^\circ \to K^-\pi^+\pi^\circ)/B(D^\circ \to K^-\pi^+) = 4.3 \pm 1.4$. Combining this with the current average value for the $D^\circ \to K^-\pi^+$ branching ratio, $2.4 \pm 0.4\%$,[6] yields a measurement of $B(D^\circ \to K^-\pi^+\pi^\circ) = 10.3 \pm 3.7\%$.

For the Dalitz plot study, a sample of $K^-\pi^+\pi^+\pi^\circ$ events was chosen with somewhat looser Cherenkov cuts and with $M_{K^-\pi^+\pi^\circ}$ within 50 MeV/c^2 of the D° mass. Figure 2 shows the ΔM spectrum for these events, with a clear peak at $\Delta M = 0.1454$ GeV/c^2. To obtain a clean sample for this analysis the 82 events with ΔM between 0.1440 and 0.1470 GeV/c^2 were selected; a fit to the ΔM spectrum determines the background to be 45% in this region. The Dalitz plot for these events is shown in Fig. 3(a). A high-statistics background sample was constructed by taking events in the D° mass range but with ΔM outside the D^* range. (The D° fraction for these events is small.) The Dalitz plot for this sample, shown in Fig. 3(b), gave a good fit to uniform phase space times an efficiency which depended linearly on $M^2(K^-\pi^+)$, due to the energy dependence of the π° efficiency. We also examined this background for ρ and K^* and found it was consistent with no contribution from these vector mesons. We made a maximum likelihood fit to the Dalitz plot from the D^* region, allowing a flat background with the acceptance correction as for the background, plus resonant contributions from $K^-\rho^+$, $K^{*-}\pi^+$, and $\overline{K}^{*\circ}\pi^\circ$. Each vector meson was described by a Breit-Wigner with the appropriate decay angular distribution. Interference effects are small compared with the quoted errors, and are neglected. The results are shown in Table 1. Only in the $K^-\rho^+$ mode is there evidence of a strong resonant contribution. We note that the $\cos^2\theta$ distribution for the $\rho \rightarrow \pi\pi$ decay means that the ρ band is populated primarily at the edges of the Dalitz plot. (Here θ is the angle in the $\pi\pi$ center of mass, with $\theta=0$ along the K^- direction in that frame.) Fig. 4 shows the $M^2(\pi^+\pi^\circ)$ spectrum for events with $|\cos\theta| > 0.5$, a cut which keeps 1/2 of the smooth $\pi\pi$ spectrum but 7/8 of the ρ. Thus this plot projects the region of the Dalitz plot most sensitive to the ρ contribution. The value of $0.31\ ^{+0.20}_{-0.14}$ for the ratio $B(D^\circ \rightarrow K^-\rho^+)/B(D^\circ \rightarrow K^-\pi^+\pi^\circ)$ compares to the earlier value of $0.85\ ^{+0.11}_{-0.15}$.[1] Combining this fraction with the $B(D^\circ \rightarrow K^-\pi^+\pi^\circ)$ ratio above gives a branching ratio $B(D^\circ \rightarrow K^-\rho^+) = 3.2\ ^{+2.3}_{-1.8}\%$. The low fractions quoted in Table 1 for the $K^{*-}\pi^+$ and $\overline{K}^{*\circ}\pi^\circ$ contributions agree with the earlier experiment. Branching ratios listed in Table 1 for the $D^\circ \rightarrow K^*\pi$ modes take into account the branching ratios for $K^* \rightarrow K\pi$ decay.

One of the crucial problems in the study of D decays is to determine whether the dominant mode is one in which the light quark is a spectator, or one in which both the quark and antiquark couple to the weak vertex. If the non-spectator quark decay dominates (W exchange), the D^+ lifetime is longer than the D°, since the only such modes available to the D^+ are Cabibbo-suppressed. The non-spectator diagram leads to an $I = 1/2$ final state, although an $I = 1/2$ state does not rule out spectator-quark decay. The $I = 1/2$ state is characterized by the ratios:

$$\frac{B(D^\circ\to K^-\pi^+)}{B(D^\circ\to\overline{K}^\circ\pi^\circ)} = \frac{B(D^\circ\to K^{*-}\pi^+)}{B(D^\circ\to\overline{K}^{*\circ}\pi^\circ)} = \frac{B(D^\circ\to K^-\rho^+)}{B(D^\circ\to\overline{K}^\circ\rho^\circ)} = 2.$$

Existing data for the first two channels were consistent with the ratio of 2, but the measurements for the last ratio were $B(D^\circ\to K^-\rho^+) = 7.2 ^{+3.0}_{-3.1}\%$ and $B(D^\circ\to\overline{K}^\circ\rho^\circ) = 0.1 ^{+0.6}_{-0.1}\%$.[1] The present result, $B(D^\circ\to K^-\rho^+) = 3.2 ^{+2.3}_{-1.8}\%$ can be compared with twice the measured ratio for $D^\circ \to \overline{K}^\circ\rho^\circ$, or $0.2 ^{+1.2}_{-0.2}\%$. Thus the present result is in approximate agreement (1.4 standard deviations) with the expectation for a pure $I = 1/2$ state.

We wish to acknowledge the assistance of the staff of Fermilab and the technical support staffs of all of the groups involved. This research was supported in part by the U.S. Department of Energy and by the Natural Science and Engineering Research Council of Canada through the Institute of Particle Physics of Canada and the National Research Council of Canada.

(a) Present address: University of California, Irvine, California.

(b) Present address: Institute for Research at Particle Accelerators, Palo Alto, California.

(c) Also at: California State University, Northridge, California.

(d) Present address: University of Washington, Seattle, Washington.

(e) Present address: Comavid Corporation, North Aurora, Illinois.

(f) Present address: University of California, San Diego, California.

(g) On sabbatical leave from NIKHEF-H, Amsterdam, Netherlands.

(h) Present address: University of California, Berkeley, California.

(i) Present address: University of Oklahoma, Norman, Oklahoma.

(j) Present address: Bell Laboratories, Holmdel, New Jersey.

(k) Present address: Fermi National Accelerator Laboratory, Batavia, Illinois.

REFERENCES

1. R.H. Schindler, et al., Phys. Rev. D24, 78 (1981); and George Trilling, Physics Reports 75, 57 (1981).
2. The spectrometer is described in detail in A. Duncan, Ph.D. thesis, University of Colorado, 1982 (unpublished), and B.H. Denby, Ph.D. thesis, University of California, Santa Barbara, 1983 (unpublished).
3. G. Hartner, et al., to appear in Nucl. Inst. Meth.
4. E. Barsotti, et al., IEEE Trans. Nucl. Sci. NS-26, 686 (1979); J. Martin, et al., Proceedings of the Topical Conference on the Application of Microprocessors to High Energy Physics Experiments, CERN 81-07, p. 164 (1981); T. Nash, ibid., p. 132.
5. V. Bharadwaj, et al., Nucl. Inst. Meth. 155, 411 (1978).
6. Review of Particle Properties, Phys. Lett. 111B (1982).

TABLE I

Contributions to $D^\circ \rightarrow K^-\pi^+\pi^\circ$ Decay

Channel	Fraction of $D^\circ\rightarrow K^-\pi^+\pi^\circ$ Decays	Branching Ratio
$K^-\rho^+$	$0.31\ ^{+.20}_{-.14}$	$3.2\ ^{+2.3}_{-1.8}\%$
$\overline{K}^{*\circ}\pi^\circ$	$0.06\ ^{+.09}_{-.06}$	$0.9\ ^{+1.4}_{-0.9}\%$
$K^{*-}\pi^+$	$0.11\ ^{+.12}_{-.08}$	$3.4\ ^{+3.9}_{-2.8}\%$
Non-resonant decays	$0.51 \pm .22$	$5.2 \pm 2.9\%$

Table I: Results of the fit to the $D^\circ \rightarrow K^-\pi^+\pi^\circ$ Dalitz plot. The category "non-resonant decays" does not include the contribution to the Dalitz plot from background below the D°.

FIGURE CAPTIONS

Figure 1: The Tagged Photon Spectrometer at Fermilab

Figure 2: $\Delta M = M_{K\pi\pi\pi} - M_{K\pi\pi}$ for events with $M_{K^-\pi^+\pi^\circ}$ within 50 MeV/c^2 of the D°. The smooth curve is a fit to the background of the form described in the text.

Figure 3: The Dalitz plot for (a) the D° region and (b) the background sample. The boundary is drawn for the center of the $K^-\pi^+\pi^\circ$ mass range.

Figure 4: $M^2(\pi^+\pi^\circ)$ for events from the $D^\circ \rightarrow K^-\pi^+\pi^\circ$ sample with $|\cos\theta| > 0.5$ for the $\pi^+\pi^\circ$ system. The upper curve shows the result of the fit to the entire Dalitz plot, projected on the $M^2(\pi^+\pi^\circ)$ axis. The lower curve shows the result of the fit with the ρ contribution removed.

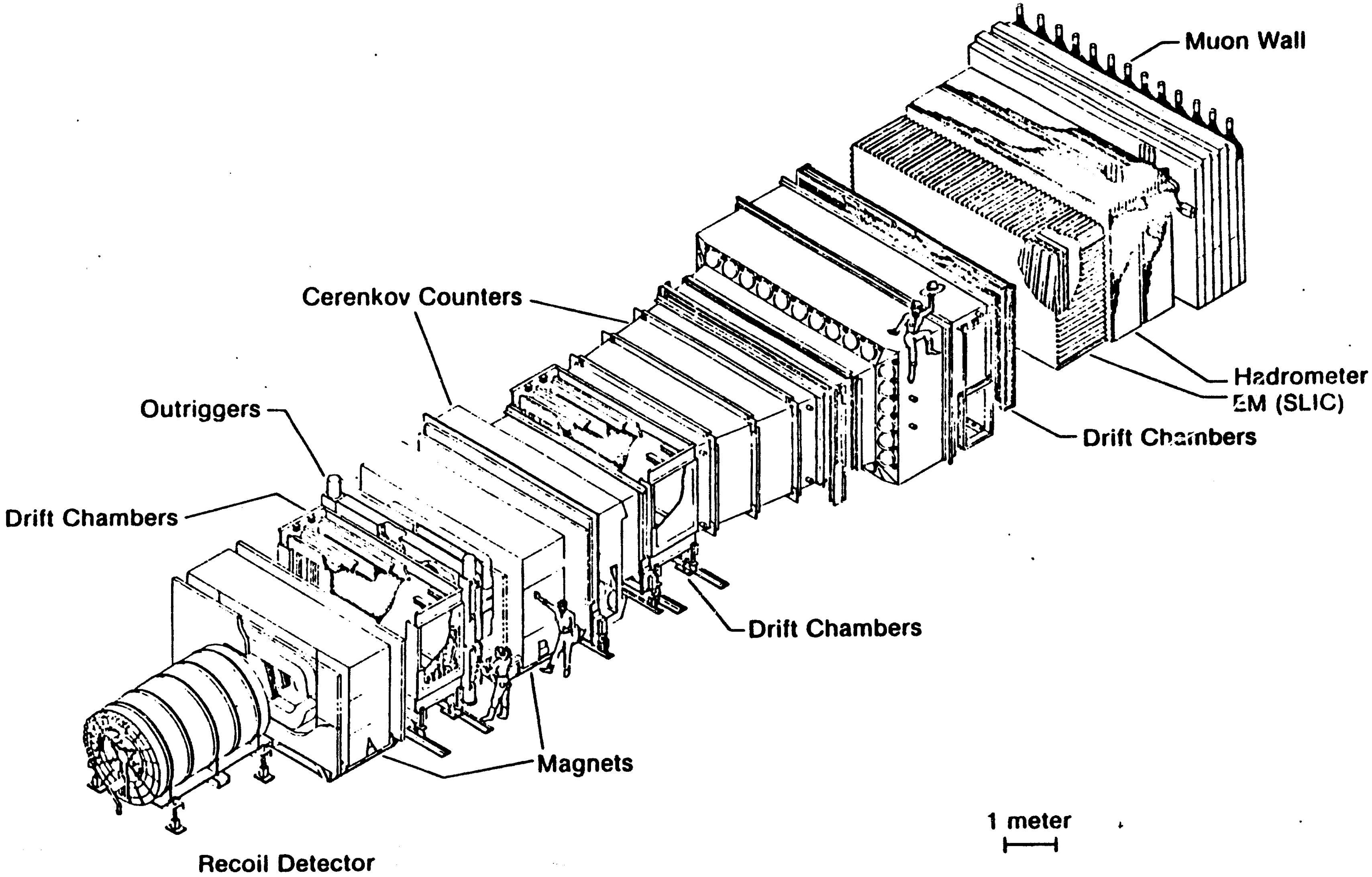
Muon Wall
Cerenkov Counters
Outriggers
Drift Chambers
Hadrometer
EM (SLIC)
Drift Chambers
Drift Chambers
Magnets
Recoil Detector
1 meter

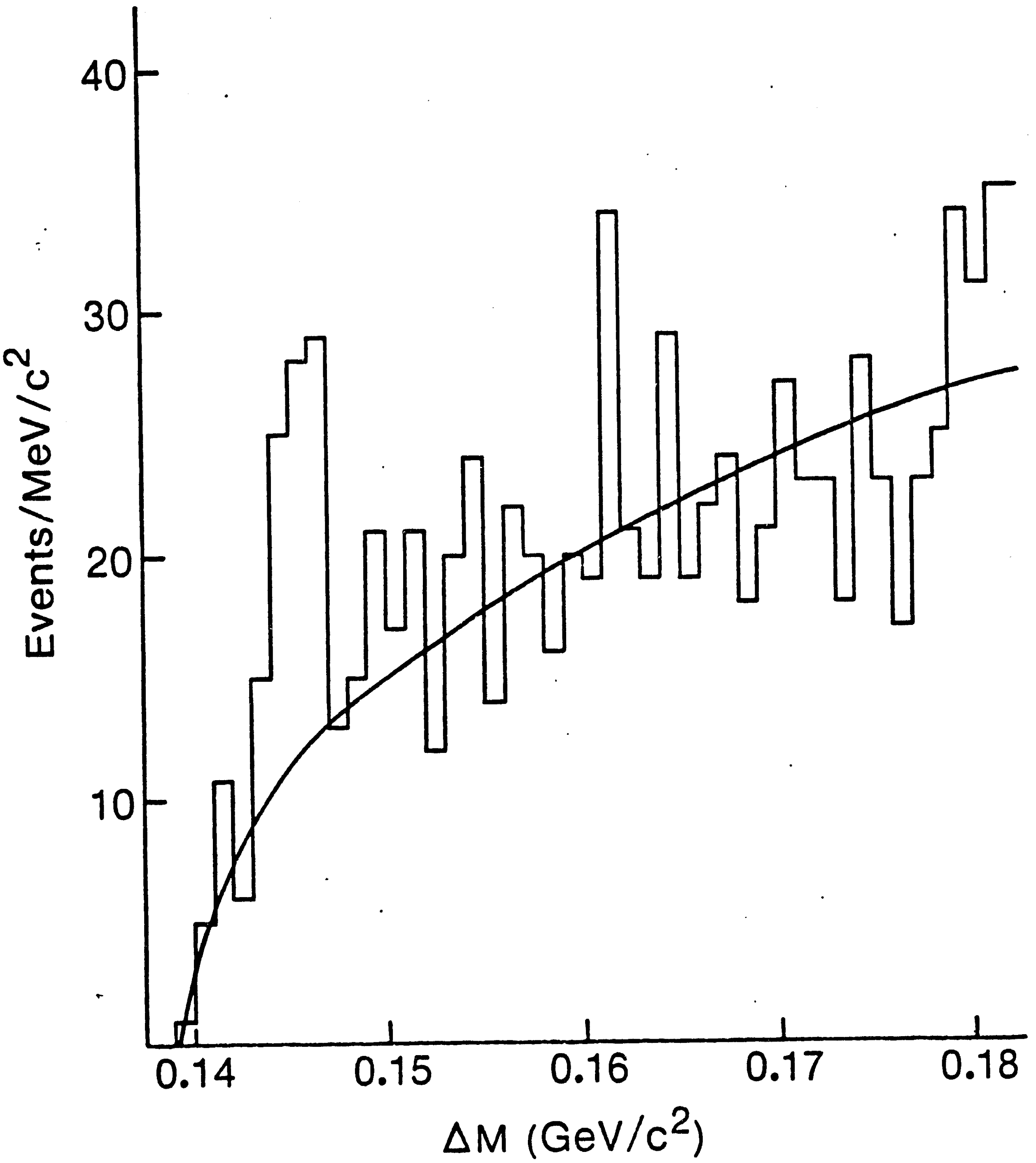
Events/MeV/c^2
40
30
20
10
0.14
0.15
0.16
0.17
0.18
ΔM (GeV/c^2)

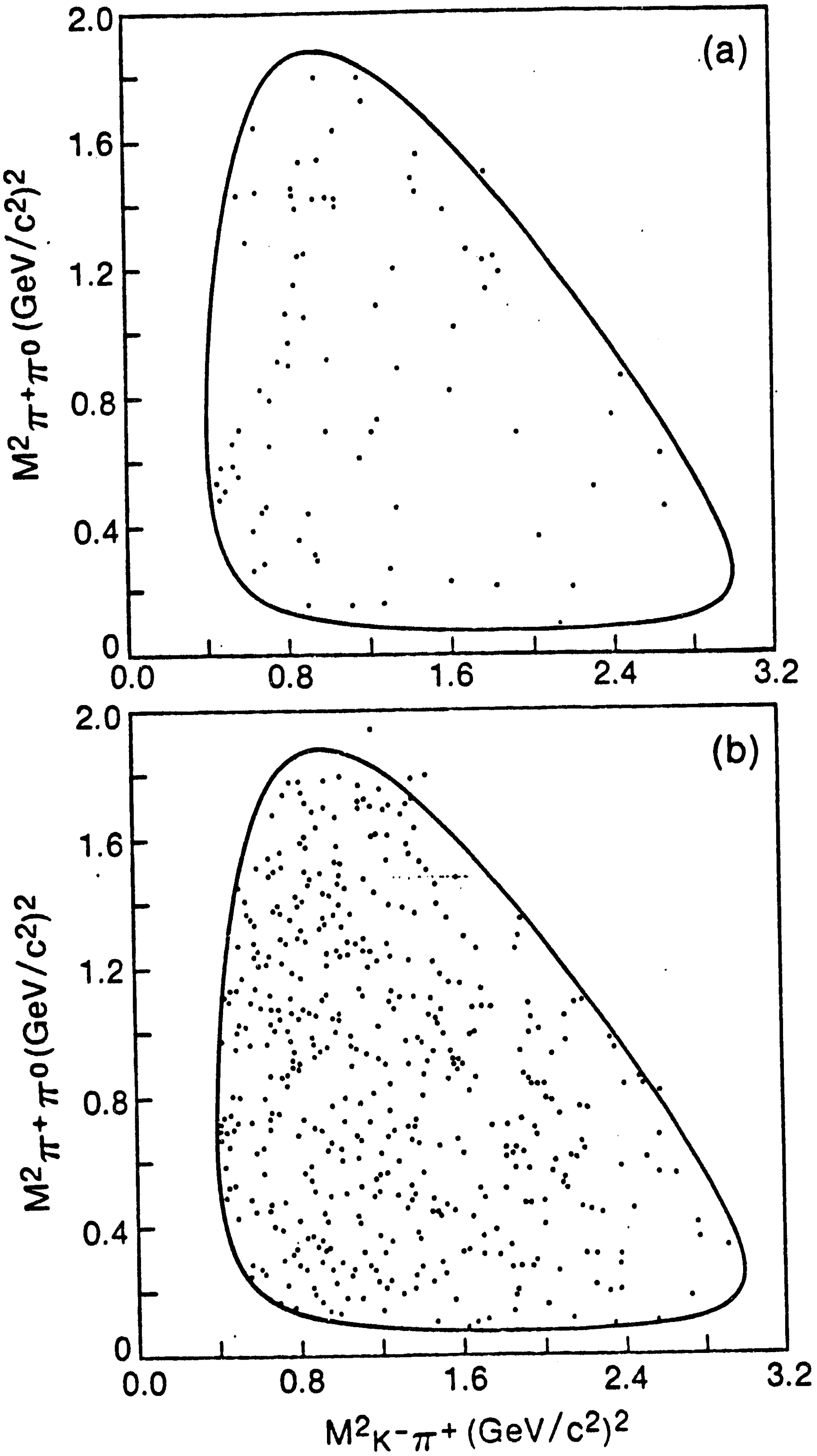
(a)
(b)
2.0
1.6
1.2
0.8
0.4
0
0.0
0.8
1.6
2.4
3.2
$M^2_{\pi^+\pi^0}$ (GeV/c^2)^2
$M^2_{K^-\pi^+}$ (GeV/c^2)^2

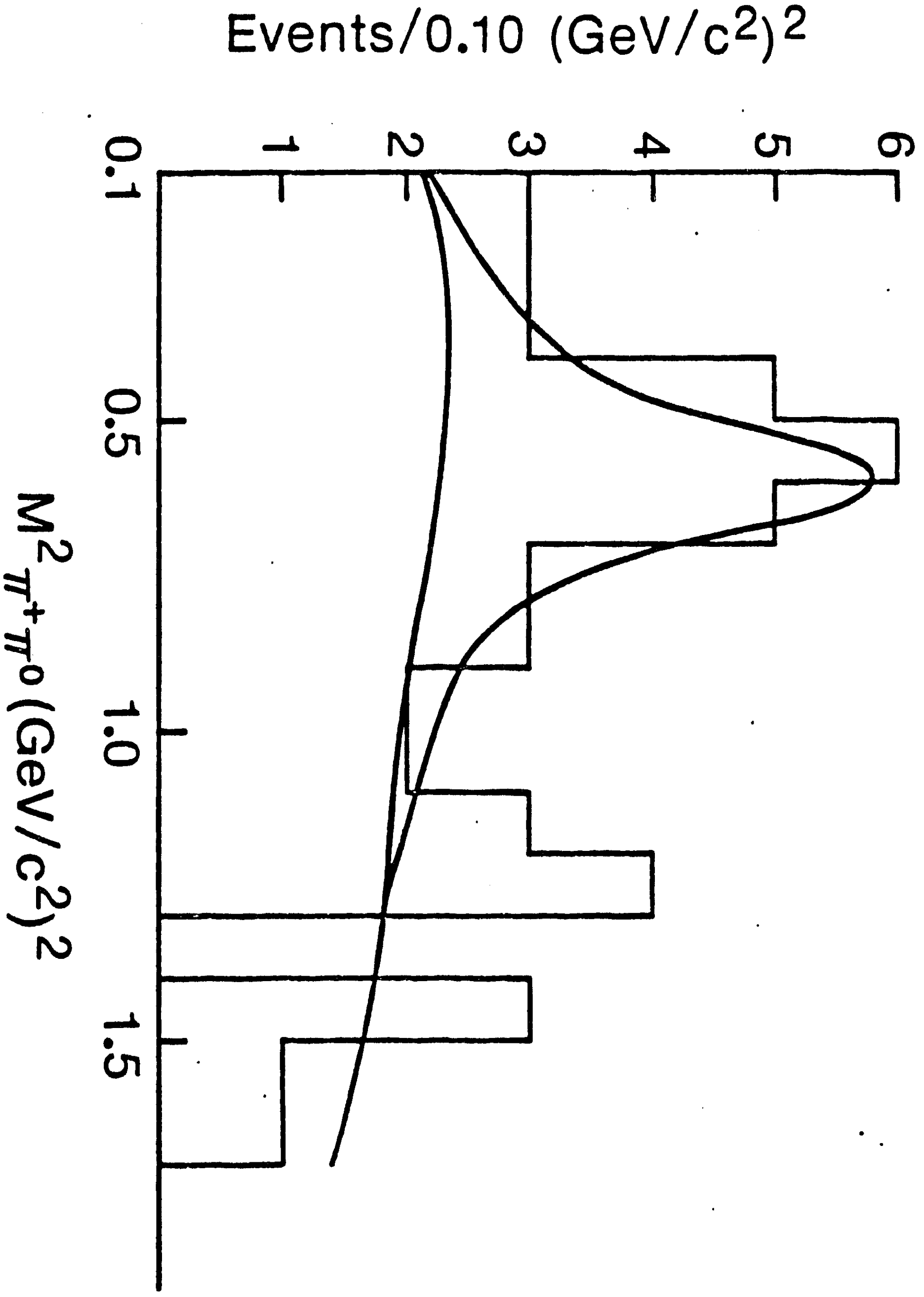
Events/0.10 (GeV/c^2)^2
0.1
1
2
3
4
5
6
0.5
1.0
1.5
M$^2_{\pi^+\pi^0}$ (GeV/c^2)^2

Draft 7 Sept 83

WILLIS

G-15

Inelastic and Elastic Photoproduction of J/ψ(3097)

B.H. Denby, V.K. Bharadwaj,(a) D.J. Summers, A.M. Eisner,(b) R.G. Kennett,(c)
A. Lu, R.J. Morrison, M.S. Witherell, S.J. Yellin
University of California, Santa Barbara
Santa Barbara, California 93106

P. Estabrooks, J. Pinfold
Carleton University, Ottawa K1S 5B6, Canada

D.F. Bartlett, S. Bhadra, A.L. Duncan,(d) J.R. Elliott, U. Nauenberg
University of Colorado, Boulder, Colorado 80309

J.A. Appel, J. Biel, D. Bintinger,(e) J. Bronstein,(f) C. Daum,(g)
P.M. Mantsch, T. Nash, W. Schmidke(h) K. Sliwa, M.D. Sokoloff,
K.C. Stanfield, M. Streetman, S.E. Willis(i)
Fermi National Accelerator Laboratory
Batavia, Illinois 60510

M.J. Losty
National Research Council of Canada

G.R. Kalbfleisch, M. Robertson(j)
University of Oklahoma, Norman, Oklahoma 73019

D.E. Blodgett, S.B. Bracker, G.F. Hartner, B.R. Kumar, G.J. Luste
J.F. Martin, K.K. Shahbazian, W.J. Spalding,(k) C.J. Zorn
University of Toronto, Toronto M5S 1A7, Canada

SEP 17 1983

PRELIMINARY

ABSTRACT

Inelastic and elastic J/ψ photoproduction on hydrogen is investigated at a mean energy of 103 GeV. The inelastic cross section with $E_{\psi}/E_{\gamma} < 0.9$ is significantly lower than the corresponding result for muoproduction on iron targets, but is consistent with a second order perturbative QCD calculation. The mean p_{+} of the inelastic events is larger than that of the elastic events, again in accord with the QCD calculation.

There has been considerable interest in the use of perturbative QCD to describe J/ψ production by real and virtual photons (1-5). Success has been achieved in describing the energy dependence, and, to a lesser extent, the magnitude of of the elastic cross section (5,6). Recent measurements of inelastic muoproduction cross sections on iron targets (7,8) confirm the dependence upon $z \equiv E_{\psi}/E_{\gamma}$ predicted (2) by QCD, but greatly exceed the predictions in magnitude. In what follows, we describe the inelastic and elastic production of J/ψ mesons on hydrogen by real photons.

The experiment was performed at the Fermilab Tagged Photon Spectrometer, which is described elsewhere in detail (9). Tagged photons with energies $60 \leq E_{\gamma} \leq 160$ GeV impinge upon a 1.5 meter liquid hydrogen target. The forward spectrometer has nearly full acceptance for charged particles, whose momenta are determined by a system of four drift chambers and two magnets, and photons, whose positions and energies are measured in two large electromagnetic calorimeters. A recoil detector (10), consisting of a set of PWC's and scintillators of cylindrical geometry surrounding the hydrogen target, is used to analyze tracks emerging from the target at large angles.

The J/ψ is detected through both e^+e^- and $\mu^+\mu^-$ decay modes. Hits in two or more muon hodoscopes, located downstream of an iron muon filter, create a dimuon trigger. Offline, events with dimuon triggers are required to have at least two oppositely charged tracks which match muon hits, are minimum ionising in the hadron calorimeter, and verticize within the target. For the dielectron mode, the trigger processor (11) determines the presence in the recoil detector of a single recoil proton consistent with a forward mass of 2.0 GeV or greater, which, in conjunction with the presence of energy in the electromagnetic and/or hadronic calorimeters, forms a recoil trigger. Offline, dielectron events are required to have at least two oppositely charged tracks, identified as electrons in the electromagnetic

? calorimeters, which verticize within the target. The resulting dimuon and dielectron mass plots are shown in figure 1. The J/ψ mass region is taken to be 2.8 to 3.4 Gev/c^2. The dielectron events are, due to the recoil trigger, predominantly elastic and are excluded from the analysis that follows.

A dimuon events is classified as inelastic if:

1. Additional forward tracks, photons, or hadronic neutrals accompany the J/ψ ("forward inelastic"), and/or,

2. The data from the recoil spectrometer are ~~is~~ inconsistent with the single recoil proton calculated from the incident photon and the reconstructed J/ψ, assuming elastic production ("recoil inelastic").

The uncertainty in assigning the 147 dimuon events is about ±4 events for forward and ±6 events for recoil.

The data were divided into seven categories based upon the above classifications (and upon a z cut, as discussed below). In table I, column 1, the raw numbers of events in each category are displayed. Background was estimated by joining the mass regions above and below the J/ψ with a smooth curve. The hashed area in figure 1b is the mass spectrum for the forward inelastic events.

The efficiencies for detection of elastic and inelastic events were calculated by separate Monte-Carlos. Elastic events were generated diffractively from a distribution $e^{\beta t}$ with B=4 and a $1+\cos^2\theta$ decay distribution. The inelastic Monte-Carlo diffractively (B=4) generated a spectrum of forward masses which subsequently decayed to a J/ψ and two pions. The use of just 2 additional pions is appropriate since very few of the real events had more than two extra tracks. The J/ψ decayed uniformly in its center of mass. The parameters of this Monte-Carlo were chosen to maximize the agreement of the generated J/ψ p_+ vs. z distribution with that predicted by Berger and Jones (2). The efficiencies calculated were relatively insensitive to the value of B, decay angular distribution, and, in the inelastic case, p_+ vs. z distribution used.

The z value for each event was determined by $z = E_\psi/E_\gamma$, for the case of low z events, and for the higher z events, where
? tagging energy resolution can create ~~force~~ $z>1$, by the formula $z = E_\psi/(E_\psi+F.\,E_x)$, where E_x is the detected energy accompanying the J/ψ and F is a correction factor. Events that are inelastic only in the recoil system are assigned to the highest z bin. The

resulting z spectrum, corrected for efficiency, is shown in figure 2. A cut of $z<\sim.9$ (category 7) is often used both experimentally (7,8) and in the theory (2) to isolate the truly inelastic process from elastic and quasi-elastic processes.

The cross sections in each category and fractions of total are shown in table I, columns 2 and 3. The cross sections have an additional 25% normalization uncertainty.

Four of the forward inelastic events were fully reconstructed as $\psi'\rightarrow\psi\pi^+\pi^-$. This implies, after efficiency corrections, a ψ' photoproduction cross section consistent with previously measured results (8,12). For purposes of comparison with theory it is desireable to measure direct inelastic ψ production as opposed to cascade production from higher mass charmonium states. To this end, we present in table I, columns 4,5 the cross sections and fractions in each category after subtracting out the contributions estimated from the known ψ' cross section and branching ratios to ψX. The z spectrum of this contribution, determined by Monte-Carlo, is indicated by the points in figure 2.

In table II elastic and $z<\sim.9$ inelastic cross sections from this experiment, and their ratio, are compared to those (where available) of the BFP (7), EMC (8), and Wide-Band (13) groups. The elastic numbers agree within the rather large errors, but it is clear that the inelastic cross section and the ratio from this experiment are substantially smaller than those from EMC and BFP. After ψ' subtraction, the numbers from this experiment become even smaller (table I), and are consistent with the second order perturbative QCD inelastic cross section calculated by Berger and Jones (2); the muoproduction cross sections are roughly a factor of 5 larger than the QCD predictions (7,8).

Table I can be used to show that (31±6)% of the forward elastic events are recoil inelastic, in excellent agreement with the (30±4)% reported by the Wide-Band group (13).

Figure 3 shows that the forward inelastic J/ψ p_+ distribution is much flatter than that of the forward elastic, recoil elastic events. This phenomenon is predicted by perturbative QCD (2), and is reported also by the BFP (7) and EMC (8) groups.

We wish to acknowledge the assistance of the staff of Fermilab and the technical support staffs of all of the groups involved. This research was supported in part by the U.S. Department of Energy and by the Natural Sciences and Engineering Research Council of Canada through the Institute of Particle Physics of Canada and the National Research Council of Canada.

REFERENCES

1. H. Fritzsch and K. Streng, Phys. Lett. 72B (1978) 385.

2. E. Berger and D. Jones, Phys. Rev. D23 (1981) 1521.

3. D. Duke and J. Owens, Phys. Lett. 96B (1980) 184.

4. T. Tajima and T. Watanabe, Phys. Rev. D23 (1981) 1517.

5. L. Jones and H. Wyld, Phys. Rev. D17 (1978) 2332.

6. T. Weiler, Phys. Rev. Lett. 44 (1980) 304.

7. T. Markiewicz, Ph.D. thesis, U.C. Berkeley, 1981.

   M. Strovink, Review of Multimuon Production by Muons, Proceedings of the 1981 International Symposium on Lepton and Photon Interactions at High Energies, Bonn, W. Germany, p. 594.

8. J.J. Aubert et al., EMC, Nuc. Phys. B213 (1983) 1.

9. B. Denby, Ph.D. thesis, University of California, Santa Barbara, 1983.

   A. Duncan, Ph.D. thesis, University of Colorado, 1982.

   G. Gidal, B. Armstrong, and A. Rittenberg, Major Detectors in Elementary Particle Physics, LBL-91 Supplement UC-37, March 1983.

10. G. Hartner et al., A Recoil Proton Detector Using Cylindrical Proportional Chambers and Scintillation Counters, accepted for publication, Nucl. Inst. Meth., 1983.

11. E. Barsotti et al., IEEE Trans. Nucl. Sci. NS-26 (1979) 686.

12. M. Binkley et al., Phys. Rev. Lett. 50 (1983) 302.

13. M. Binkley et al., Phys. Rev. Lett. 48 (1982) 73.

FIGURE CAPTIONS

1. a) Dielectron mass spectrum. There are 63 events in the J/ψ mass region, $2.8 \leq M < 3.4$ Gev/c². b) Dimuon mass spectrum. There are 147 events in the J/ψ region. The hashed region represents the forward inelastic events (category 3 of table I).

2. Z distribution for inelastic J/ψ photoproduction. Dashed line indicates the contribution of the recoil inelastic events (category 4 of table I). Points are an estimate of the contamination of the inelastic sample by ψ′ production.

3. p_+ distributions for totally elastic and forward inelastic J/ψ events. The inelastic events have a much flatter p_+ distribution. Mean p_+ for the totally elastic is .39 ± .11 Gev/c; for the forward inelastic, .96 ± .11 Gev/c.

TABLE CAPTIONS

1. The J/ψ data are divided into seven categories as indicated. Figures in parentheses are statistical and systematic errors, respectively. Cross sections (only) have an additional ~25% normalization uncertainty.

2. Comparison of inelastic and elastic J/ψ data with other experiments. Numbers in parentheses are statistical and systematic errors respectively where double, and overall errors where single. The systematic errors for this experiment here also contain the normalization uncertainty.

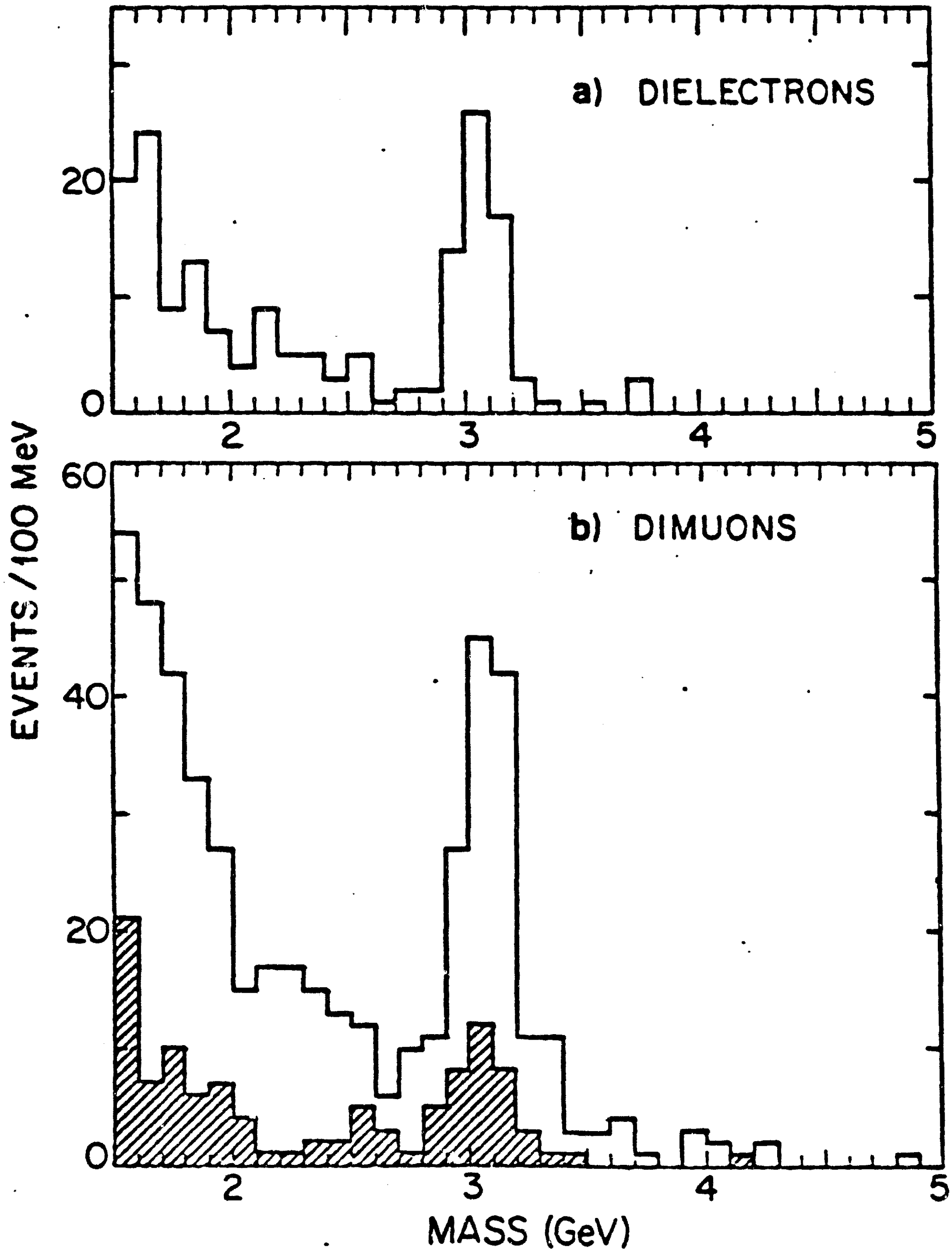
a) DIELECTRONS
b) DIMUONS
EVENTS / 100 MeV
0
20
40
60
2
3
4
5
MASS (GeV)

Figure 1

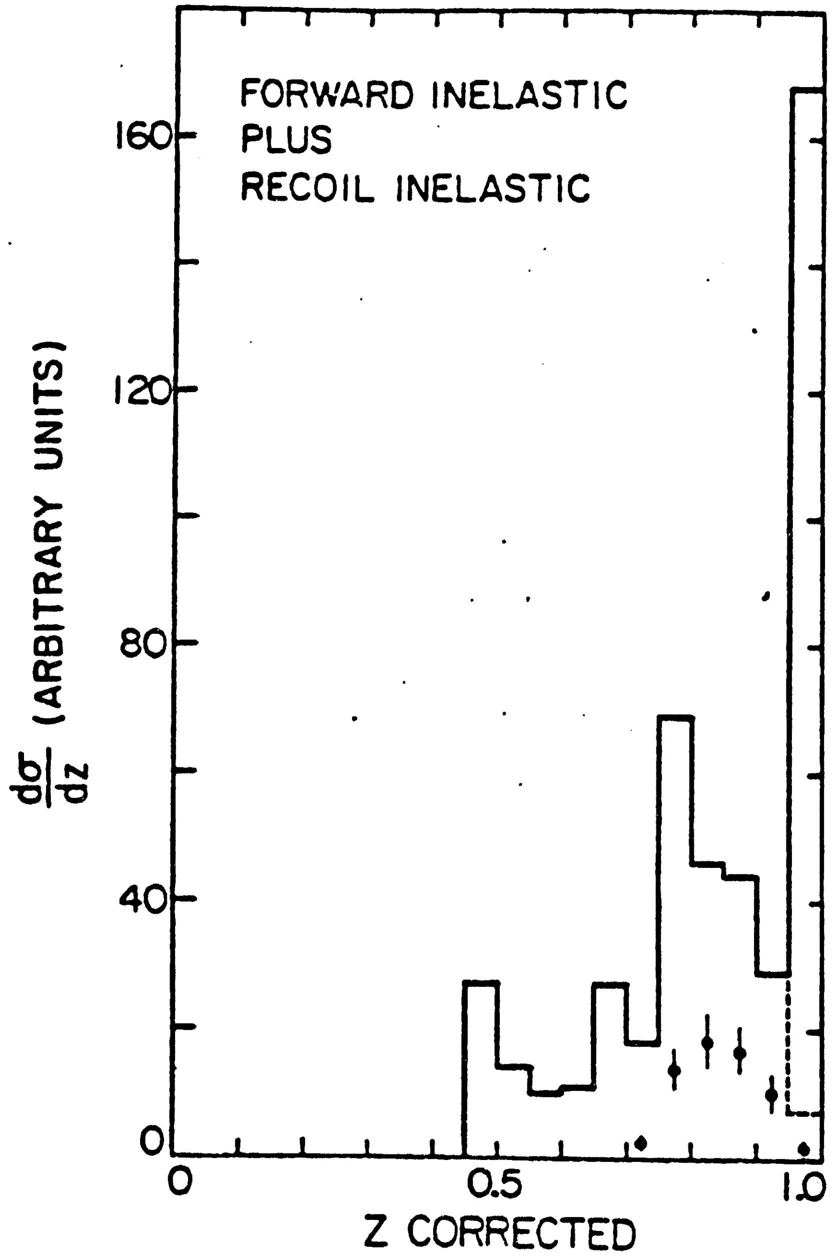
FORWARD INELASTIC
PLUS
RECOIL INELASTIC
$\frac{d\sigma}{dz}$ (ARBITRARY UNITS)
160
120
80
40
0
0
0.5
1.0
Z CORRECTED

Figure 2

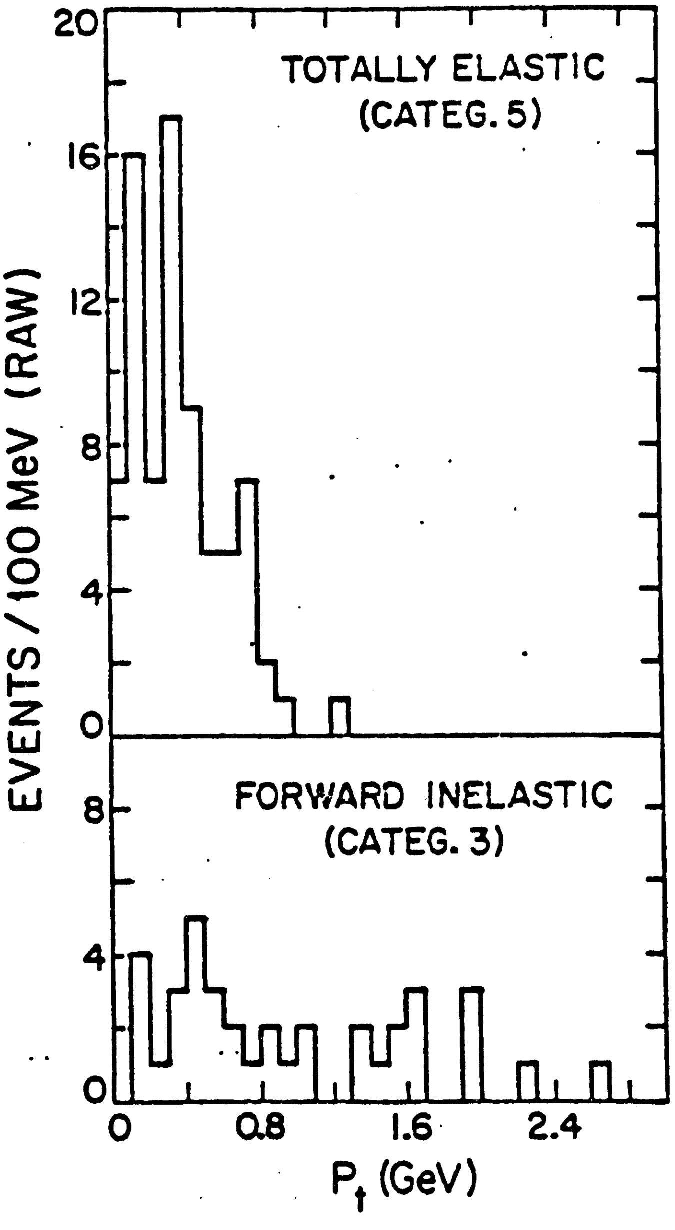
TOTALLY ELASTIC
(CATEG. 5)
FORWARD INELASTIC
(CATEG. 3)
EVENTS / 100 MeV (RAW)
20
16
12
8
4
0
8
4
0
0
0.8
1.6
2.4
P_t (GeV)

Figure 3

TABLE I

	EVENTS		σ	FRACTION	σ-ψ'	FRAC.-ψ'
	RAW	BKD				
1) All	147	23	21.5(2.1)(1.4)	1. (.00)(.00)	19.6(2.1)(1.4)	1. (.00)(.00)
2) Fwd. Elas.	110	18	14.2(1.6)(1.3)	.67(.03)(.07)	14.2(1.6)(1.3)	.73(.03)(.08)
3) Fwd. Inel.	37	4	7.3(1.3)(1.0)	.34(.05)(.06)	5.4(1.3)(1.1)	.28(.04)(.05)
4) Fwd. El. & Rec. Inel.	33	5	4.4(.9)(1.1)	.21(.03)(.05)	4.4(.9)(1.1)	.22(.03)(.06)
5) Fwd. El. & Rec. El.	77	13	9.8(1.4)(1.5)	.46(.04)(.08)	9.8(1.4)(1.5)	.51(.04)(.08)
6) Fwd. In. or Rec. In.	70	9	11.7(1.6)(1.3)	.55(.05)(.07)	9.8(1.6)(1.3)	.50(.04)(.07)
7) Inel. z<.9	30	3	6.6(1.3)(.7)	.31(.05)(.04)	5.1(1.3)(.8)	.26(.04)(.04)

TABLE II

THIS EXPT.	BFP[7]	EMC[8]	WIDE BAND[13]
$\sigma_{\text{Fwd. Elas.}}$	σ_{Elastic}	$\sigma_{z\geq.95}$	$\sigma_{\text{Fwd. Elas.}}$
14.2(1.6)(3.8)	19.5(.7)(2.9)	12.9(1.1)	21(3)
$\sigma_{z<.9}$	$\sigma_{z<.9}$	$\sigma_{z<.95}$	
6.6(1.3)(1.8)	15.5(.7)(3.1)	20.6(1.8)	not quoted
$\frac{\sigma_{z<.9}}{\sigma_{\text{Fwd. Elas.}}}$	$\frac{\sigma_{z<.9}}{\sigma_{\text{Elastic}}}$	$\frac{\sigma_{z<.95}}{\sigma_{z\geq.95}}$	
.46(.07)(.08)	.81(.08)	1.6(.2)	not quoted

APPENDIX H

Analysis of Data from the CLEO Experiment

One of us (PS.) is continuing work on the CLEO experiment at the Cornell Electron Storage Ring (CESR). CLEO is an all purpose magnetic detector (Fig. 1 ab) incorporating charged particle tracking, electromagnetic shower detection, and particle identification. Our work on the experiment started in 1978 at Rutgers University, and involved the construction of the primary electromagnetic shower detector (Ref. 1), installation and maintenance of the shower detector at Cornell, development of the shower detector analysis program, and general data analysis (Ref. 2).

The most significant recent result is the evidence for $B\overline{B}$ production from the 4S upsilon state. The visible inclusive electron ($p>1$ GeV/c) cross section resulting from a preliminary analysis of all CLEO data is shown in Fig. 2 along with the visible hadronic cross section. The large enhancement in high energy electron cross section and energy spectrum (Fig. 3) has been interpreted as evidence for $B\overline{B}$ production (Ref. 3).

Institutions within the CLEO collaboration have access to one PDP-10 and five VAX computers exclusively dedicated to research, including the OU VAX. The CLEO off-line analysis programs are operational on the OU VAX including the interactive event display. The OU effort is coordinated in close cooperation with the Rutgers group and is directed toward completion of the inclusive electron measurements in the Υ (4S) resonance region (Ref. 3). This effort crucially depends on the successful operation of the shower detector and development of its analysis software. Refinement of the final event selection including detailed event scanning is presently underway at OU. In conjunction with the inclusive electron analysis, OU based efforts will be made to improve the shower detector analysis and Monte Carlo simulation programs. Electromagnetic shower generation programs EGS (Ref. 4) and hadronic shower generation programs HETC (Ref. 5) have been installed on OU computers and should greatly aid in this effort. The EGS program gives reasonable agreement with electron test beam data taken with one octant of the CLEO detector. (See Figures 4,5 and 6.)

Finally, the OU-HEP groups important involvement in U.S. solid state detector development leads to the exciting prospect of using such detectors in colliding beam experiments. One attractive possibility involves use of large area (1 in^2) Si detectors for dE/dX measurements (Ref. 6). Measurements have been made of dE/dX with commercial Si detectors for π's, p's, and electrons in the momentum range 100-650 MeV/C at LAMPF. Good agreement (to within 5%) has been obtained between the measurements and the peak and the width of the theoretical Laudau distribution. These results indicate that a dE/dX Si detector consisting of four layers surrounding the beam pipe could separate π's and K's of 500 MeV/C momenta with greater than 90% efficiency and with a contamination of the K sample of less than 6% (assuming a π/K ratio of 10). To study radiation damage in the environment of the interaction region, an ORTEC Si detector was mounted to the beam pipe inside the CLEO Solenoid. After four months of normal machine operation, no degradation in the detector has been observed.

References

1. The CLEO Electromagnetic Calorimeter, P. Skubic, ~~The CLEO Photon Shower Detector~~, ~~J. J. Mueller, et. al.~~, Proceedings of the ~~1980 IEEE Nuclear Science Symposium~~. Gas Calorimeter Workshop, Fermilab, 1982,

2. First Physics Results from the CLEO Detector at CESR, B. Gittelman and P. Skubic, Proceedings of the XVth Recontre de Moriand (1980).

3. C. Bebek, et. al., Phys. Rev. Lett. 46, 84 (1981).

4. Richard Ford and Walter Nelson, SLAC Report No. SLAC-210, June 1978.

5. T. A. Gabriel and W. Schmidt, Nucl. Instr. and Meth. 134, 271 (197).

6. S. Csorna, F. Sannes, P. Skubic, "A Silicon DEDX Detector for CLEO II," CLEO internal report.

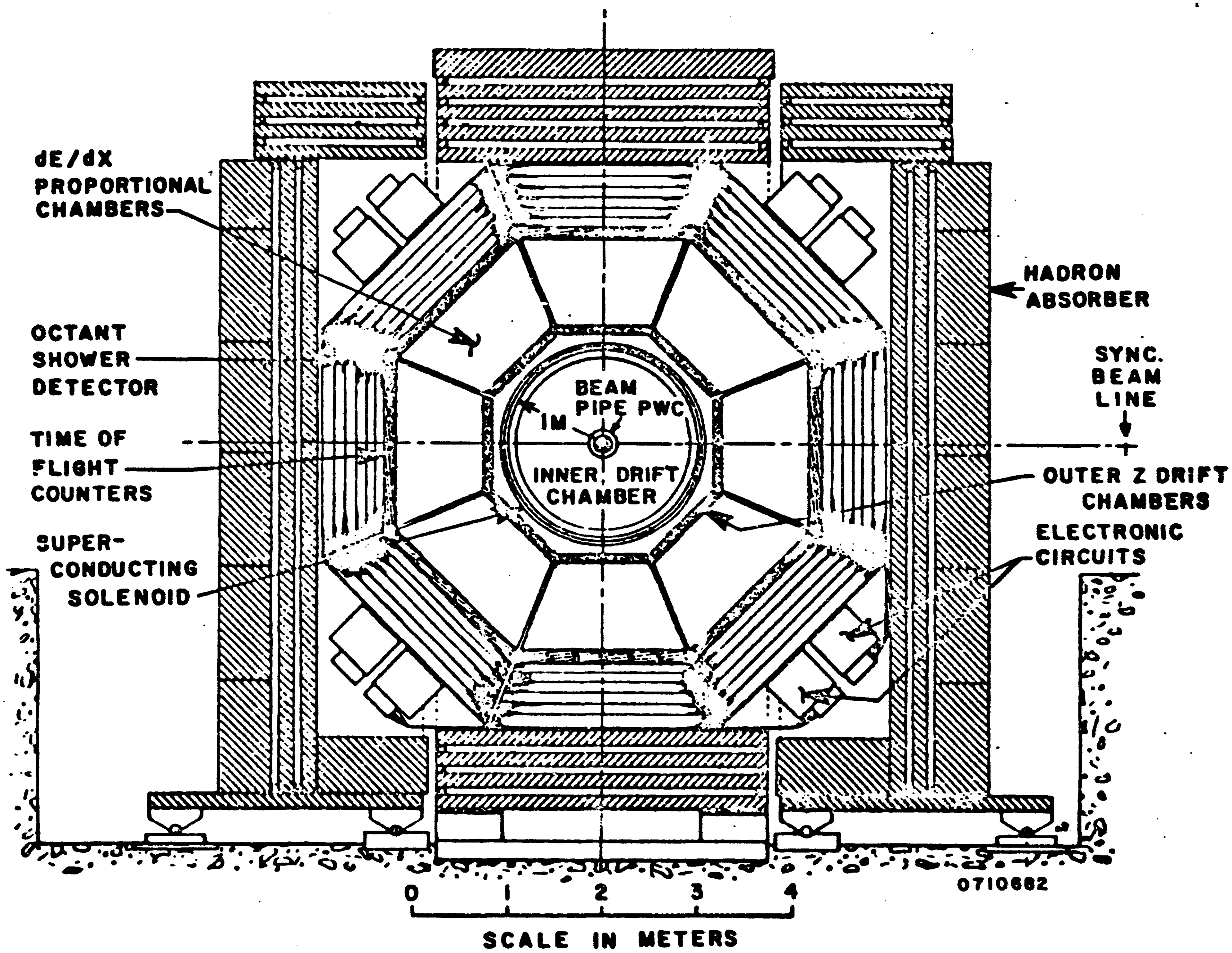
dE/dX PROPORTIONAL CHAMBERS
OCTANT SHOWER DETECTOR
TIME OF FLIGHT COUNTERS
SUPER-CONDUCTING SOLENOID
HADRON ABSORBER
SYNC. BEAM LINE
BEAM PIPE
PWC
IM
INNER DRIFT CHAMBER
OUTER Z DRIFT CHAMBERS
ELECTRONIC CIRCUITS
0710682
0
1
2
3
4
SCALE IN METERS

Fig. 1a

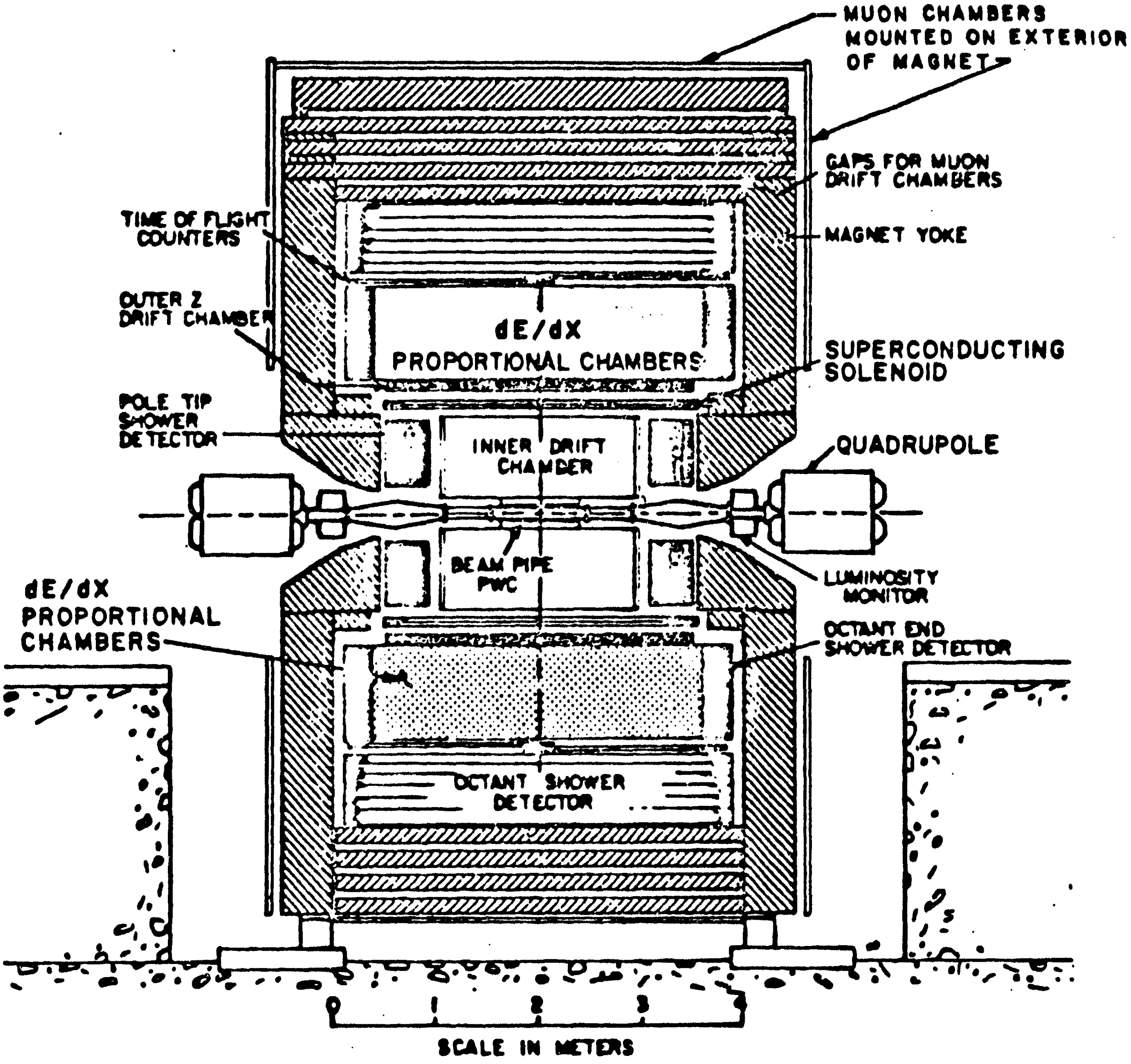

Fig. Ib

0710282

FIGURE 2

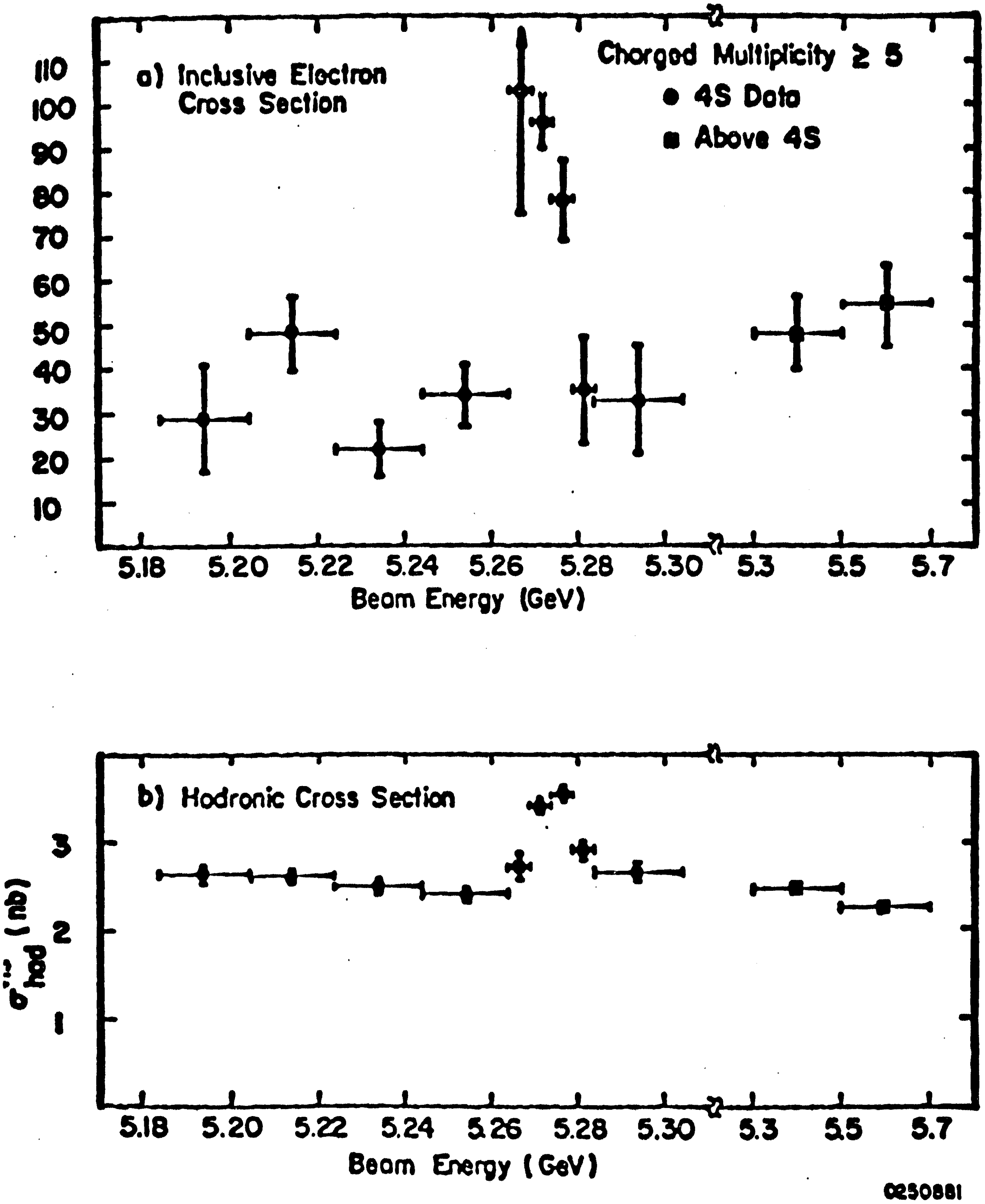
a) Inclusive Electron
Cross Section
Charged Multiplicity ≥ 5
● 4S Data
■ Above 4S
110
100
90
80
70
60
50
40
30
20
10
5.18
5.20
5.22
5.24
5.26
5.28
5.30
5.3
5.5
5.7
Beam Energy (GeV)
b) Hadronic Cross Section
σ_{hod} (nb)
3
2
1
5.18
5.20
5.22
5.24
5.26
5.28
5.30
5.3
5.5
5.7
Beam Energy (GeV)
0250881

FIGURE 3

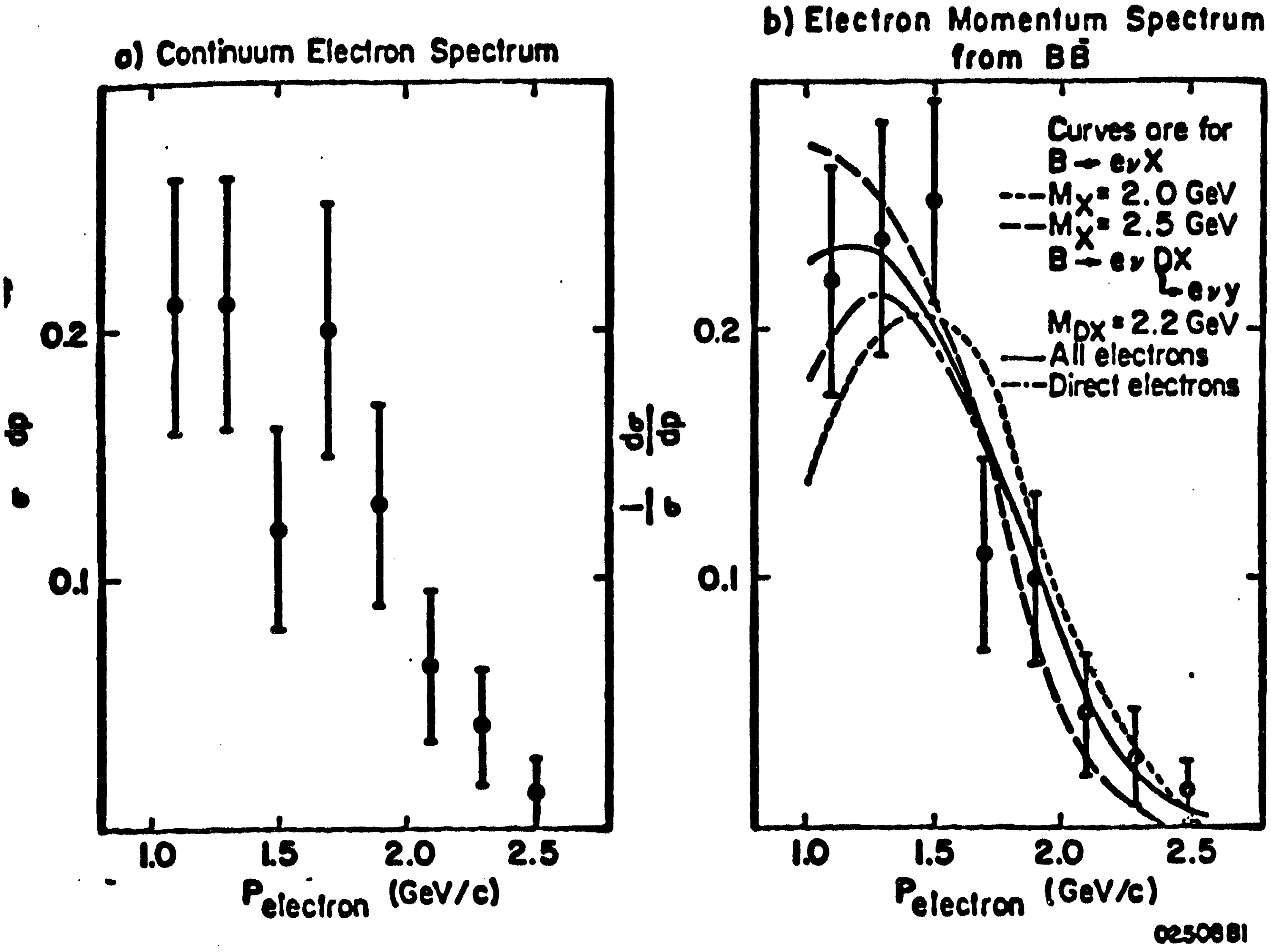

a) Continuum Electron Spectrum

b) Electron Momentum Spectrum from $B\bar{B}$

FIGURE 4

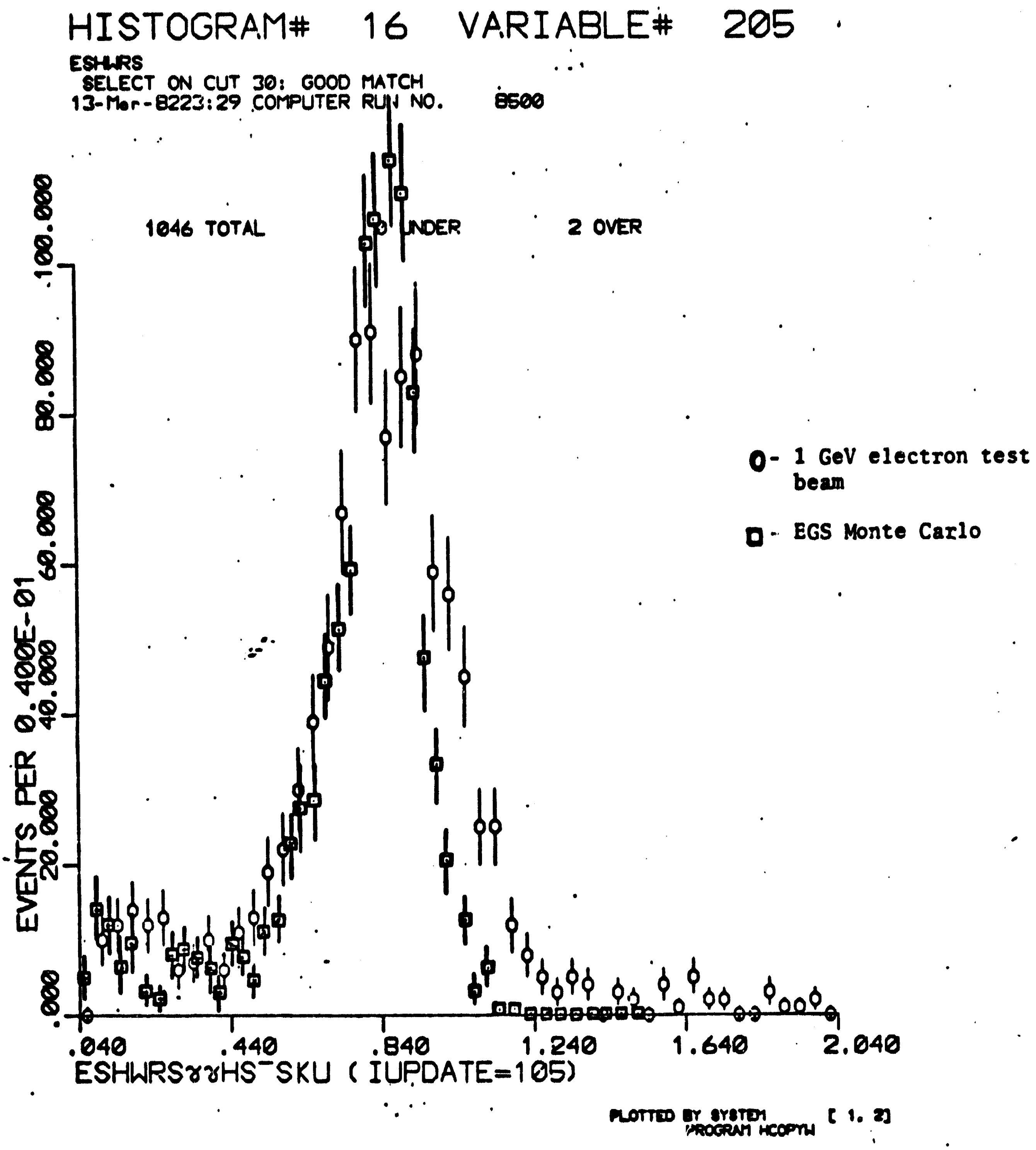

TOTAL SHOWER ENERGY

FIGURE 5

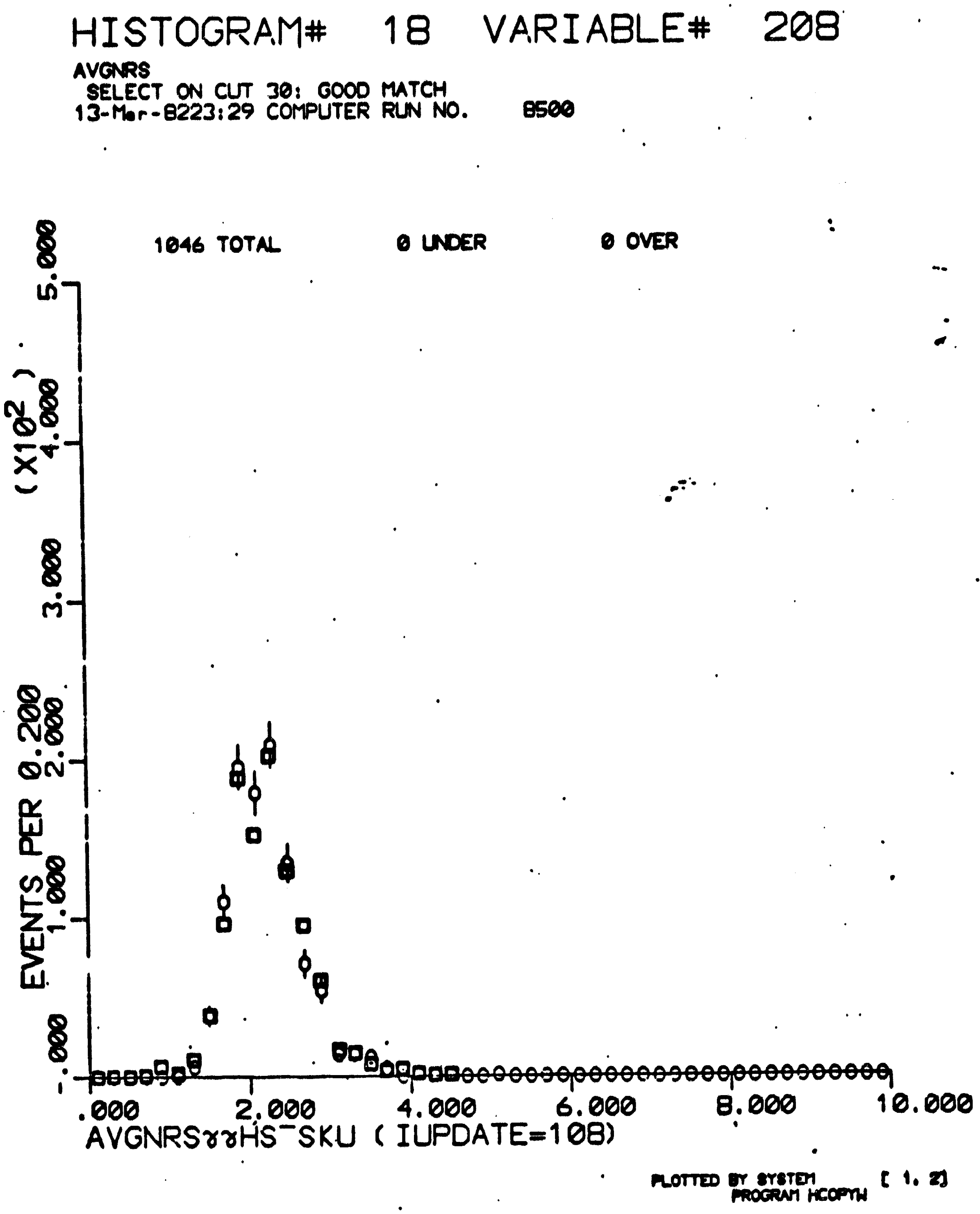

AVERAGE NUMBER OF HITS PER LAYER

FIGURE 6

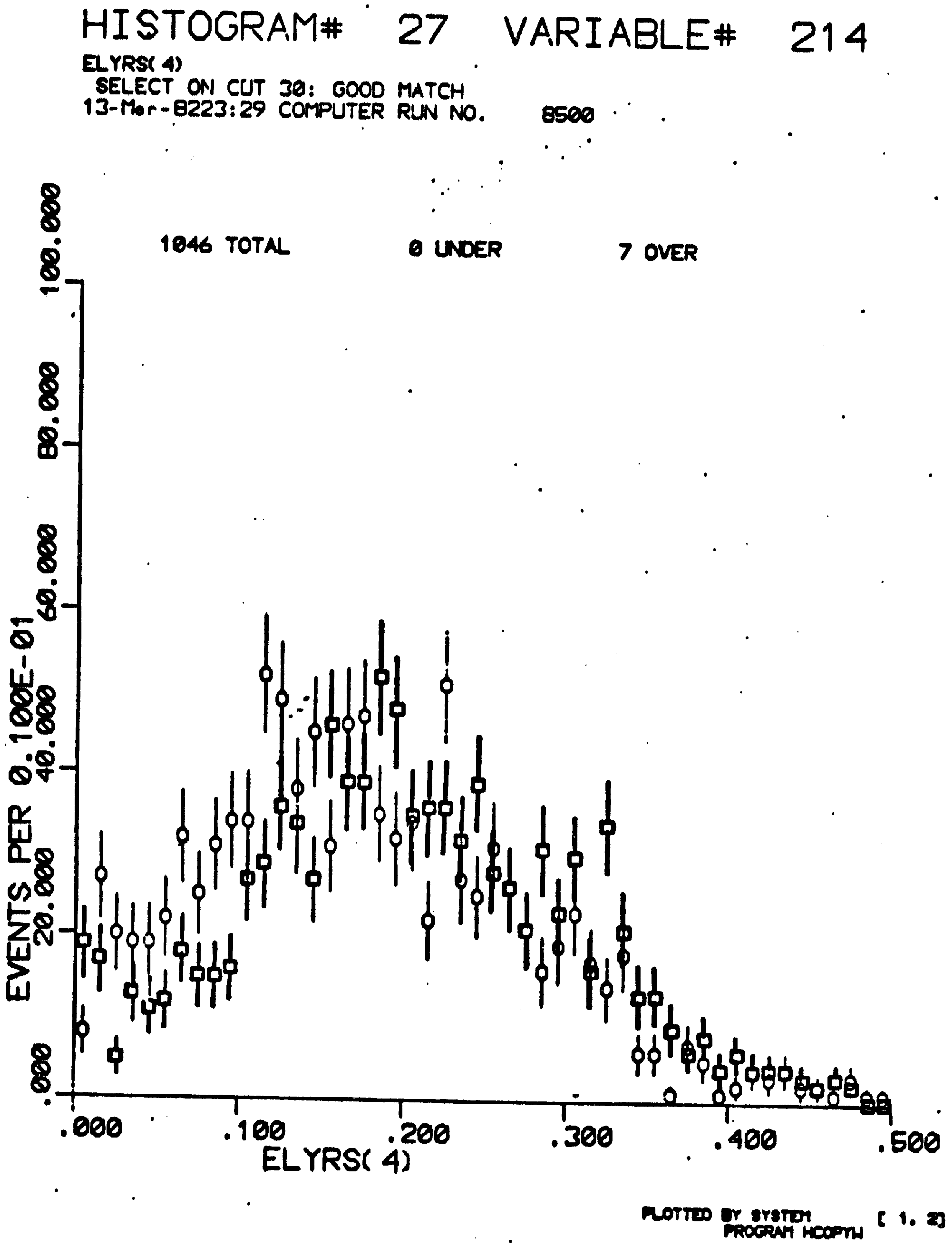

ENERGY IN LAYER FOUR
(Out of 7)

OU-HEP MEMO 1

SSD RESULTS 1983

George R. Kalbfleisch

3/1/83

Appendix C
The SSD Prototyping and Testing Program

The SSD prototyping and testing program has basically three goals:

a) Check charge collection,
b) Check track point resolution,
c) Check vertex reconstruction resolution.

All of the above checks have been made with the OU testing of five 1 cm^2 LBL (Walton) detectors instrumented with 160 prototype amplifiers. The result is that the detectors perform as theoretically expected. A discussion of the basics, the amplifier design etc. is to be found in the 1981 Fermilab SSD Workshop.[1] A description of the Fermilab M5 beam test (May-June, 1982) is appended as a subappendix to this Appendix C.

In addition, OU and Ohio State have been cooperating on testing of 8 cm^2 Centronic detectors (LAMPF beam test in progress, data taking to commence Nov. 27--Dec. 15, 1982). In addition, six 25 cm^2 United Detector Technology and six 25 cm^2 Centronic's detectors square in cross-section built on three inch silicon disks SSD's should be in hand in two or three months. At that time we will bench test them and subsequently beam test them. The ultimate twelve sided regular polygonal 35 cm^2 (on 3" Si disks) SSD's should be specified and ordered early next year (with delivery expected late in the year).

The charge collection results are shown in Figures C-1 and Figure C-2. Figure C-1 shows the charge distribution of 46 GeV/c pions compared to a Landau distribution convoluted with a 0.25 fc noise distribution. The shape and the magnitude of the charged collected (1.7 fc observed vs. 1.8 fc predicted) agree well. Figure C-2 shows 650 MeV/c protons in excellent agreement with the theoretical shape (Landau convoluted with a momentum spread of 7% and a noise of 0.25 fc). And the observed ratio of the pulse heights of 650 MeV/c protons to

550 MeV/c pions of 2.7 ± 0.2 agrees well with the theoretical ratio of 2.6. Assuming that the spatial track point accuracy is given by the microstripe spacing (pitch) divided by the $\sqrt{12}$, the observed chisquare distribution for the fits of straight through beam tracks for all 3, 4, and 5 point 46 GeV/c pion tracks are shown in Figure C-3. The average (χ^2/DOF) for this data is 1.2 ± 0.2. This implies that the accuracy is within (10 ± 10)% of the theoretical pitch/$\sqrt{12}$ value including residual misalignments of the detector array. The detector array was aligned better than ½ the pitch of 80 microns both rotationally and translationally.

The transverse resolution of through beam tracks extrapolated from the SSD's to the position of the veto counter is illustrated by the data in Figure C-4. The veto would ideally cast a rectangular shadow on the downstream SSD's. Beam divergence (corresponding to less than ≤ 80 μ), the veto angular misalignment (≤ 60 μ), multiple scattering in the copper target pieces (~40 μ) and the errors in the fitted parameters (~20 μ) put a slope on the edge of the shadow of (≤ 110 μ). The data have a sloped box shape with a slope of ~100μ. However please note that the shadow edge goes from fully bright to fully dark in one stripe width!

Finally multiprong interactions are observed in the SSD's. A typical three track event is displayed in Figure C-5. The "dashes" represent the stripes each connected to its own amplifier. The letters of the alphabet represent proportionally the charge deposited on the appropriate strip for those stripes which have a signal larger than the pedestal plus three noise standard deviations. The numbered lines represent the tracks. One sees that the three tracks intersect nicely in a small region (triangle). The estimated vertex errors from the fitted track parameters are ± .01 mm transversly and ± 0.4 mm longitudally. The transverse errors are roughly independent of the event details for vertices close to the detector array. The longitudal errors should be linear in the pitch, the reciprocal of the (largest) opening angle of the tracks, and the distance from the SSD array to the interaction point (i.e. vertex). Alternatively, the RMS deviation of the pairwise intersections of the tracks from the overall fitted vertex can be examined in lieu of the calculated transverse and longitudal errors for events with 3 or more tracks. The RMS for the transverse direction averages 20 μ, as compared to the track point standard deviation of pitch/$\sqrt{12}$ = 23μ in this set up. The RMS for the longitudal direction depends strongly on the reciprocal of the opening angle and averages 500μ for an opening angle of 50 mr. Monte Carlo shows that bottom and charm decays from hadronic production at Tevatron energies will have an average opening angle between pairs of 70mr. The actual SSD's for E-653 will have a pitch of 40μ. Thus we expect an RMS longitudal error in predicting vertices in the emulsion of E-653 of 500/2/$\sqrt{2}$ = 200μ, as advertised in the proposal (Appendix I, page 12).

The above results show that SSD's perform as theoretically expected. We have gained needed experience in SSD's, low noise amplifiers, charge sharing, and the diverse software required to analyze the data from such a system. The SSD's are well understood. Thus we can proceed to prosecute this experiment, having SSD technology well in hand.

---

1. Kalbfleisch, George R., "Status of Some of the Silicon Detector Development in the United States," in Silicon Detectors for High Energy Physics, Proceedings of a Workshop held at Fermilab, Ocotober 15-16, 1981, page 45.

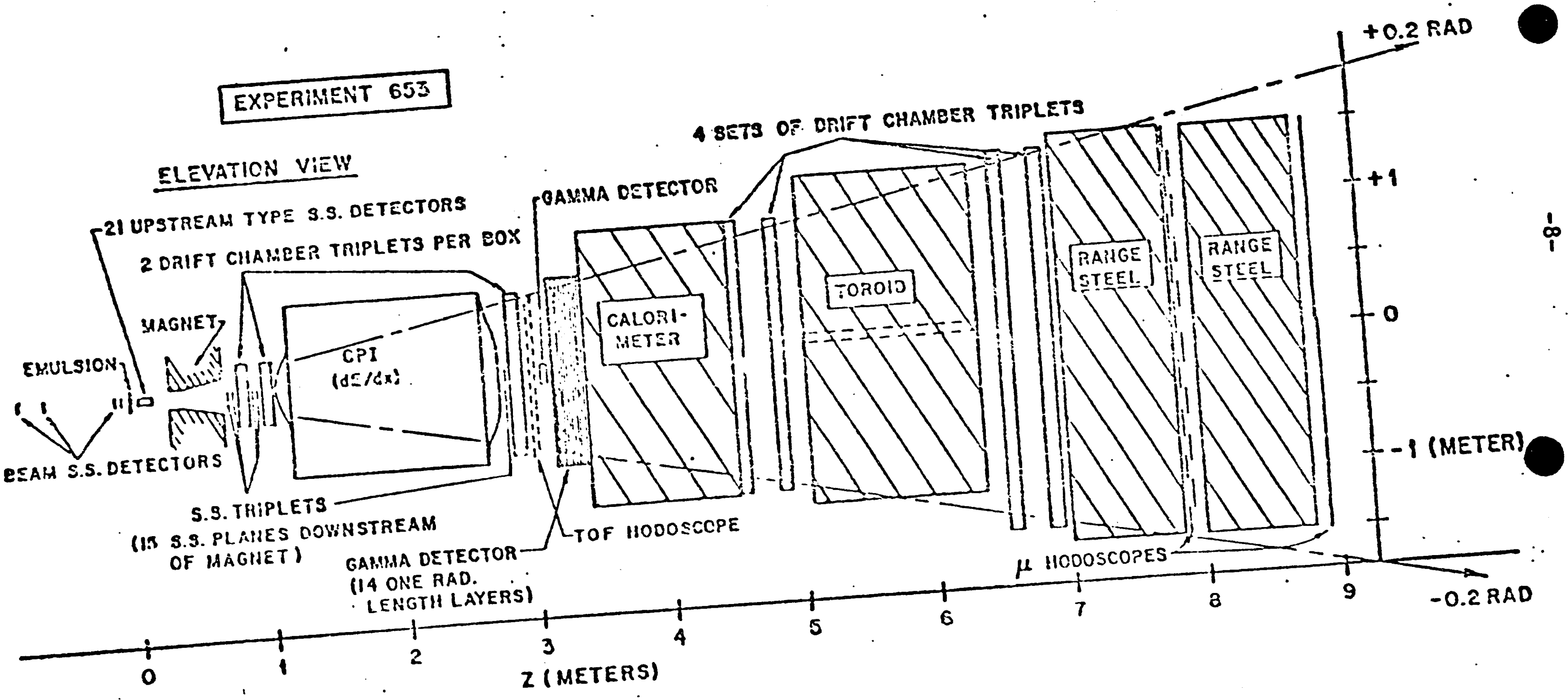
EXPERIMENT 653
ELEVATION VIEW
21 UPSTREAM TYPE S.S. DETECTORS
2 DRIFT CHAMBER TRIPLETS PER BOX
MAGNET
EMULSION
BEAM S.S. DETECTORS
CPI (dE/dx)
S.S. TRIPLETS (15 S.S. PLANES DOWNSTREAM OF MAGNET)
GAMMA DETECTOR
GAMMA DETECTOR (14 ONE RAD. LENGTH LAYERS)
TOF HODOSCOPE
CALORI-METER
4 SETS OF DRIFT CHAMBER TRIPLETS
TOROID
RANGE STEEL
RANGE STEEL
μ HODOSCOPES
+0.2 RAD
-0.2 RAD
+1
0
-1 (METER)
0
1
2
3
4
5
6
7
8
9
Z (METERS)

Figure 2.

8-LBL DEVICES:

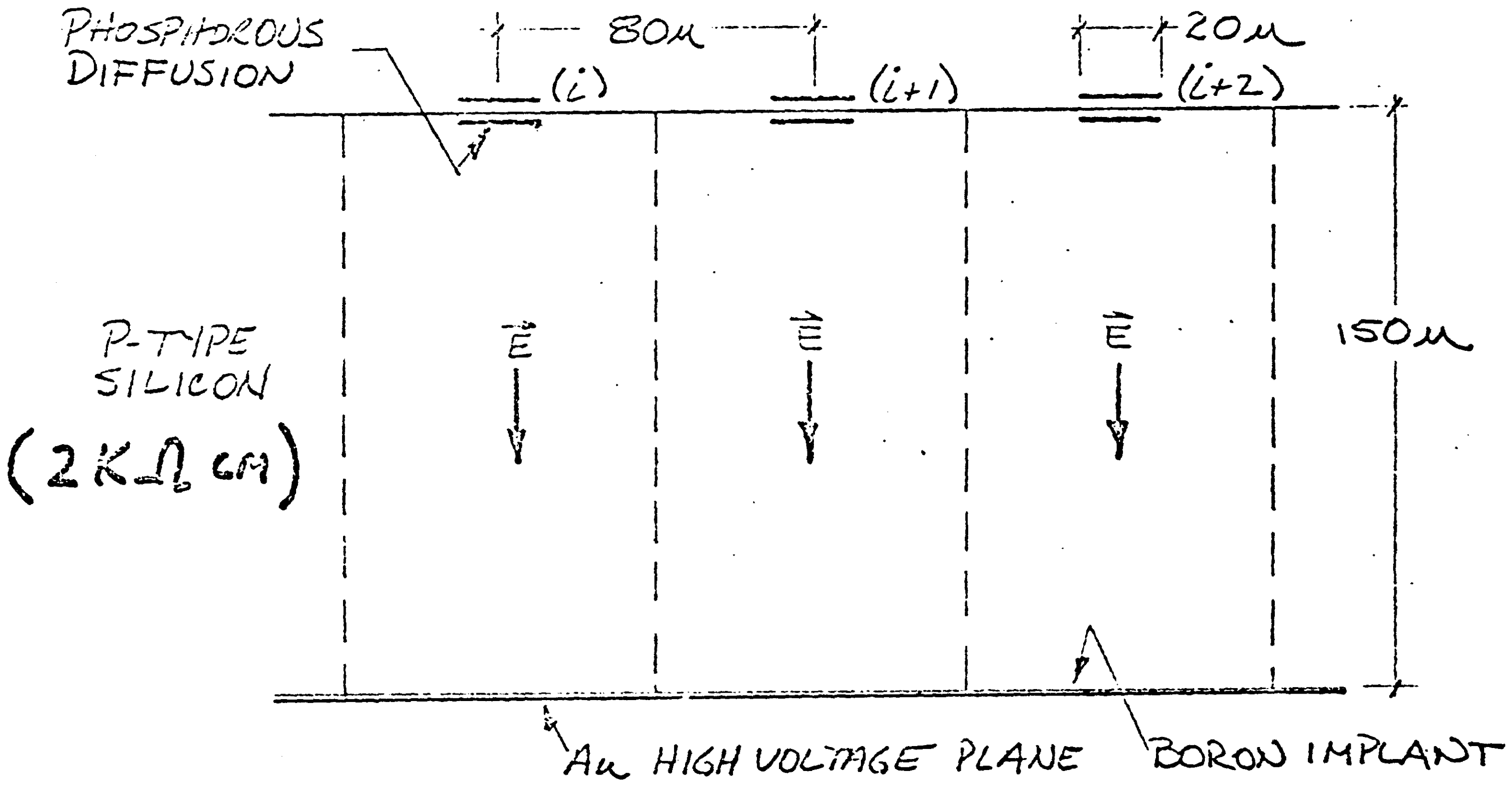

48 - 1 CM LONG STRIPES EACH

(EACH [illegible]) [illegible]

"M5" BEAM TEST (FNAL)

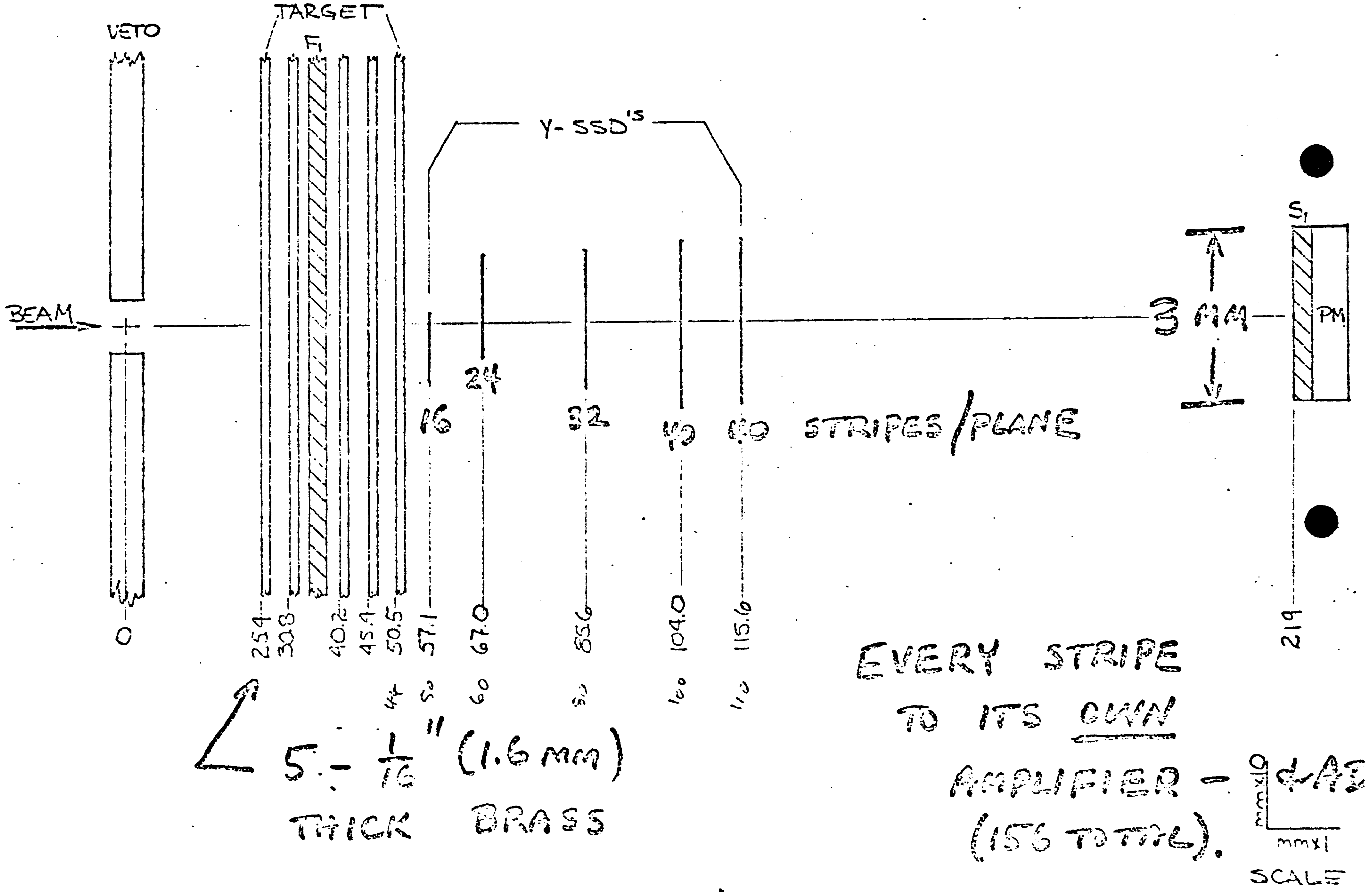

∠ 5 - 1/16" (1.6 mm)
THICK BRASS

EVERY STRIPE
TO ITS OWN
AMPLIFIER - ∠∆E
(156 TOTAL).

```
FIT AGAIN--THROWING OUT A POINT ?   BEAM
Y
DELETE OR RESTORE OR SAVE <D,R,S>      |   ← HOLE IN VETO AT  Z=0MM
S
FIT AGAIN--THROWING OUT A POINT ?      ↓
N
**VTX***-EV,NT,XV,DXV,ZV,DZV=  21  3    -0.015     0.010     40.849     0.535
       Z <X> -1                                                  1 MM
        28 MM ++++++++++++++++3+++++++++++++1++++++++++++++++++++
        30 MM                   3          1
        32 MM +++++++++++++++++++3+++++++++1+++++++++++++++++++++
        34 MM                     3     2 1
        36 MM +++++++++++++++++++++3++++21+++++++++++++++++++++++     TARGET
        38 MM                       3   12
        40 MM +++++++++++++++++++++++3   2+++++++++++++++++++++++
        42 MM                         13 2
        44 MM +++++++++++++++++++++++1++3+2++++++++++++++++++++++
                                   1   3 2
                                   X - - 3 X - - - - - - - - - - -     50 MM
                               1           2 3                            SSD^1_Δ
Z=60MM - - - - - - - - - - X - - - - - - - 2 X 3 - X -
                       1                     2       3
         - - - - - 1 - - - - - - - - - - - -   - 2 -   -   - 3 -   -   -   80MM
             1                                   2               3
 - - - - 1 X - - - - - - - - - - - - - - - - - - - 2 - - - - - - - - - 3 X - - -   100MM
       1                                           2                       3
 - - X - - - - - - - - - - - - - - - - - - - - - - - X - - - - - X - - X - - X -   110MM
                         *************************************************
                         **          FILE  57   EVENT  21
                         ** TRACK    ZMID    INTER    SLOPE    CHISQ    # HITS
                         **     1    80.000   -9.750   -0.235   19.615     4.000
                         **     2    80.000    4.355    0.091    4.222     3.000
                         **     3    80.000   10.638    0.293   22.024     4.000
                         **        XV=    -0.015 -+     0.010 MM.
                         **        ZV=    40.849 -+     0.535 MM.
                         *************************************************

N
AGAIN WITH ANOTHER FILE
N
```

Figure C-5

A typical 46 GeV/c 3 prong event as seen in the 5 LBL microstripe array.

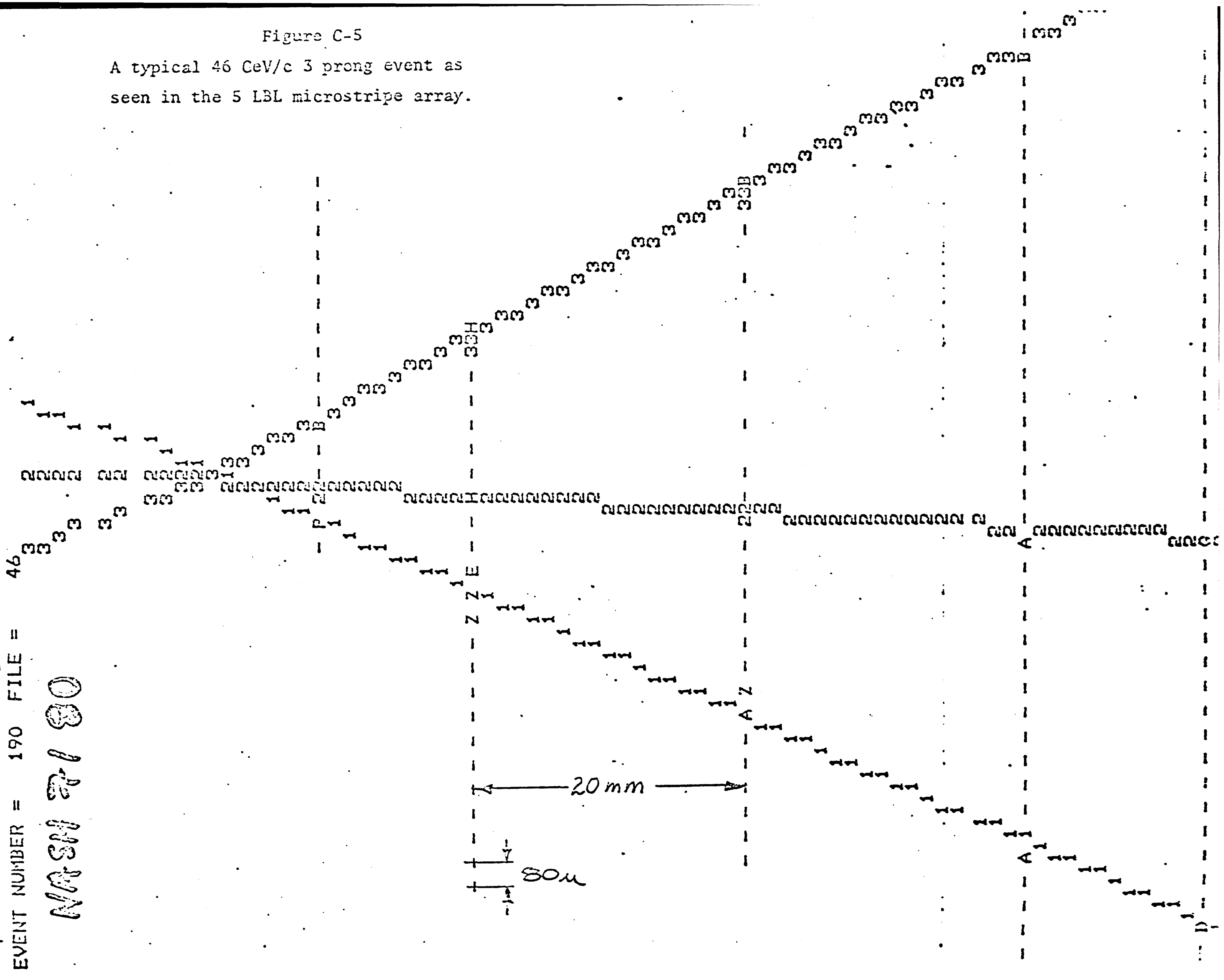

10/22/82

EVENT NUMBER = 133 FILE = 28

NSH III 120

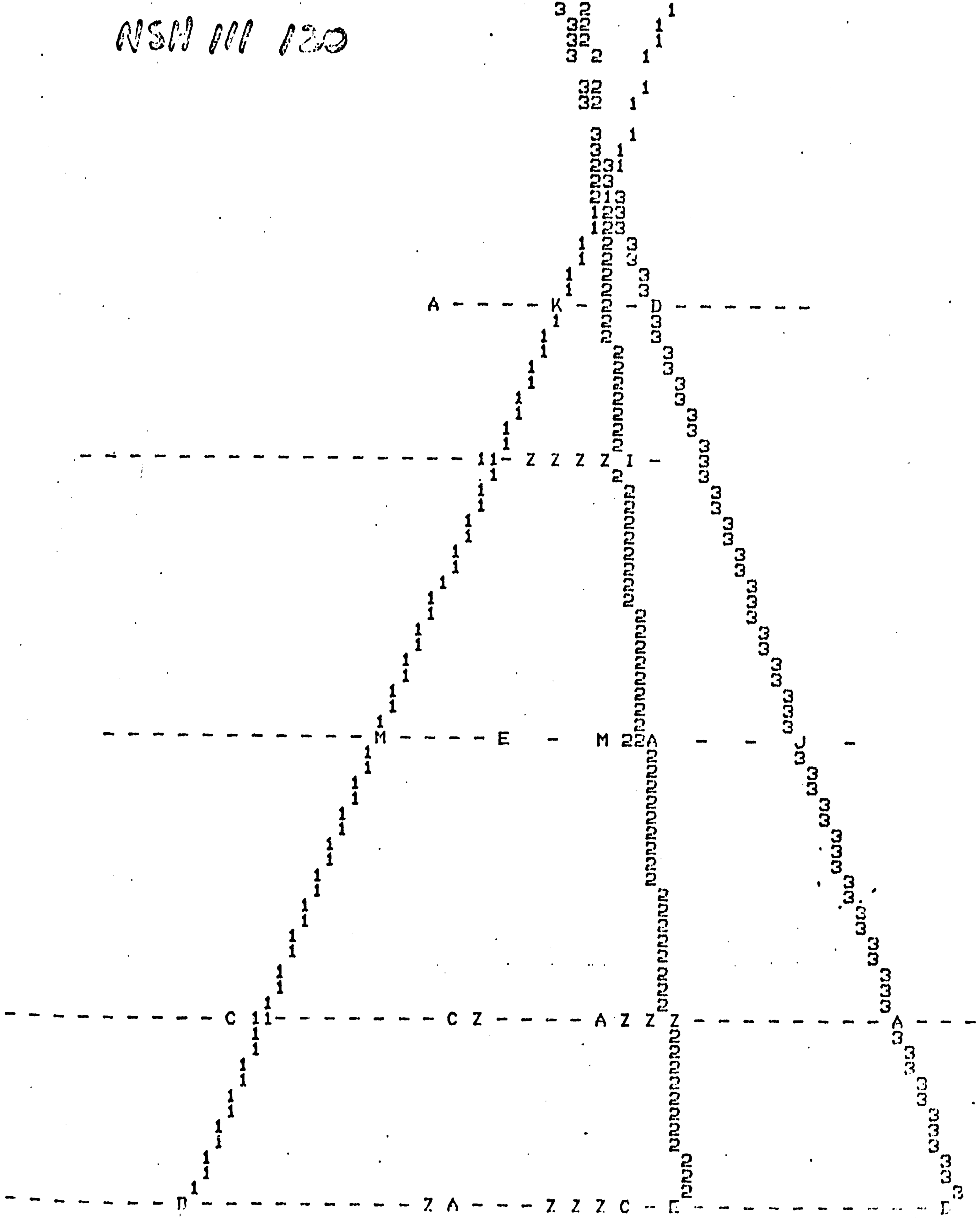

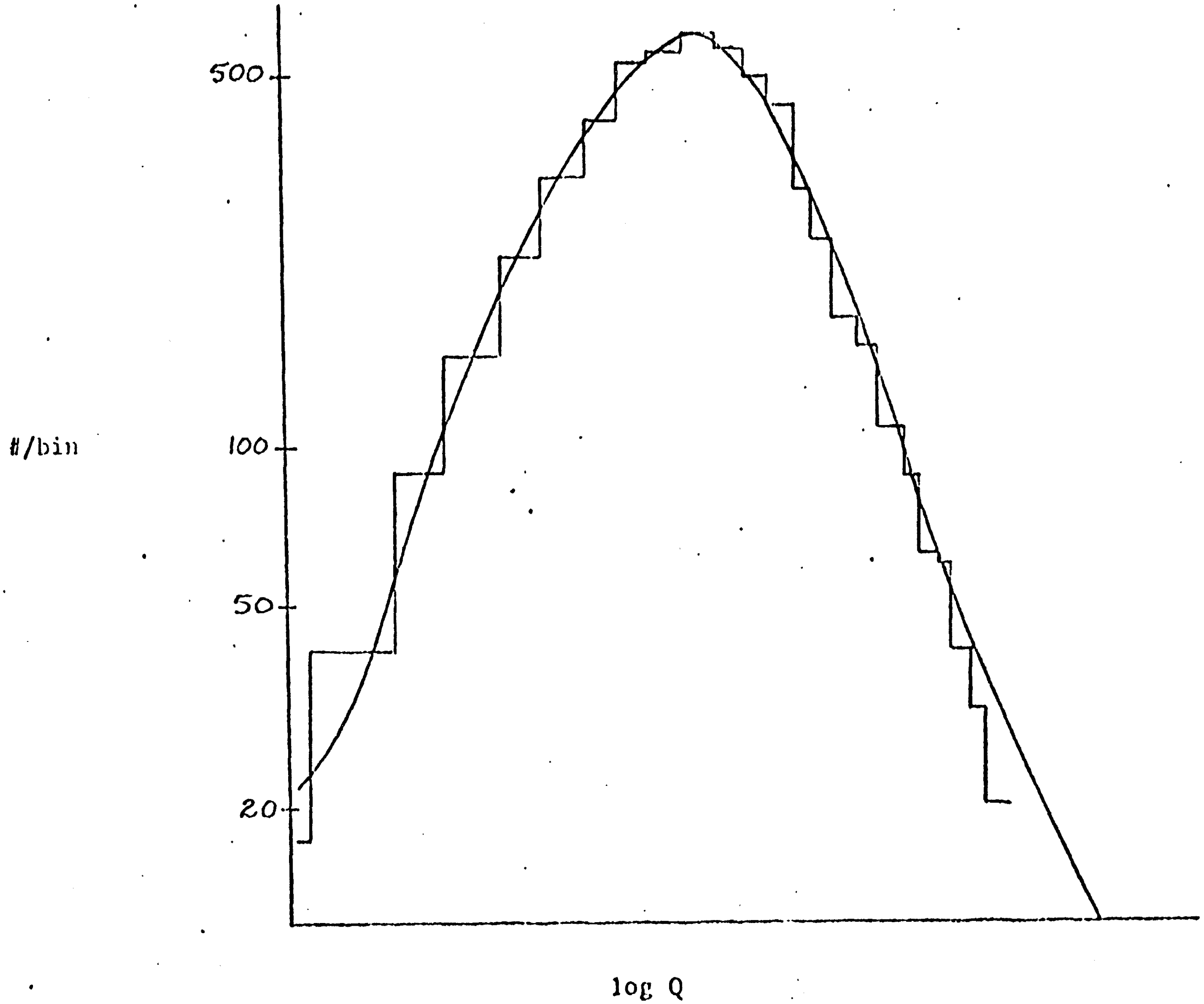

Figure C-1
Charge Distribution
6196 Tracks, 46 GeV/c Pions

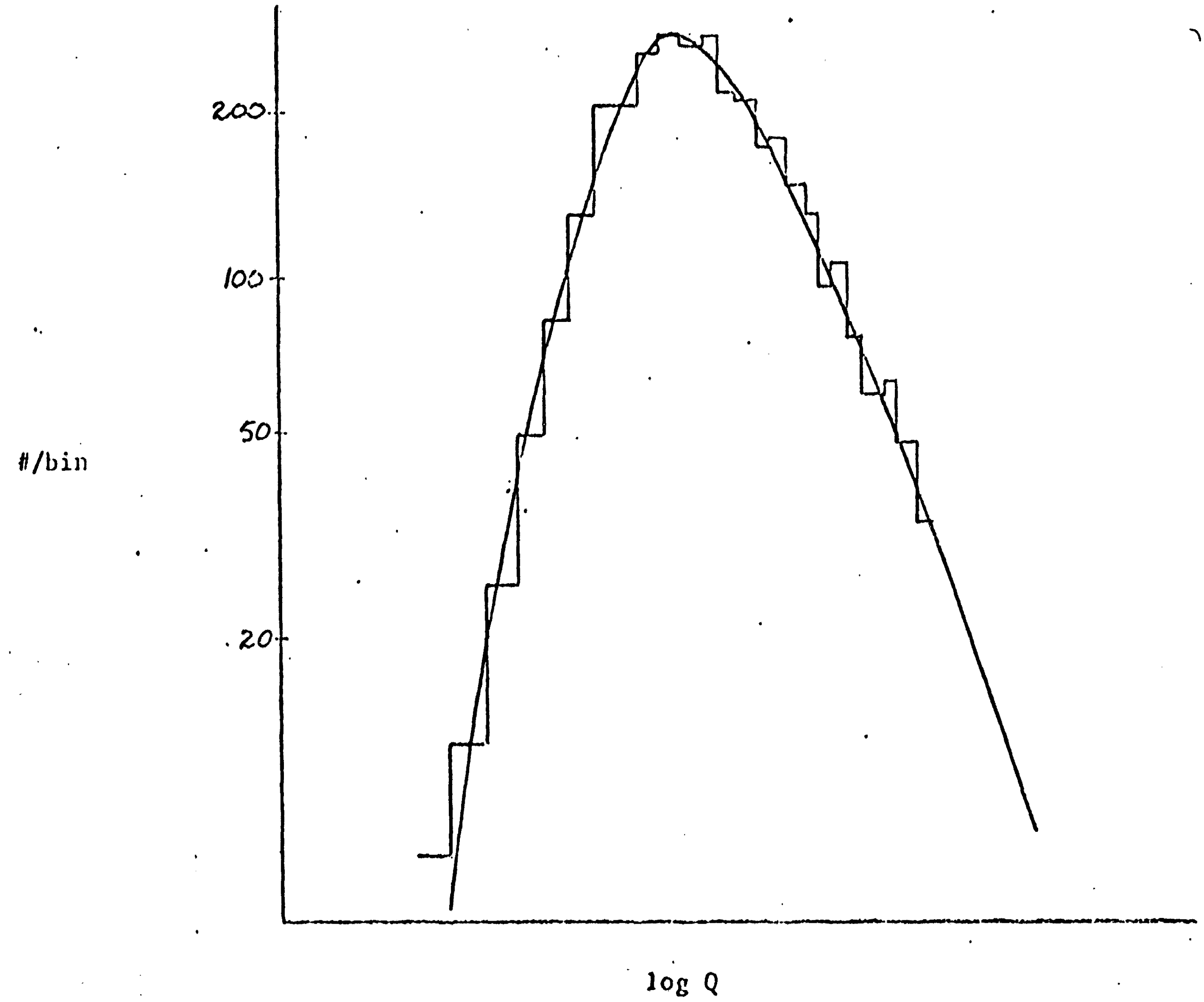

Figure C-2
Charge Distribution
3905 Tracks, 650 MeV/c Protons

χ^2 Distristributions

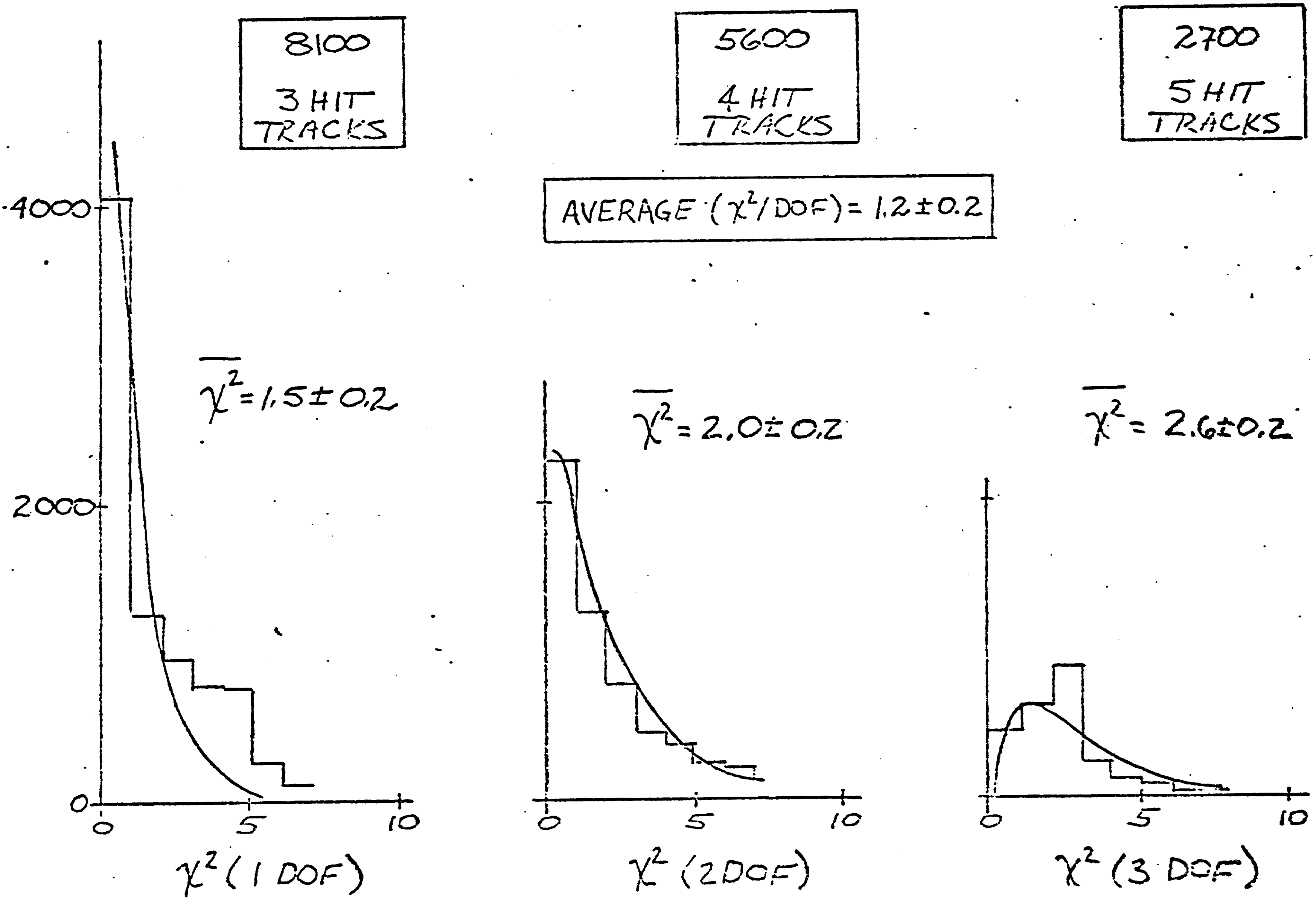

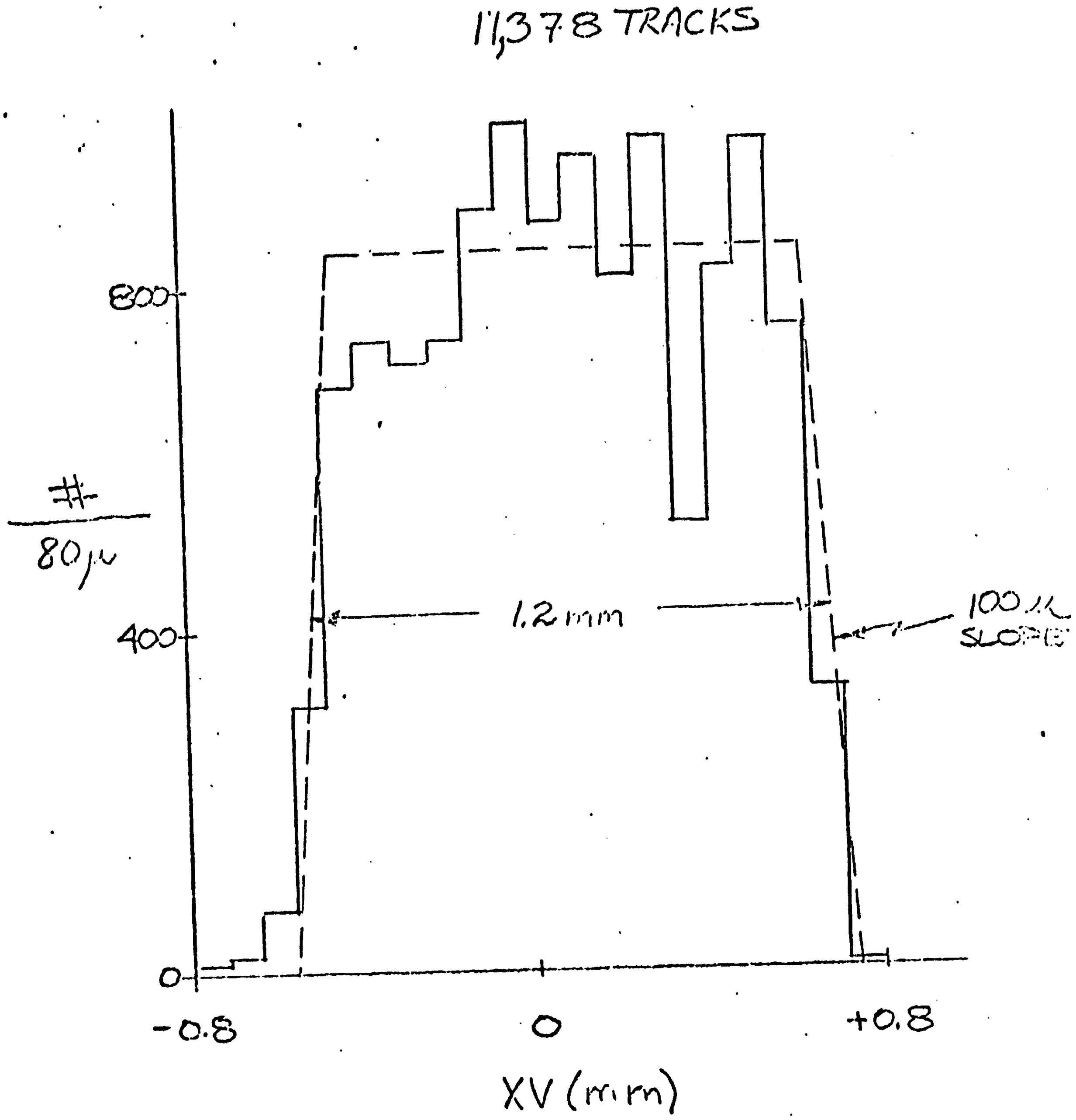

Figure C-4

Transverse position of 46 GeV/c pion tracks at the 3-positions of the VETO counter (its "shadow").

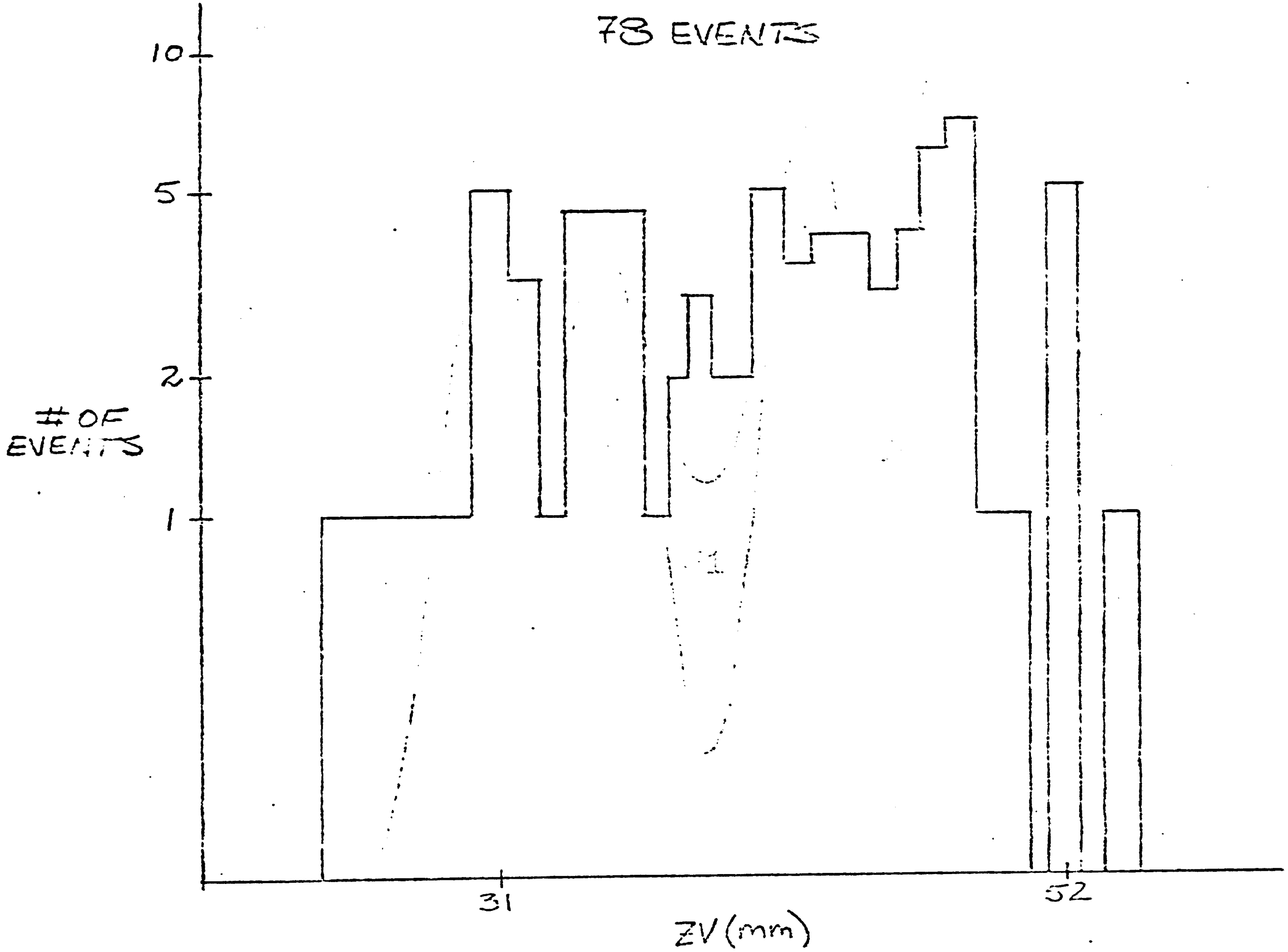
78 EVENTS
10
5
2
1
OF EVENTS
31
52
ZV (mm)

THE OHIO STATE TEST OF 1 (OF 3) CENTRONICS (LONDON) DETECTORS USES CAPACITIVE CHARGE DIVISION READOUT INTO 2 AMPLIFIE

THE RAW $Q = Q1 + Q2$ DISTRIBUTION HAS (AS SHOWN) A FWHM ≈ 50%.

HOWEVER, WHEN EACH Q_i IS CORRECTED FOR BRIDGING EFFECTS OF THE CAPACITANCES TO "GROUND" THE FWHM BECOMES 26%.

VS. EXPECTED 23%.

4/30/82 MIT/GL

③/⑤

OHIO STATE (REAY)

SPRING
1982

CENTRONICS + 2 CHANNELS AMPLIFIER

$\sigma_{A+D} \sim .05\,fc$ (300 ELECTRONS)

$\Longrightarrow S/N > \frac{50}{1}$!!

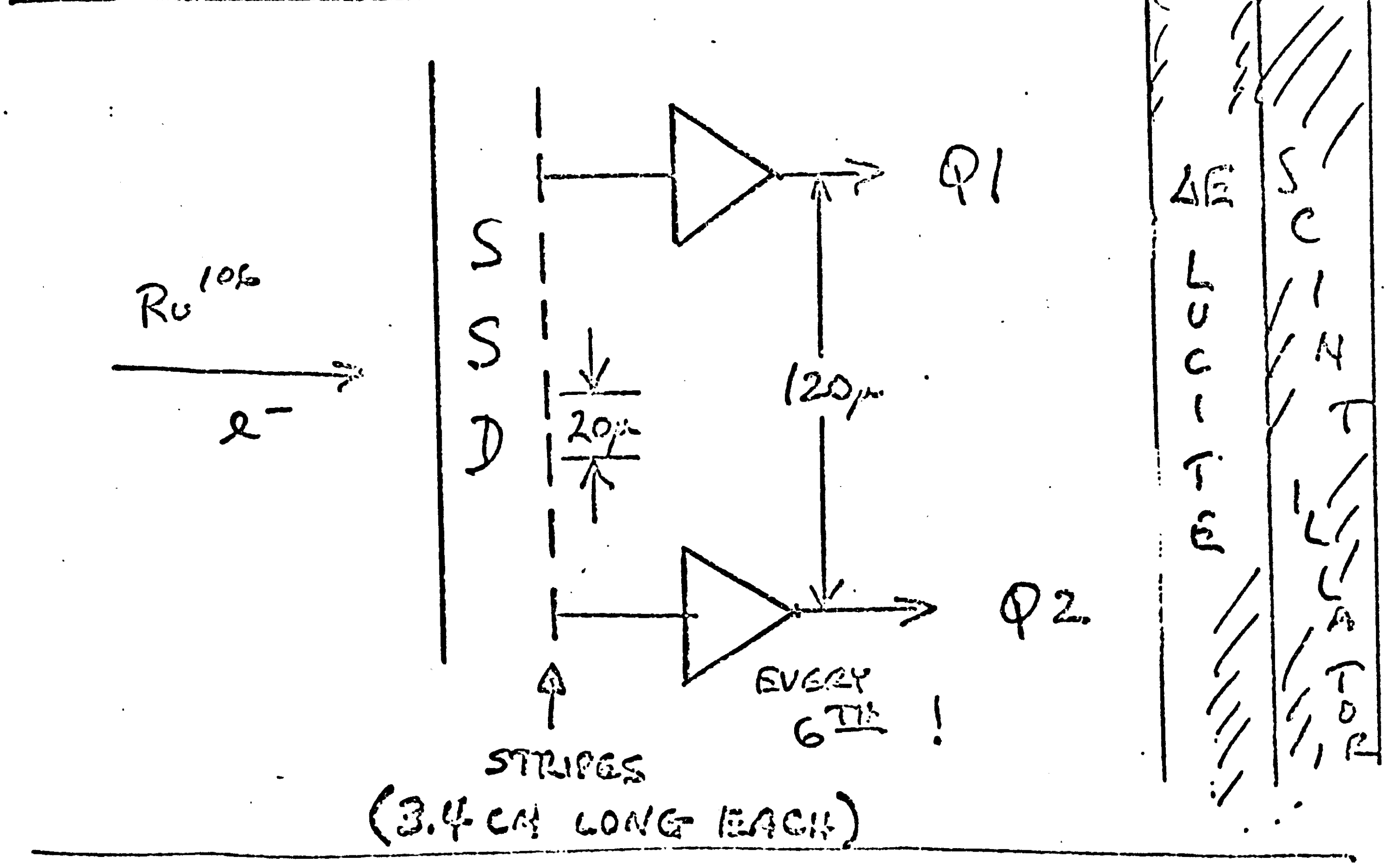

TRIGGER: $\left\{ \begin{array}{l} ① = (Q1 > T1) \cdot S \\ ② = (Q2 > T2) \cdot S \end{array} \right\} \rightarrow \text{ADC} \}$

$\Sigma_1 = ① + ②$ → TOTAL Q (SOFTWARE).

CORRELATION: $(Q1+Q2)$ VS $(Q1-Q2)$

4/29/82 [illegible]
MET

OSU - CENTRAL

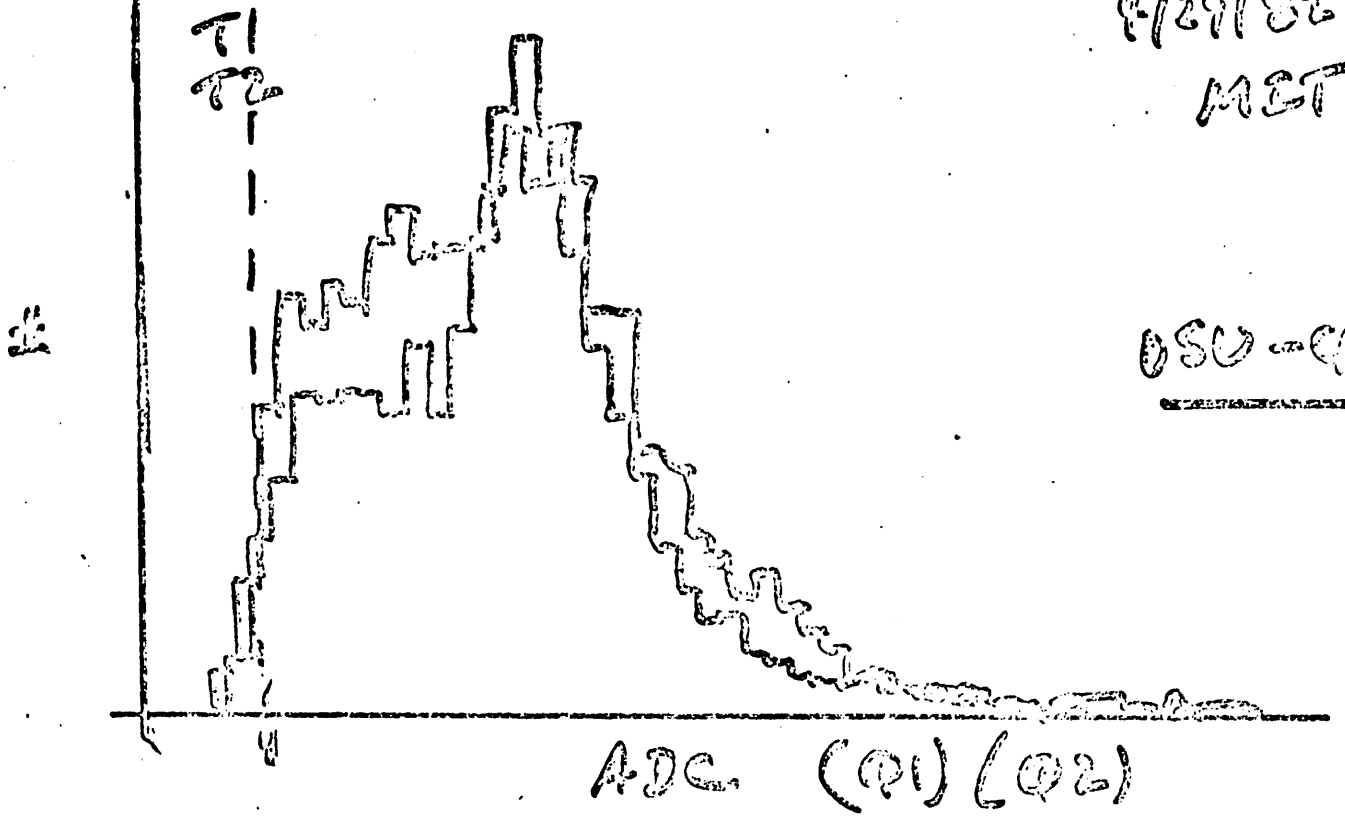

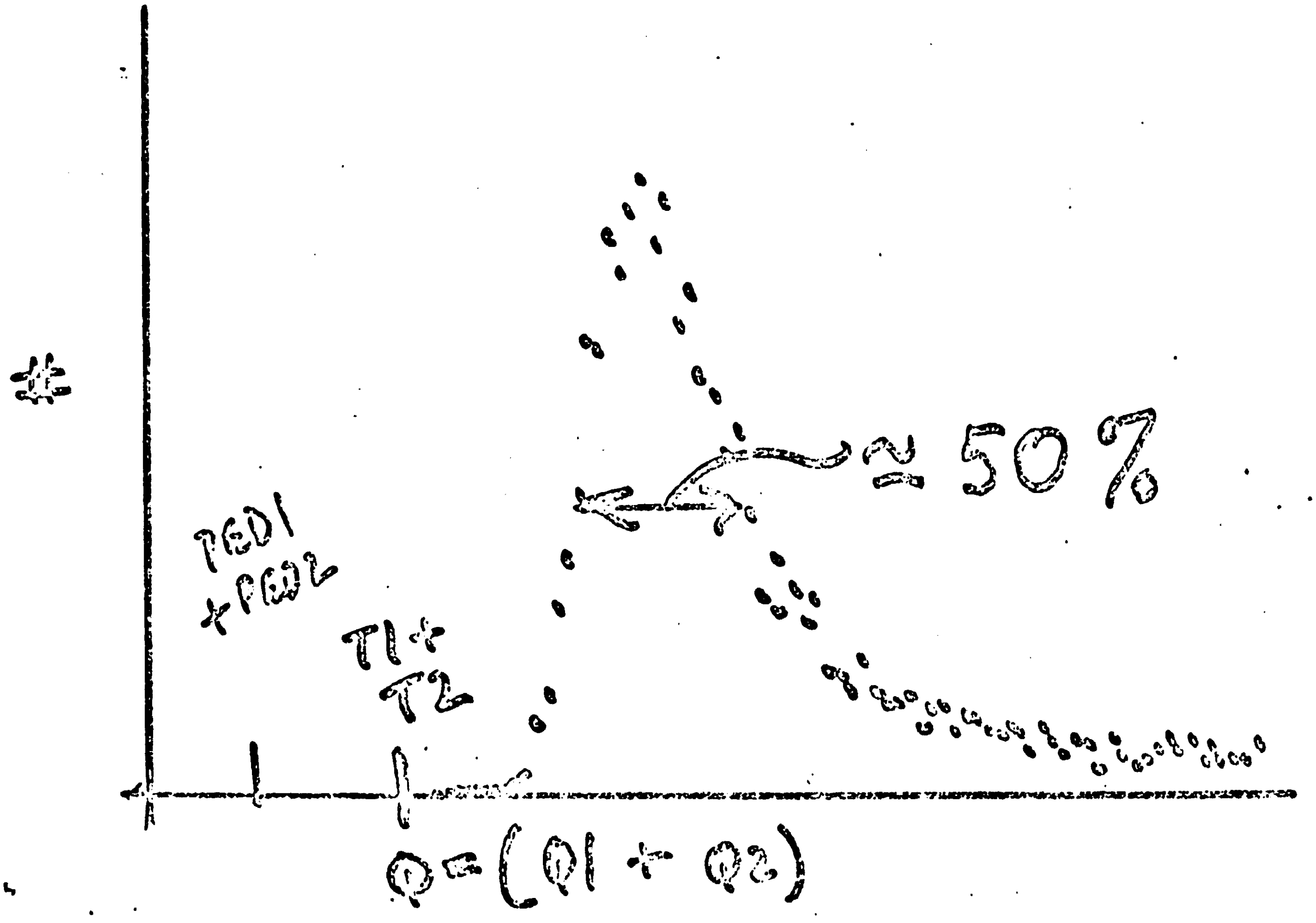

(5/5)

OSU - CENTRONI

4/29/82

GAIL

MIE

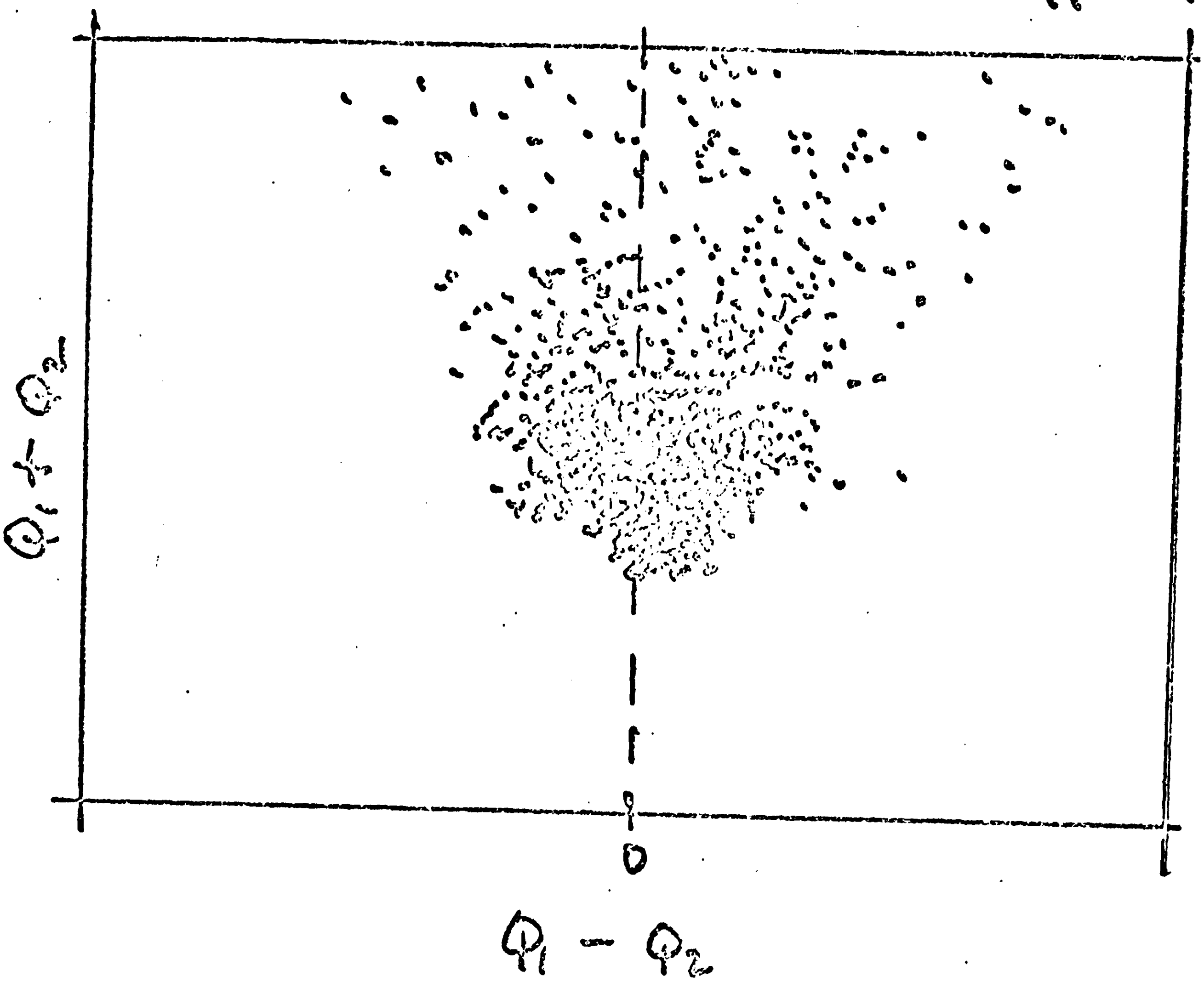

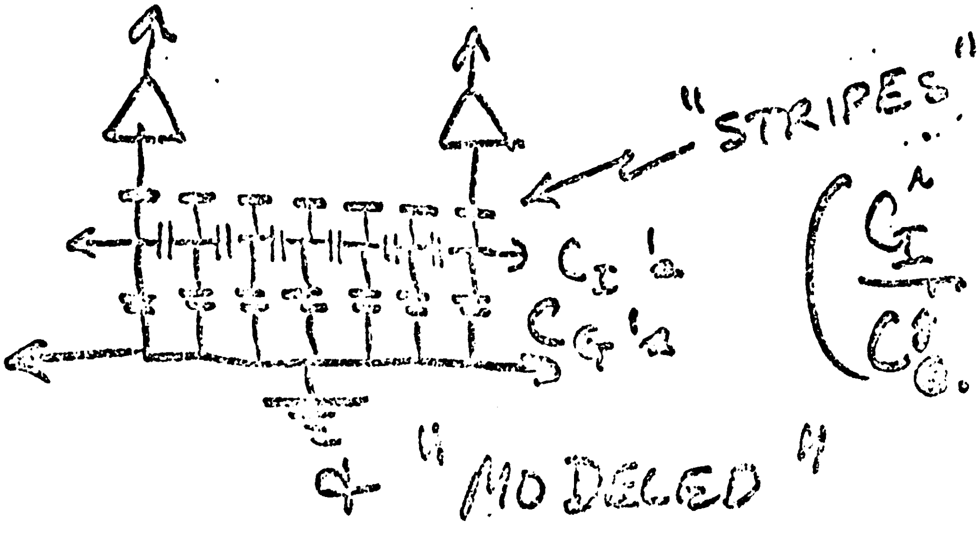

$$\left(\frac{C_I}{C_G} \approx 10\right.$$

June 10, 1982

Enclosure 1
of Appendix C

(LBL - J. Walton, R. Ely
OU-HEP - G. R. Kalbfleisch, P. Skubic, S. Willis, T. Nicol, R. Palmer, J. White,
M. Ho, D. Maher, F. Maher, K. Palmer, L. Palmer, R. Sirochman)

OU-HEP and LBL-Berkeley have continued prototype SSD testing. Eight devices were made in April 1982 at LBL. Two of these are still at LBL for bench testing, one was accidentally broken and the other five are being tested in the M5 beam at Fermilab (E653, May 15-June 14, 1982). Some preliminary results from 2000 triggers of some 50,000 taken (or to be taken) are presented here.

SSD's

These April 1982 devices are 3 cm diameter 150μ thick p-type (2 KΩ cm resistivity) silicon wafers, with 48 stripes (each 10 mm long) 20μ wide spaced on 80μ centers. Forty stripes are wire bonded to the P.C. card fanout (see Appendix I E-653 Proposal June 1981). The devices which were wired to the 160 channel amplifier setup at OU had few faults. Of 240 stripes examined two had disconnected wire bonds, and (due to crossover-fanout problems from the silicon disks at 2 x 80 = 160μ spacing at 20 mil (1000μ) standard P.C. card traces) 7 pairs were shorted together. Thus 99 percent of the stripes worked.

Amplifiers

In setting up at M5 test beam in short order in mid-May, some amplifier channels failed or were too noisy and it was not possible to fix some of them. The SSD's were arranged in five planes on four quadrants (quadrant four has two detectors (1 and 2) on it). There are 152 stripes (16, 24, 32, 40, and 40 stripes were on planes 1, 2, 3, 4, 5 respectively) of the Y-SSD's connected (with 140 working channels) and in addition 8 - 1mm pitch x-stripes on a crossed SSD. The standard deviation of the noise of the amplifiers is less than 0.2fc (femto-coulombs; i.e., <1200 electrons) with the SSD's connected and the bias voltage (greater than a few volts) turned on. The devices were run with -80 volt bias generally (the 150μ thickness fully depleted).

The Layout

An elevation view of the layout is shown in Fig. 1a. The data from the X-SSD and the East/West (E/W) counters has not been used in the analysis so far. A beam of 46 GeV/c pions from M5 triggered the data taking. The VETO counter has a 1.0 ± 0.1 mm high (by 12 mm long) hole to define the beam size incident on the ≤ 3.2 mm (by 10 mm long) active area of the SSD's and target. The target is five layers of 1.6 mm brass ([illegible]m x 3cm) spaced by 4.8 mm re[illegible]ctively as shown in Fig. 1a. A trigger was provided by F1 • S1 • $\overline{\text{VETO}}$ to gate 168 channels of LRS 2280 ADC's, readout by a CROMEMCO computer onto 5" diskettes. An event is displayed in Fig. 1b. The VETO hole, SSD's 1-5 and S1 were aligned (translationally and rotationally) with a transit. Some alignment data runs were made to check it. Some few small adjustments were made. Final adjustments will be made in the final analysis in the software.

Preliminary Data Analysis

Some 2000 events have been partially analyzed at this time. A scattergram of the hits on SSD plane 4 vs SSD plane 5 is shown in Fig. 2. The enhancement on the diagonal from stripes 13 through 27 represents the shadow of the 1.0 ± 0.1 mm high hole of the VETO on planes 4 and 5. The fifteen stripe width (13 to 27) is 15 x 0.08 = 1.2 mm. The narrowness perpendicular to the diagonal shows that the alignments (translational and rotational) of the VETO and planes 4 and 5 are all good to 1 stripe width (80μ) over their 10 (to 12) mm lengths.

A scan for (interaction) event candidates (2 or more tracks pointing to the target with at least 3 points each) was made. These tracks were fitted and a vertex found (XV and ZV); an example was shown above in Fig. 1b. Plots of XV and ZV should show the height of the hole in the veto counter and the position of the brass target pieces respectively. The resolution DXV is better than 0.02 mm. The resolution DZV depends inversely on the opening angle of the tracks as well as on how far upstream the event occurred (the average opening angles get smaller for interactions occurring farther upstream). Please remember that the maximum opening angle is very small (averaging some 25 milliradians (less than 2 degrees!)).

The distributions in XV and ZV are shown in Fig. 3a and 3b. We see the VETO hole (Fig. 3a) and the downstream brass pieces (Fig. 3b) clearly. The upstream brass pieces are not resolved yet (horizontal bars in Fig. 3b represent the average DZV at the ZV). With greater statistics in the final analysis of the total sample we can cut on the larger opening angles (smaller DZV's) and see all the brass pieces. The slopes of the edges of the XV and ZV peaks will give an experimental measure of the resolution to compare to the (theoretical) calculated values (such as those printed out in Fig. 1b). At this level of statistics such agreement appears to exist.

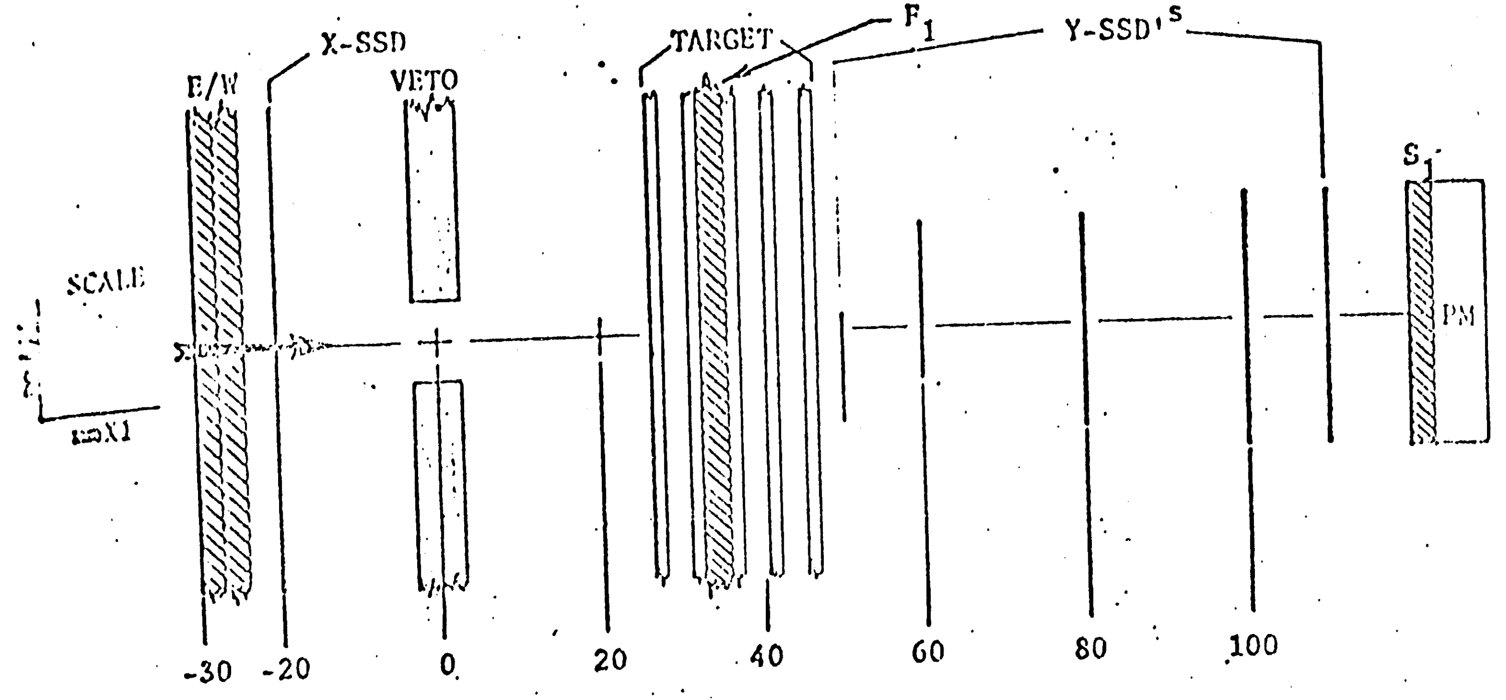

FIGURE 1A

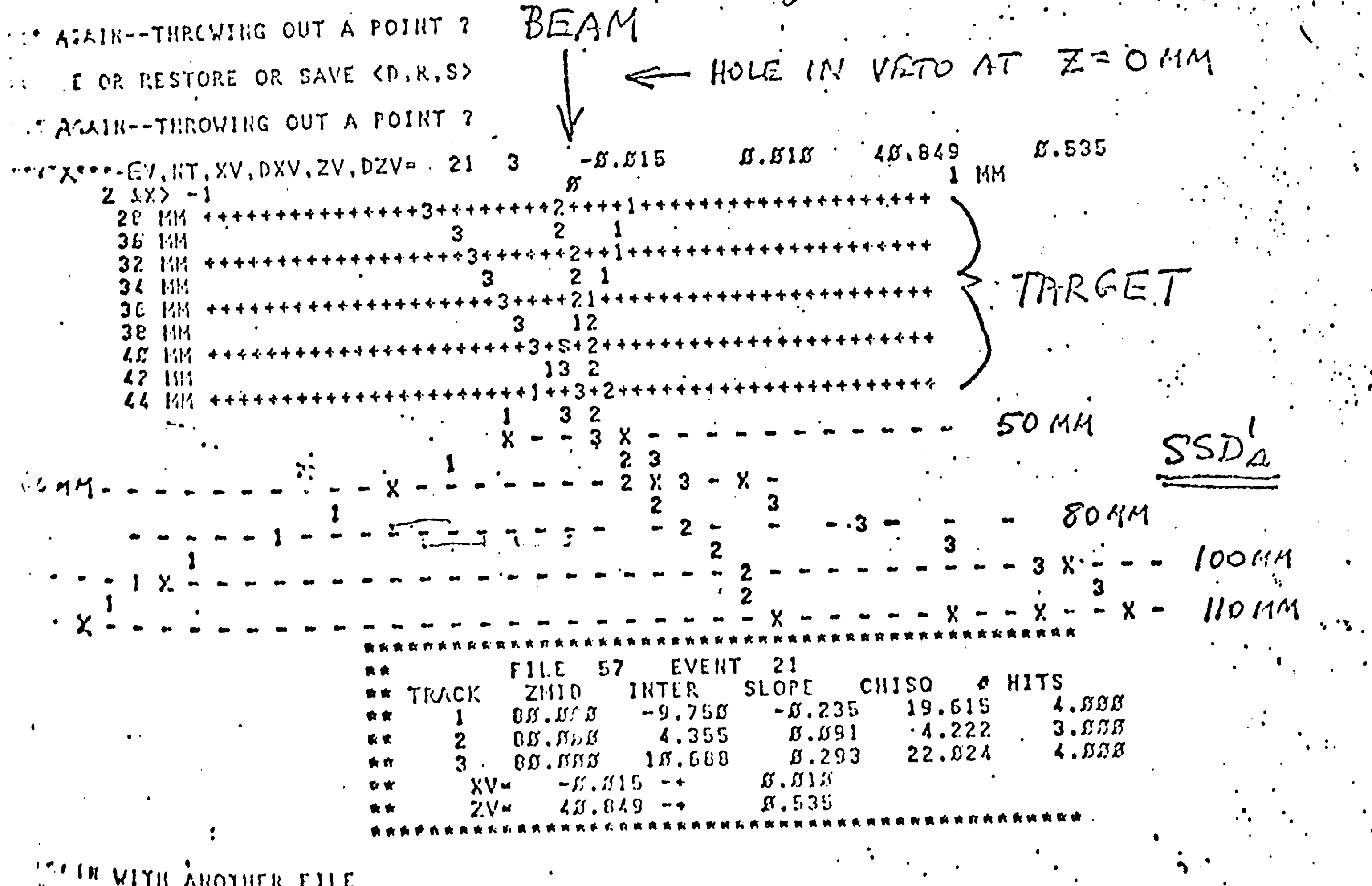

```
 AGAIN--THROWING OUT A POINT ?
 E OR RESTORE OR SAVE <D,R,S>
 AGAIN--THROWING OUT A POINT ?
 X***-EV,NT,XV,DXV,ZV,DZV=  21   3      -0.015      0.010     40.849      0.535
                                          0                              1 MM
    2 X> -1
     28 MM ++++++++++++++3++++++++2++++1++++++++++++++++++++
     30 MM                  3          2    1
     32 MM +++++++++++++++++3++++++2++1+++++++++++++++++++++
     34 MM                     3        2 1
     36 MM ++++++++++++++++++++3++++21++++++++++++++++++++++
     38 MM                        3     12
     40 MM ++++++++++++++++++++++3+S+2+++++++++++++++++++++++
     42 MM                          13 2
     44 MM ++++++++++++++++++++++1++3+2++++++++++++++++++++++
                                1   3 2
                                X - - 3 X - - - - - - - - - - - - -
                  1                       2 3
 MM- - - - - - - - - - X - - - - - - - - 2 X 3 - X -
                     1                    2       3
   - - - - - - - 1 - - - - - - - - - -   - 2 -    -    - 3 -   -   -
         1                                    2               3
 - - - 1 X - - - - - - - - - - - - - - - - - - 2 - - - - - - - - - 3 X - - -
   1                                              2                   3
 X - - - - - - - - - - - - - - - - - - - - - - - X - - - - - - X - - X - - X -
                    ***********************************************
                    **          FILE  57    EVENT  21
                    ** TRACK    ZMID    INTER    SLOPE    CHISQ    # HITS
                    **   1     80.000   -9.750   -0.235   19.615    4.000
                    **   2     80.000    4.355    0.091    4.222    3.000
                    **   3     80.000   10.680    0.293   22.024    4.000
                    **      XV=    -0.015 -+      0.010
                    **      ZV=    40.849 -+      0.535
                    ***********************************************

 IN WITH ANOTHER FILE
```

FIGURE 1B

```
AGAIN WITH ANOTHER FILE

DISKFILE?
60 + 11 + 12 + 13 + 14 + 15 + 16 + 17 + 18 + 19 + 20 + 56.
                              SCATTERGRAM
```

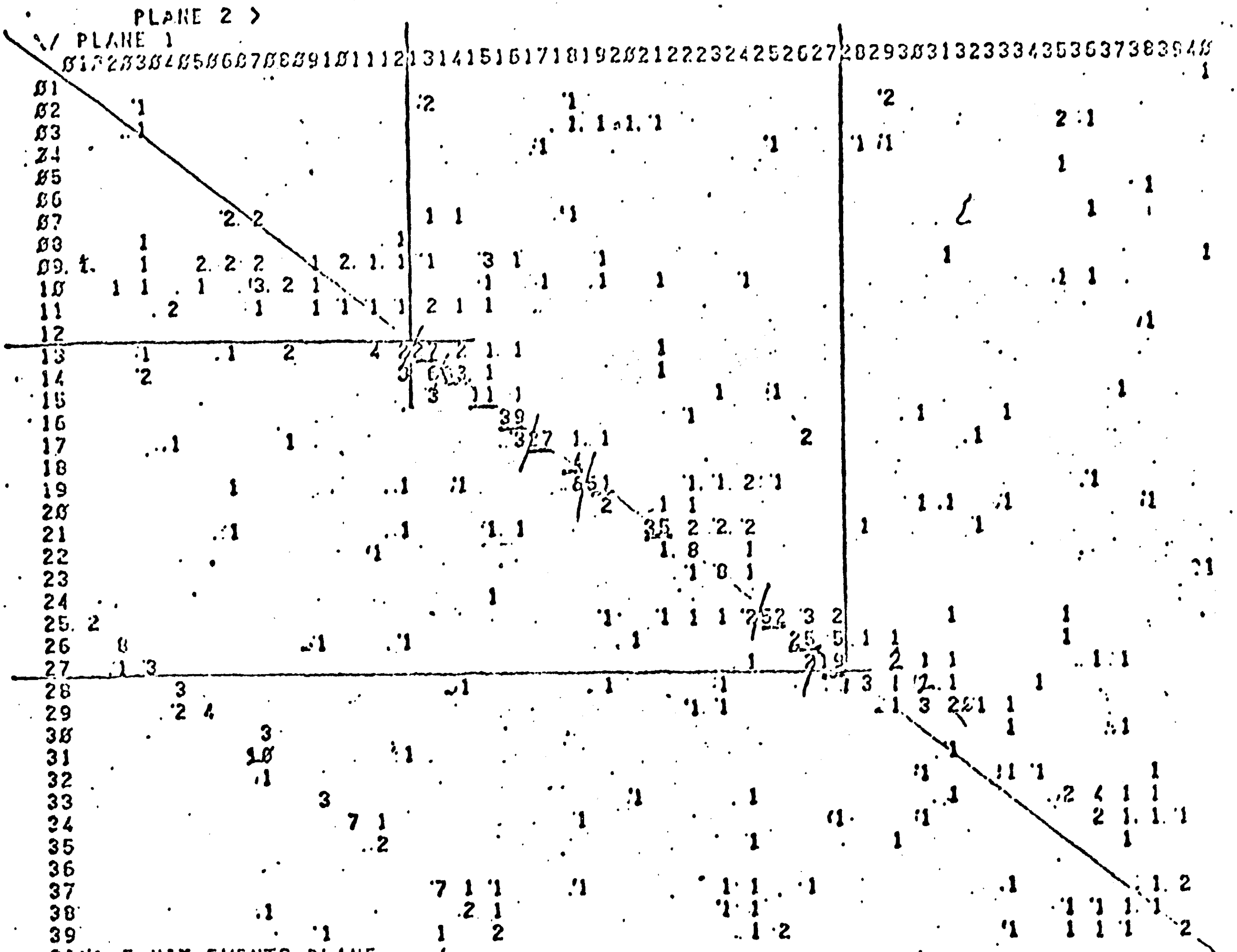

```
SINGLE HIT EVENTS-PLANE      4
     39       554      312      356      119      39      472      78     1259     1024
    :69       :39     2038     3694      822    1598     1923     436     3484     1952
   2:13       629      429      159     2933    1876     1848     546      624      675
    668       595      666      744      155      40      703     350      547        0

SINGLE HIT EVENTS-PLANE      5
     57       710      469      392      313     313      817     155      272      390
    .10       668     2190     3010     1576    3114     1691    1384     2011      167
```

FIGURE 2

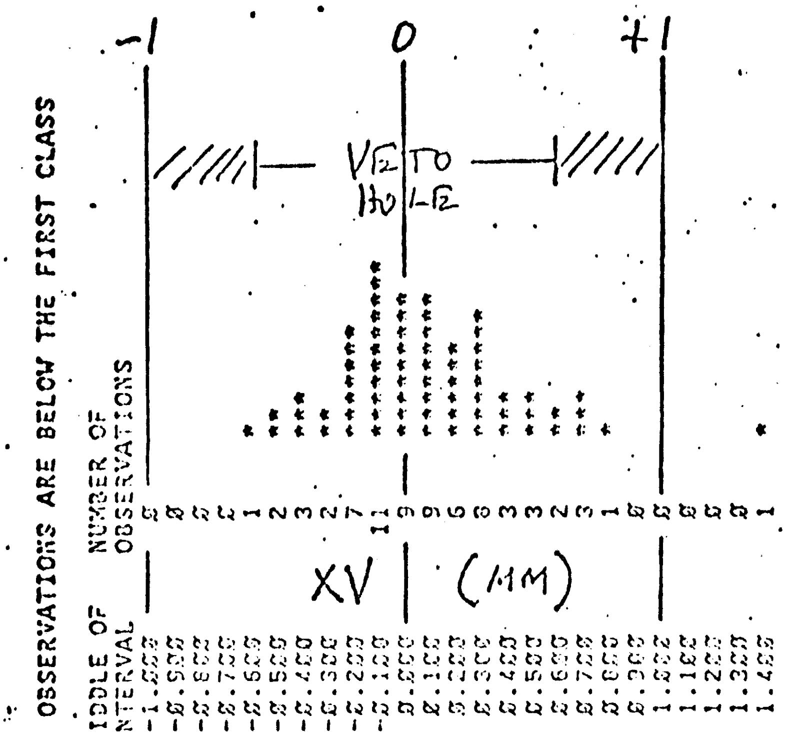

FIGURE 3a

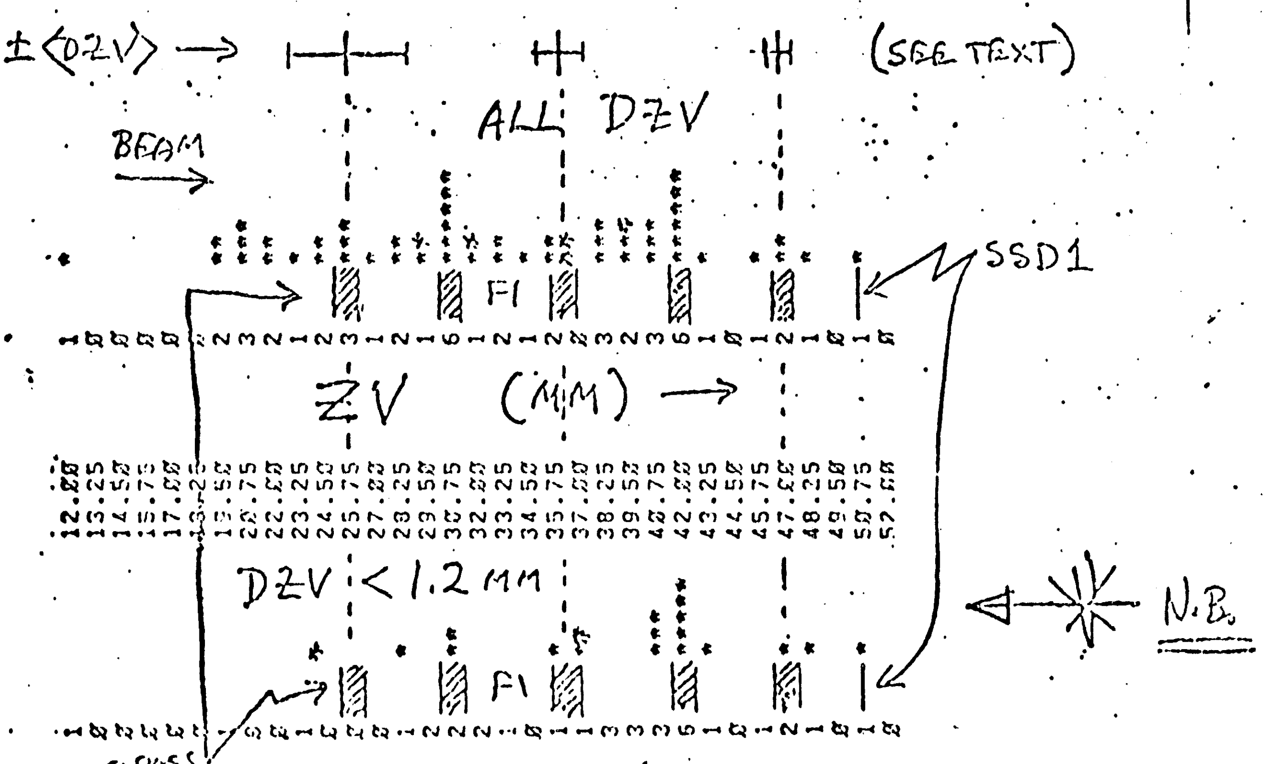

FIGURE 3b

OU-HEP MEMO #4

(GRK)

May 16, 1983

(RCV. 5/29/83).

Beam Testing of Centronic
Charge Sharing SSD's

Three 24 x 36 mm^2 Centronic detectors, 20 micron pitch (12 micron stripes and 8 micron gaps), bonded out every third stripe (alternate sides) and 300 microns thick were tested in 650 MeV/c proton and 600 MeV/c pion beams at LAMPF, Los Alamos (December 1982).

Figure 1 a. show the pulse height from one arbitrary stripe compared to the sum of pulse heights (Q1+Q2) for hit pairs. We see that charge sharing occurs. The Q12 signal is incomplete (80 percent) and somewhat wider than expected (10-20 percent). Figure 1 b. shows the collected charge from Q12 +Q03 neighbors (the stripes adjacent immediately either side) compared to the expected distribution (Landau including noise and beam momentum spread). The Q0123 pulse height is 25 percent greater than Q12 alone, and the Q0123 pulse shape and width agree with theory.

Three point proton and pion tracks (the three detectors were spaced 7 and 7 mm apart respectively) are being studied. The deviation of the position coordinate of the middle plane from a line joining the hits on the outer planes has a distribution with a standard deviation (sigma) of 18 microns for protons, and 14 microns for pion tracks. This compares with an expected sigma of:

$$\sigma(\text{proton}) = (1.5\,\sigma_m^2 + \sigma_{MS}^2 + \sigma_A^2 + \sigma_{CS}^2)^{1/2} =$$

$$= (1.5\times 6^2 + 10^2 + 4^2 + 5^2)^{1/2} = 14 \text{ microns},$$

and $\sigma(\text{pion}) = (1.5\times 6^2 + 5^2 + 4^2 + 5^2)^{1/2} = 11$ microns,

where σ_m = measurement sigma, σ_{MS} = multiple scattering sigma, σ_A = alignment error and σ_{CS} = error from the simple charge sharing algorithm. Or, "unfolding", we find "σ_m" less than or equal to 11 (9) microns for protons (pions) respectively. We note that the hit efficiency is better than 98 percent.

We see from the charge collection and track deviations that charge sharing occurs, although we have not yet achieved the theoretical optimum spatial resolution.

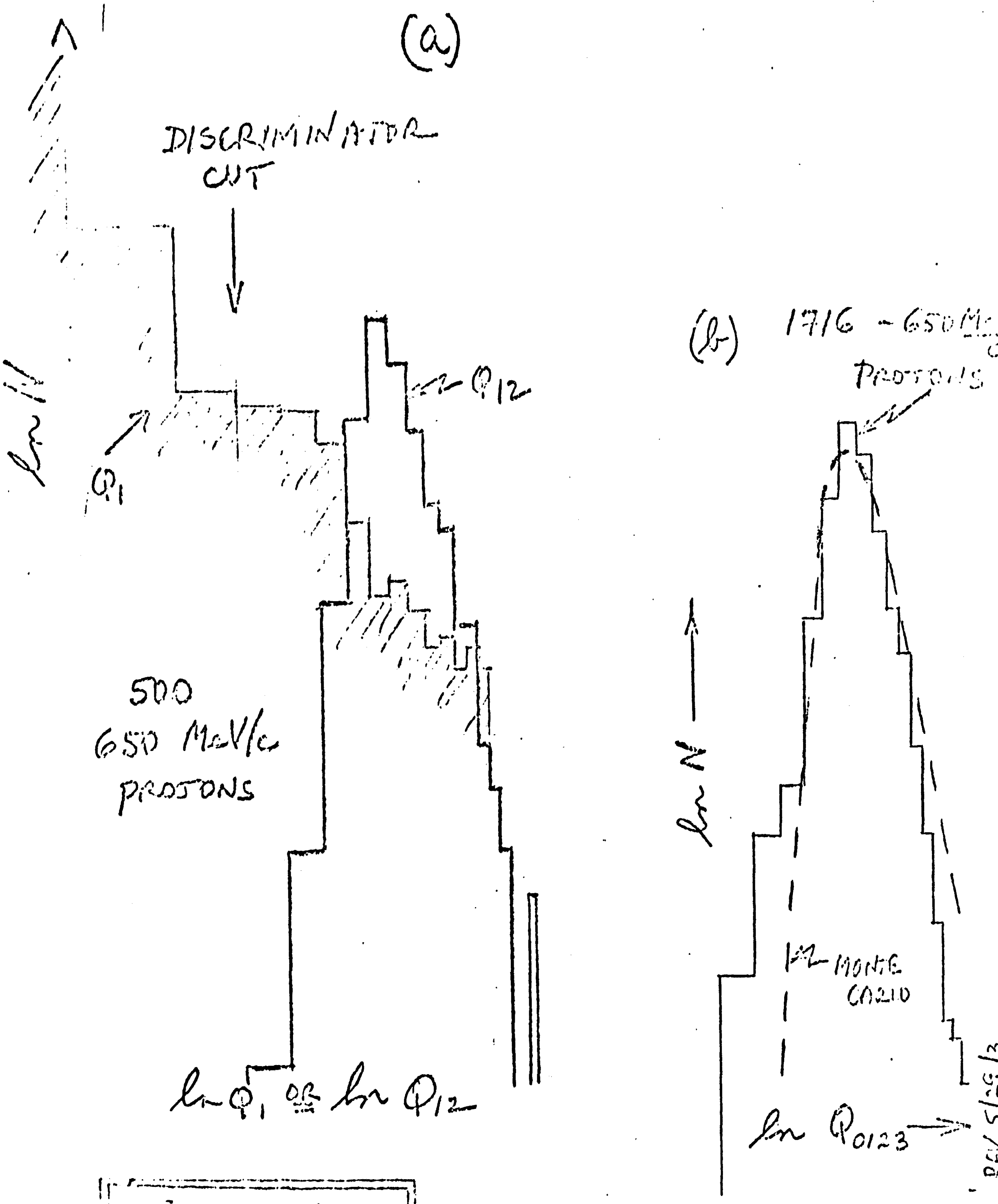

FIGURE 1

NUMBER VS. CHARGE Q VIA CHARGE DIVISION READOUT (GENTRONIC DETECTORS)

Further Results on the LBL SSD's

A set of five LBL 1cm long x 48 stripes at 80 micon pitch, with every stripe readout and 150 microns thick were tested at 46 GeV/c at Fermilab and with 650 MeV/c protons and 550 MeV/c pions at LAMPF during summer 1982. Most of these results were presented at L. Ledermans 10-25-82 E-653 Director's Review.

The track point accuracy (via chi-square distributions) was shown to obey the (pitch/$(12)^{1/2}$) standard deviation within ten percent. The charge collection was shown, see Figure 2 , to match the theoretical Landau+noise+momentum spread expectation, when the 10-20 percent collected by the neighbors was added in (ie Q012 shown is bigger and narrower than the Q1 distribution alone). The VERTEX RECONSTRUCTION was discussed, but it was not documented in detail.

46 GeV/c pions interacting in five copper sheets 1.7 mm thick spaced 5.0 mm apart and starting 5 mm from the most upstream SSD were recorded. These events were scanned for on an online VAX display and interactively fitted to stright line tracks. The largest opening angles subtended by the array (3 mm at a distance of 6.5 cm) is 50 milliradians (about 3 degrees). The X and Z of the vertex were calculated by the intersection of the 2,3 and 4 tracks of each event. A crude propagation of errors gave DX and DZ also. A Monte Carlo of the five copper target pieces and the DZ distributions gives the predicted Z vertex distribution. The experimental distribution of the 194 events having DZ less than 1.2 mm (as calculated) are compared to the Monte Carlo[a] in Figure 3 . The agreement is satisfactory. Thus, as concluded at Leon's Review, vertex reconstruction as claimed in our proposal can be done.

---

a) The errors DZ have been increased in the Monte Carlo by a factor of 1.25.

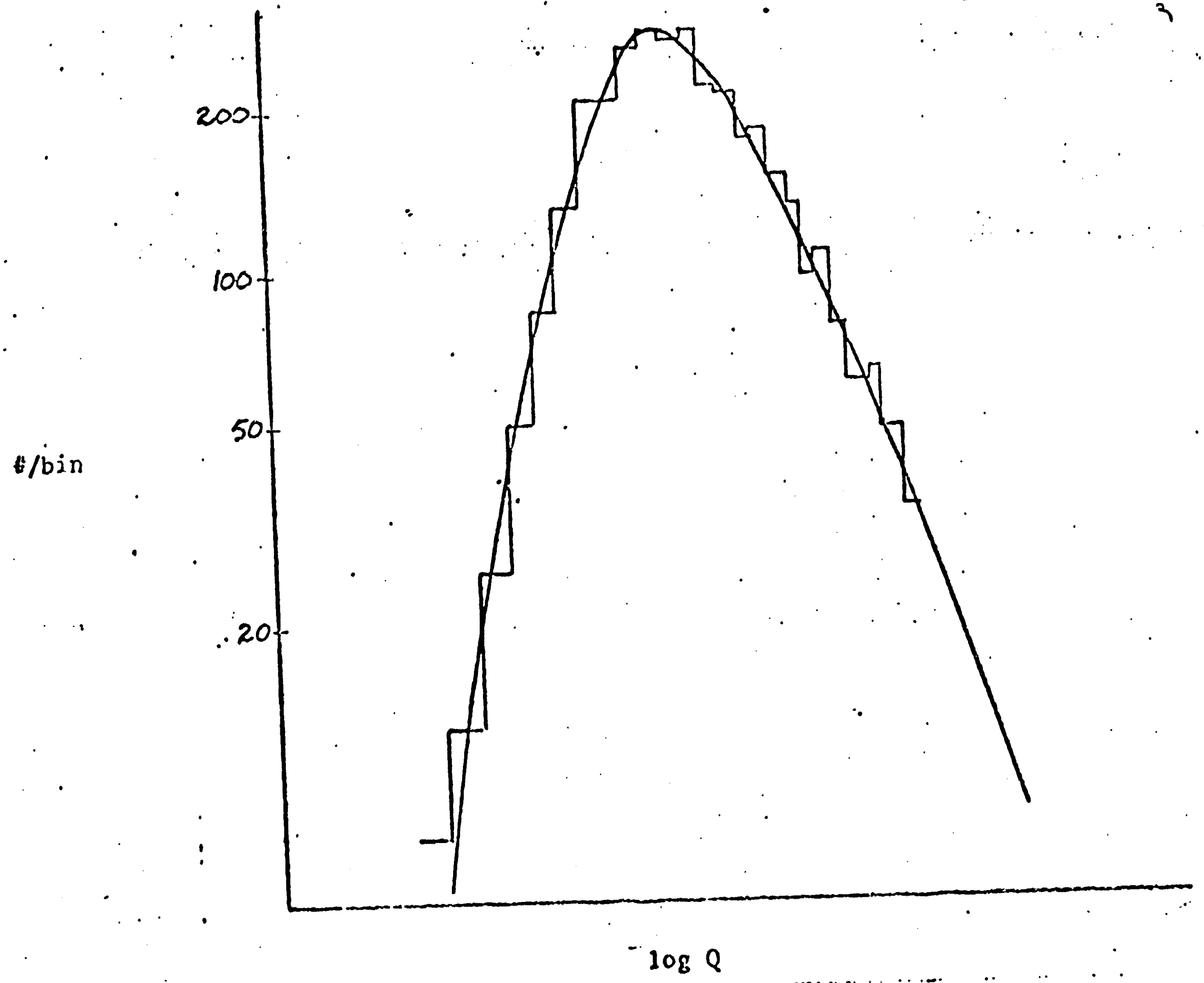

Figure 2

Charge Distribution (Q012)

3905 Tracks, 650 MeV/c Protons

(LBL - EVERY LINE READOUT).

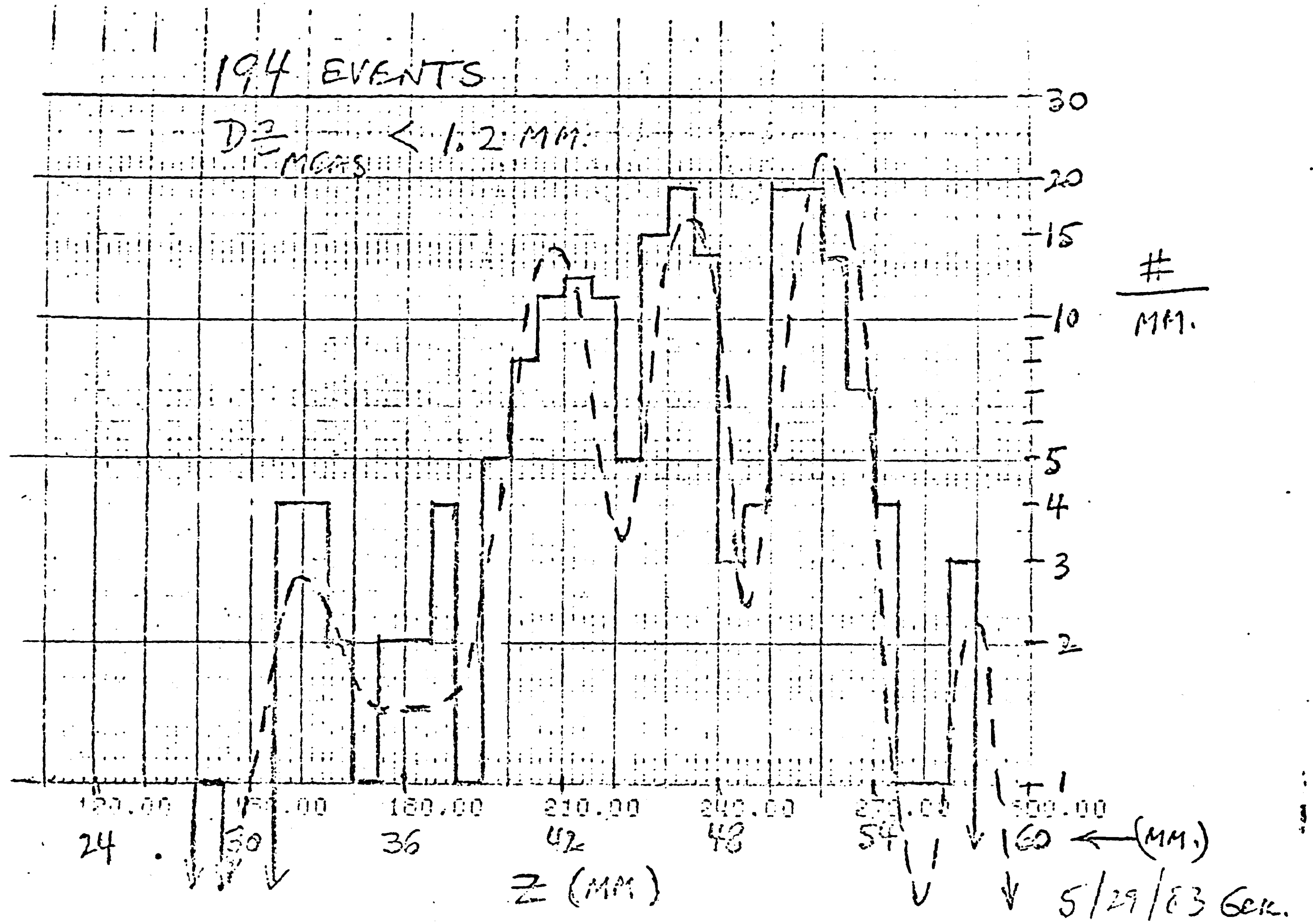

FIG. 3 – "LBL" VERTICES

OU-HEP MEMO #10

TIME-OF-FLIGHT SCINTILLATOR TESTS

S. Willis and S. Wold

9/16/83

TIME-OF-FLIGHT SCINTILLATOR TESTS

Tests of attenuation lengths and light output were made on three types of scintillator being considered for use in the E653 time-of-flight system.

1.	NE102A	2" x 2" x 67"
2.	PS12	1.75" x 2.375" x 35"
3.	PS10	1" x 4" x 35"

The attenuation length measurement setup consisted of the scintillator being tested, with a phototube on each end (56AVP), and a trigger counter, 8" x 3", also with a phototube on each end. The two trigger tubes were put in coincidence, and the trigger counter placed crosswise on the scintillator at various distances from the ends. Because much of the trigger counter did not overlap the scintillator, the pulse height distribution was quite wide, although it was adequate for the purpose.

The pulse height was measured at five points along each scintillator, and the signals at both ends were analyzed. The attenuation lengths here are the averages of those found from each end.

1.	NE102A	138 cm
2.	PS12	68 cm
3.	PS10	157 cm

From these results, the PS10 scintillator appears to be slightly better than the NE102A. However, all three pieces were received from the manufacturers with two sides cast and two rough; the rough sides were polished by the shop, but the results were not very good. The PS10 piece has the 4" sides cast, so a smaller fraction of light is lost in relections along the length than in the NE102A. Since the NE102A looks similar to the PS10, it is probably somewhat better. (This agrees with the manufacturers' data). Attempts to repolish the NE102A were not particularly successful.

The light output measurements were made with an improved trigger setup and a different phototube, Amperex XP2230, on the tested scintillator. This measurement was only performed on the NE102A. The trigger consisted of two small scintillators, one above and one below, the tested scintillator. These two were put in coincidence, and were arranged so that particles had to traverse the entire thickness of the scintillator. This gave a very nice Landau distribution of pulse heights. Then the end of the scintillator was covered, leaving a small hole. Few enough photons came through this hole that the number of photoelectrons could be measured by the width of the peak. The results are as follows:

Hole	FWHM/peak	N(PE)	N(PE)/mm^2
4 x 4 mm	0.87	6.7	0.42
5 x 6 mm	0.61	13.4	0.45

Averaging these two and extrapolating to the full 50 x 50 mm area of the end of the scintillator gives 1100 photoelectrons. The number which go into the 2" round phototube is 850. The pieces for E653 will be 1.5" instead of 2"; the number of photoelectrons arriving at the phototube in that case is 650.

The attenuation length of this scintillator was remeasured using this trigger; the result was 147 cm, in agreement with the previous measurement.

OU-HEP MEMO #12

OU Analysis of Centronics Charge Sharing SSD's

By

G. R. Kalbfleisch and L. Palmer

Fall 1983

OU Analysis of Centronics Charge Sharing SSD's

by

Dr. G.R. Kalbfleisch and L. Palmer
Sept. 16, 1983
revised Oct. 3, 1983

Data Analysis of three 24mm x 36mm x 300 micron Centronic detectors, 20 micron pitch (12 micron stripes and 8 micron gaps), bonded out every third stripe (alternate sides) which were tested in 650 MeV/c proton and 600 MeV/c pion beams at Lampf, Los Alamos (December 1982) has concluded at OU. Areas of interest in this Analysis include: checking of pulse heights of single stripes, hit pairs and hit quads vs theoretical values; resolution of three point proton/pion tracks; and characterization of Centronic devices by charge sum/difference plots of hit pairs.

Charge Collection on Centronic Detectors

Plots 1 and 2 show the pulse height for the sum of pulse heights (Q1 + Q2) for proton and pion hit pairs (a 10 sigma cut imposed on proton pairs and a 5 sigma cut imposed on pion pairs) with no pair/quad having a dead neighbor. The pair and quad plots were generated from all proton and pion data at appropriate sigma cuts. Plots 3-6 show a breakdown of pulse heights for proton and pion hit pairs "Inside" and "outside" describe the position of a particle with respect to the instrumented vs non-instrumented stripes ("inside" is between or near two non-instrumented stripes while "outside" is near an instrumented stripe). Notice that "inside" plus "outside" add to give the hit pair plots (shown in plots 7 and 8). Plots 9 and 10 show the collected charge from Q12 + Q03 neighbors forming proton and pion hit quads for all proton and pion runs. The Q12 signal for protons is nearly complete (same height as Q0123) but somewhat wider than Q0123 signal. The Q12 signal for pions is slightly incomplete and also somewhat wider than Q0123. Q0123 pulse height for protons and pions are plotted with theory plots with pulse heights dashed and with theory shown as solid lines on plots 11 and 12 (theory curves are of 650 MeV/c protons and 600 MeV/c pions with .19 fc noise folded in). Included with the pion plot are the theory curves with larger noise values folded in (.30 fc and .38 fc as shown). Notice that the quad plots agree fairly well with the theory plots but are slightly wider than theory predicts (especially in the pion case).

Characterization of Centronic Devices

Plots 13 (proton) and 14 (pion) are scatterplots of Centronics detector #1 (#2 is similar while #3 if nearly dead) for Q1 + Q2 vs Q1 − Q2 with no charge sharing algorithm correction (x=1, where x is the value multiplied by the member of a hit pair with the least charge). These plots show the sum of the gain corrected charge of adjacent (neighboring) stripes which pass a sigma cut plotted against the difference in charge for the pair. Charge sharing for protons occurs but only about 30 percent of the time (i.e. 30 percent of observed pairs had a neighbor with greater than 10 percent of the collected charge). Pions show charge sharing only about 35 percent of the time (i.e. 35 percent of observed pairs had a neighbor with greater than 10 percent of the collected charge). Notice that other charge sharing algorithm correction values have the effect "smearing out" the scatterplot (see plots 15-17 for protons and 18-20 for pions) and result in charge sharing percentages as follow:

proton x=sqrt(2) => 32 %
x=2 => 42 %
x=4 => 53 %

pion x=sqrt(2) => 44 %
x=2 => 53 %
x=4 => 68 %

Large values of x (2 and 4) are unphysical and inconsistent with charge collection ratios which are close to theory without the correction. Plots 21-24 show mean(Q1 - Q2/Q1 + Q2) vs sigma(Q1 - Q2/Q1 + Q2) for protons and pions at various correction values for the charge sharing algorithm. These plots show on average that most channels behave the same way (i.e. those clustering around a mean value of zero give uniform (Q1 - Q2/Q1 + Q2) values over the range of -1 to 1 as indicated by the sigma shown). Those means outside of the cluster are weak or neighbors of dead channels as they appear as always "on" (high mean values) or always "off" (negative mean values).

Since the method described above cannot be explained physically other tests were made on the data and cuts involving the position of Q1-Q2 vs Q1+Q2 as well as the sigma of (Q1-Q2/Q1+Q2) were made. Plot 25 shows Q1-Q2 vs Q1+Q2 as a scatterplot with points above 2500 and points below 1200 on the Q1+Q2 axis removed. This had little or noeffect on the "horns" of the histogram of Q1-Q2/Q1+Q2 as shown. Plots 26 and 27 show plots of Q1-Q2 vs Q1+Q2 for values of Q1 and Q2 with the sigma of (Q1-Q2/Q1+Q2) greater than 0.55 (determined from plot 21). Notice that these plots are better than the $x=1$ plots (plots 13,14) for both protons and pions insofar as charge sharing occurs to a greater extent (45 percent for protons compared to $x=1$ case of 30 percent for protons). Notice also that the sigma cut plots are for centronics #2 since when the cut was imposed both centronics #1 and centronics #3 displayed few or no channels which passed the cut. This is not surprising for centronics #3 since it has few good channels but is rather unexpected for centronics #1 since it has nearly as many "good" channels as centronics #2.

Proton and Pion "Window" analysis

Plots 28-30 and diagrams 1 and 2 describe the three centronic detectors over a region of non-dead channels (the non-dead "window"). This window was found by removing individual channels which did not have a statistically good charge pulse shape or which were dead completely. Diagrams 1 and 2 show typical proton and pion 3 point track displays (upper is a coarse display while lower is a blowup of the event). The blowups show charge sharing occurring on centronics #1 and #3 while no charge sharing occurs on plane #2 (for both protons and pions - coincidental). Charge pair sum vs

charge pair difference plots are shown for all "window" protons (plot 28) and pions (plot 29) and it can be seen that charge sharing occurs in this region approximately 5 percent more often than in general (35 percent for protons and 40 percent for pions with no charge sharing algorithm correction factor). Plots 30 a and b show mean (Q1-Q2/Q1+Q2) values verses sigma(Q1-Q2/Q1+Q2) for protons and pions in the "window" Notice that this small "window" still has some weal channels.

Resolution of Centronic Detectors

The "window" region needs to be used for the determination of the resolution of the Centronic detectors (since a region of good channels over all three detectors is necessary). Three point proton and pion tracks (detectors were spaced 7 and 7mm apart respectively) have been studied in this "window". Plots 31a and 32a show the deviation of the position of a hit pair on centronics 2 from hit pairs on centronics 1 and 3 verses the number of the active scintillator for the 3 point track. The general slope of the plots can be attributed to the orientation of the 8 scintillators. The deviation of the position coordinate of the middle plane from a line joining the hits on the outer planes then has a distribution with standard deviation (sigma) of 15.3 microns for proton tracks, and 14.9 microns for pion tracks. This compares with an expected sigma of:

$$\sigma(\text{proton}) = (1.5* \sigma_m^2 + \sigma_{ms}^2 + \sigma_a^2 + \sigma_{cs}^2)^{1/2} =$$

$$= (1.5* 6^2 + 10^2 + 4^2 + 5^2)^{1/2} = 14 \text{ microns}$$

and $$\sigma(\text{pion}) = (1.5* 6^2 + 5^2 + 4^2 + 5^2)^{1/2} = 11 \text{ microns}$$

where σ_m = measurement sigma, σ_{ms} = multiple scattering sigma, σ_a = alignment error and σ_{cs} = error from the simple charge sharing algorithm.

Or "unfolding", we find "σ_m" less than or equal to 5 (10) microns for protons (pions) respectively. We note the hit efficiency is better than 98 percent. Thus the resolution of 3 point proton tracks is slightly better than theory, while 3 point pion track resolution is slightly worse. In both cases the use of a "correction factor" in the charge sharing algorithm had no positive effect (see plot 31b for correction of x=2 for protons and plot 32b for x=sqrt(2) for pions (x is described in the Characterization section)).

Data Analysis Program

Diagram 3 shows a flow control diagram of the data analysis program used at OU. The initialization portion of the program sets runtime parameters, defines a reorganization map, reads a pedestal file, and reads a gain file. The main loop reads an event, reorganizes the raw data, calls the statistics package (if desired), and enters the hit analysis subroutine. The hit analysis subroutines checks each active stripe and decides if any pair or quad hits are present and further if these pairs or quads form a 3 point track after charge sharing has been determined. Results of the run are displayed as the main loop exits by subsequent calls to the statistics and histogram packages. The program is written entirely in fortran and program listings are available under separate cover.

#1

P PAIRS [261+262+271+272]

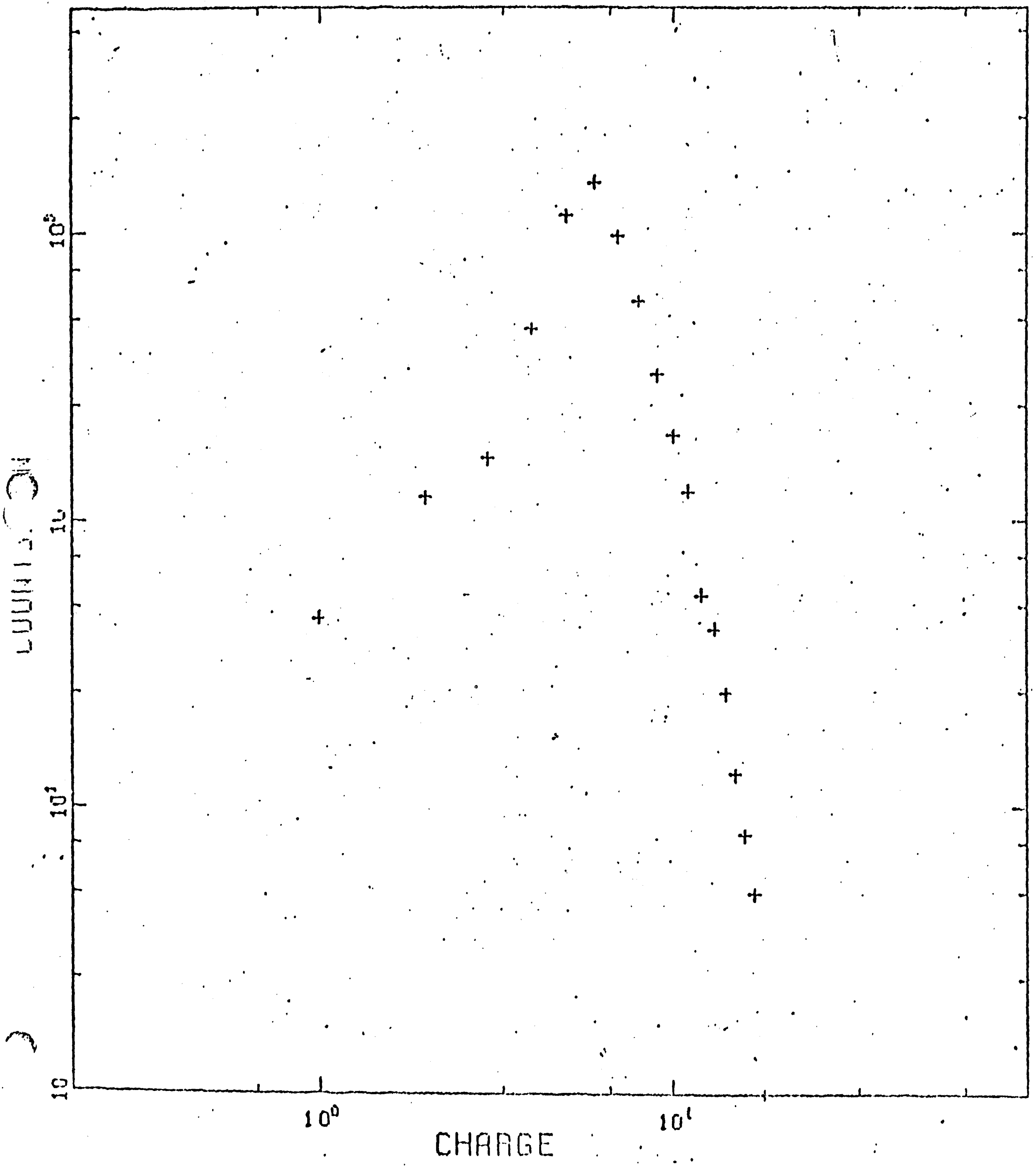

#2

Log - log Plot of

π PAIRS [261+262+271+272]

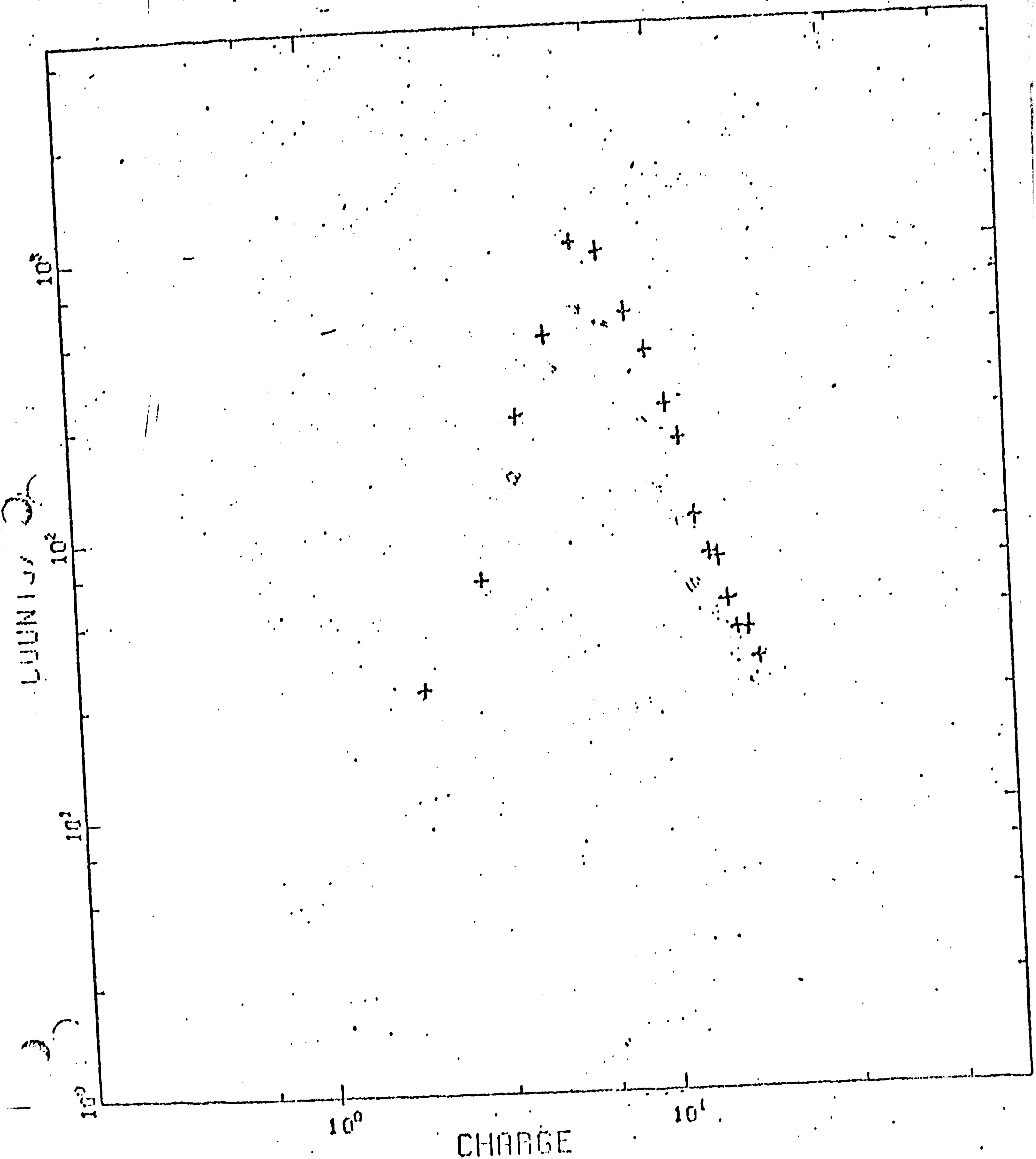

#13

Log - log Plot of

10SIGMA P [261+262] INSIDE*

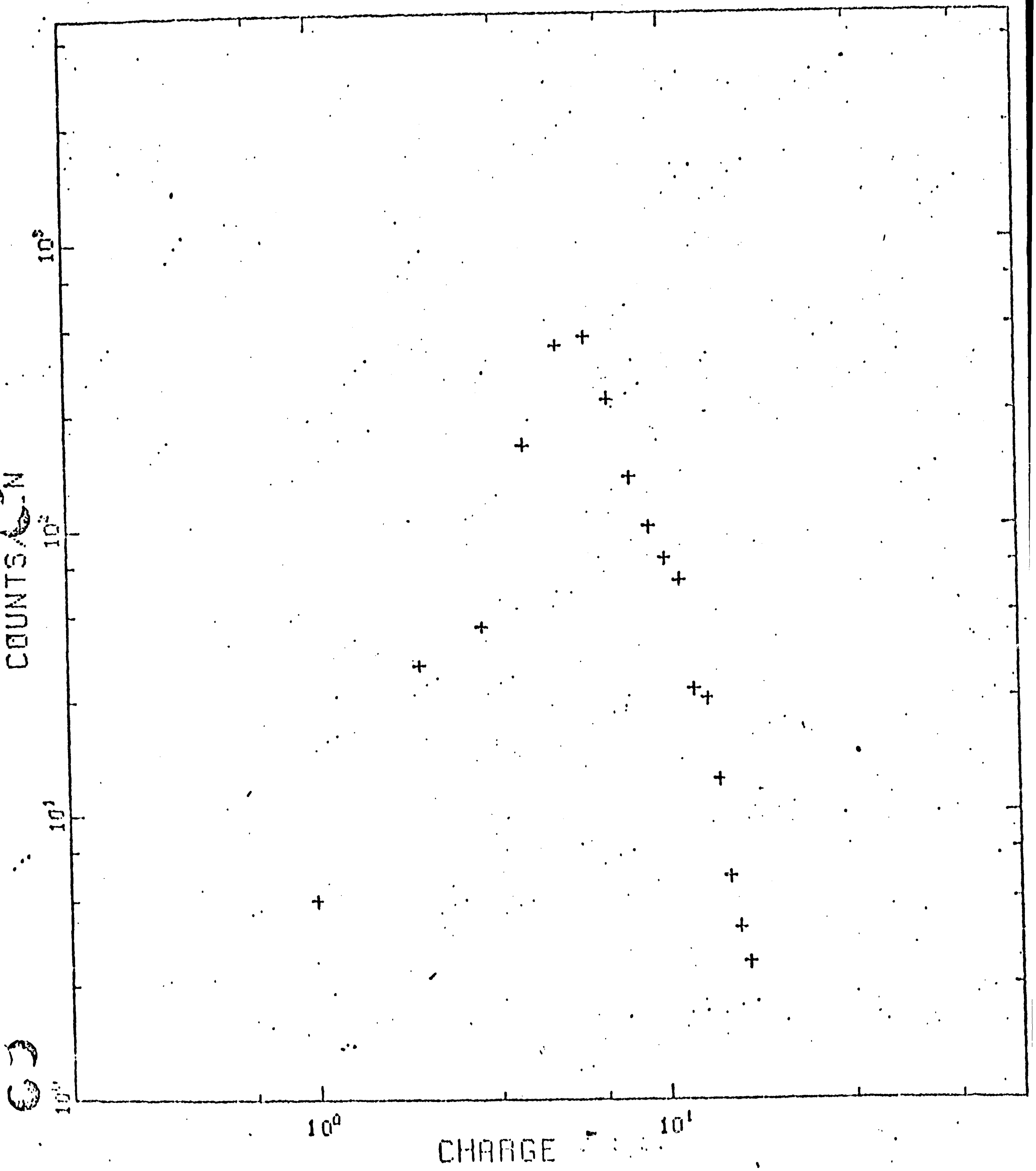

* [illegible]

#4

Log - log Plot of

10SIGMA P [271+272] OUTSIDE *

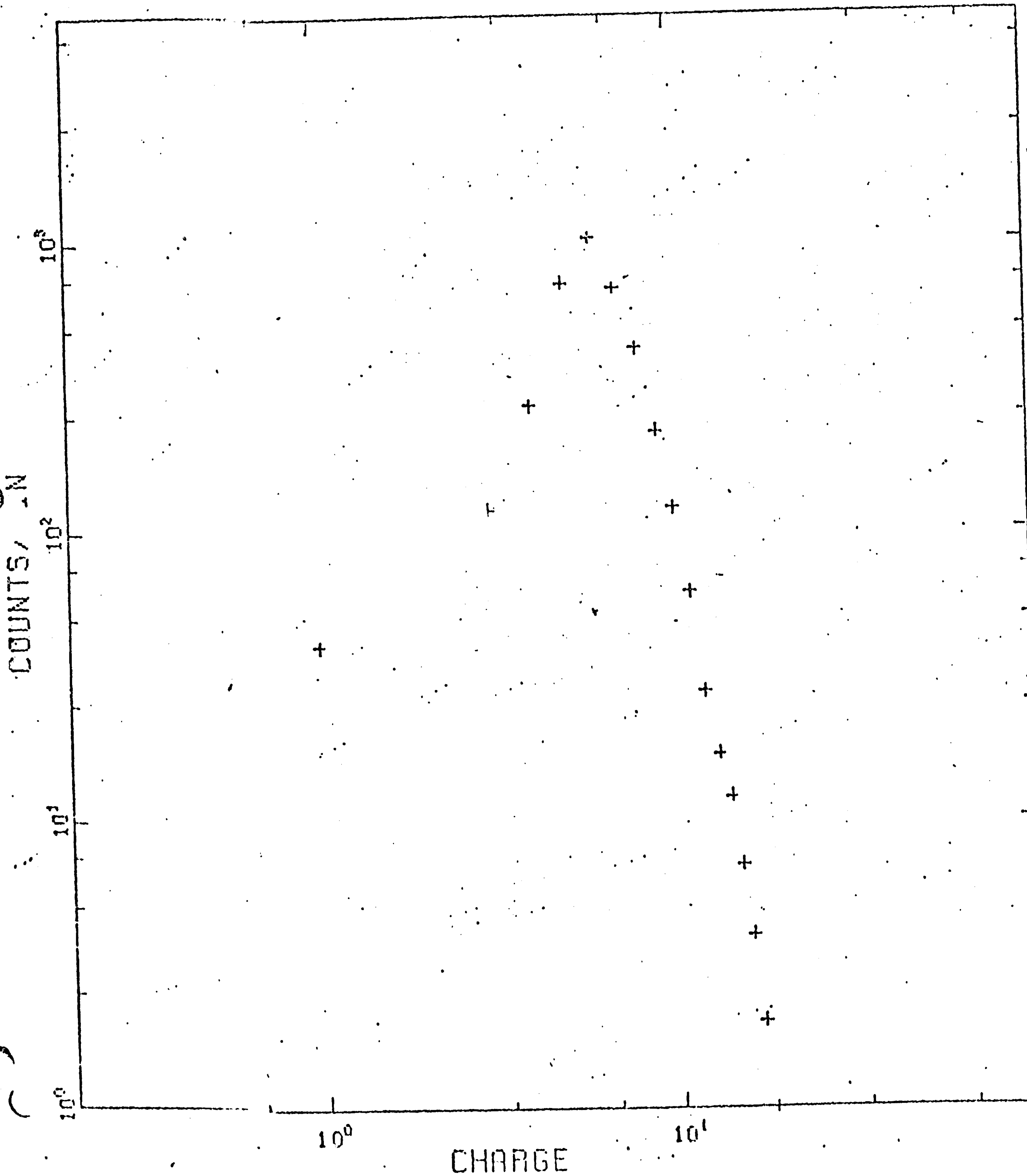

#5

Log-log Plot of
5 SIGMA π [261+262] INSIDE*

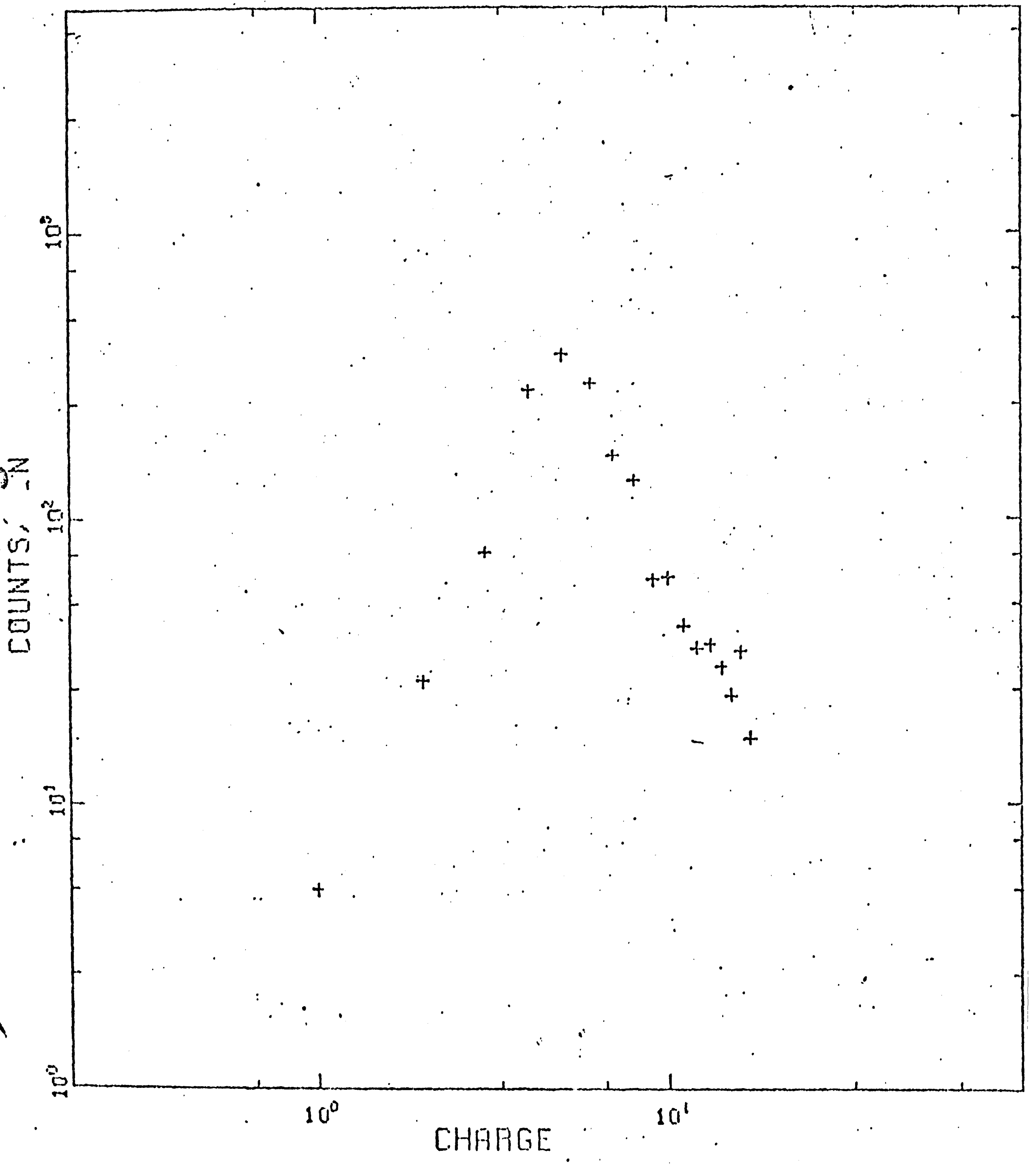

Log-log Plot of

5 SIGMA π [271+272] OUTSIDE*

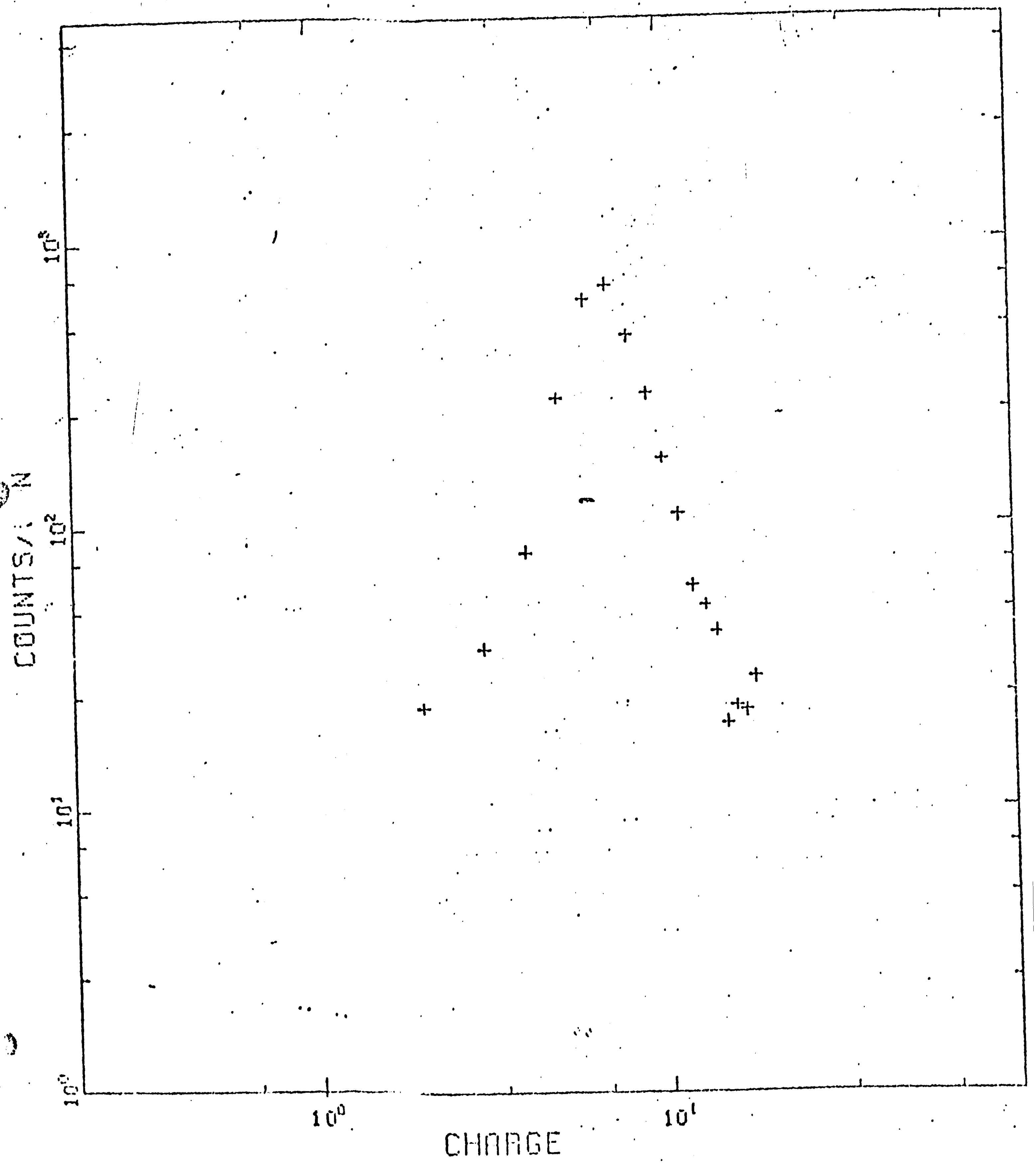

* [illegible]

#F1

Log-log Plot of 10 Sigma Proton Pairs

⊞ - Total
⊕ - outsid
+ - insid

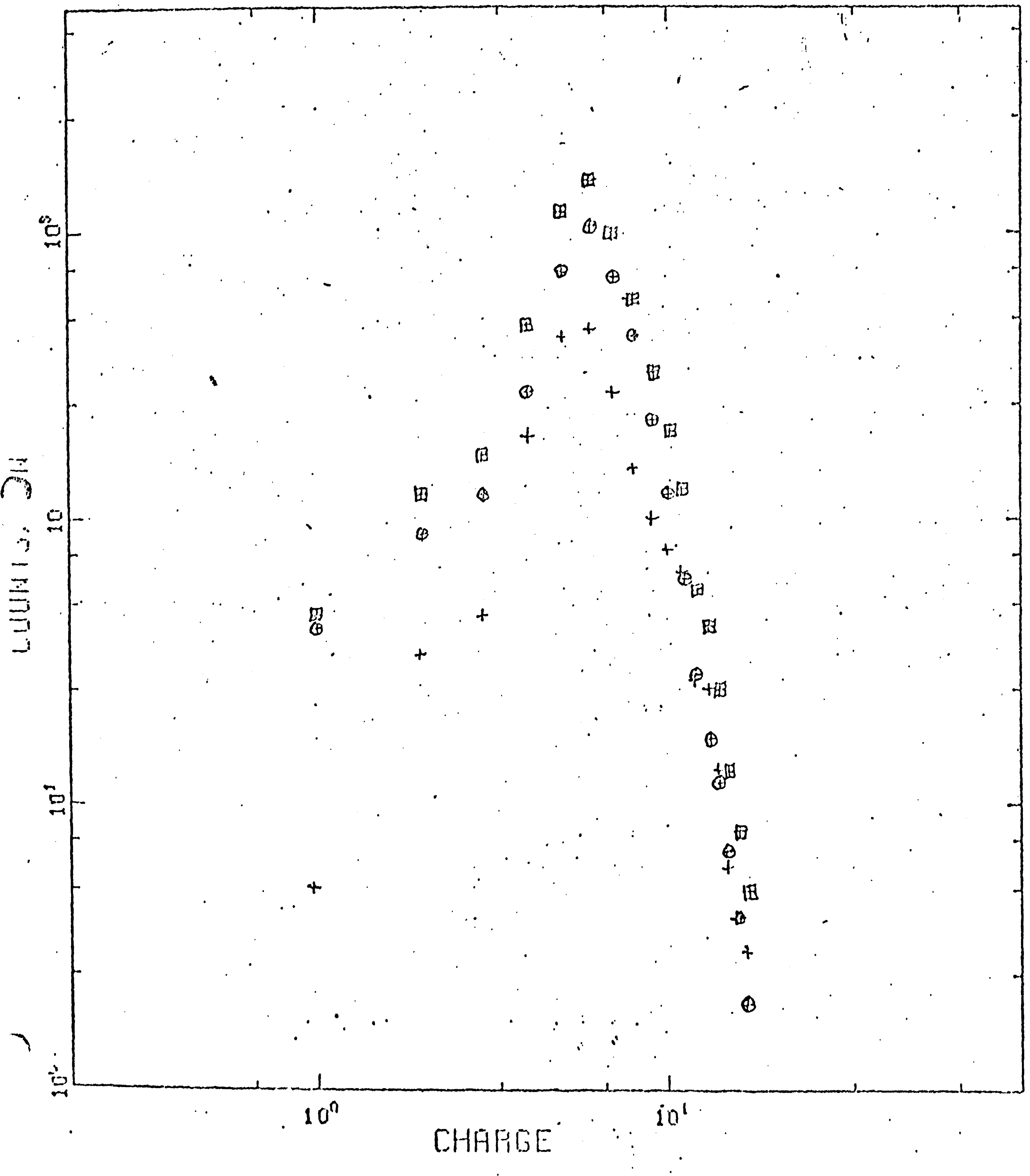

#8

Log-log Plot of 5Sigma Pion Pairs

⊞ - Total Pair
⊕ - Outside P
+ - Inside Pai

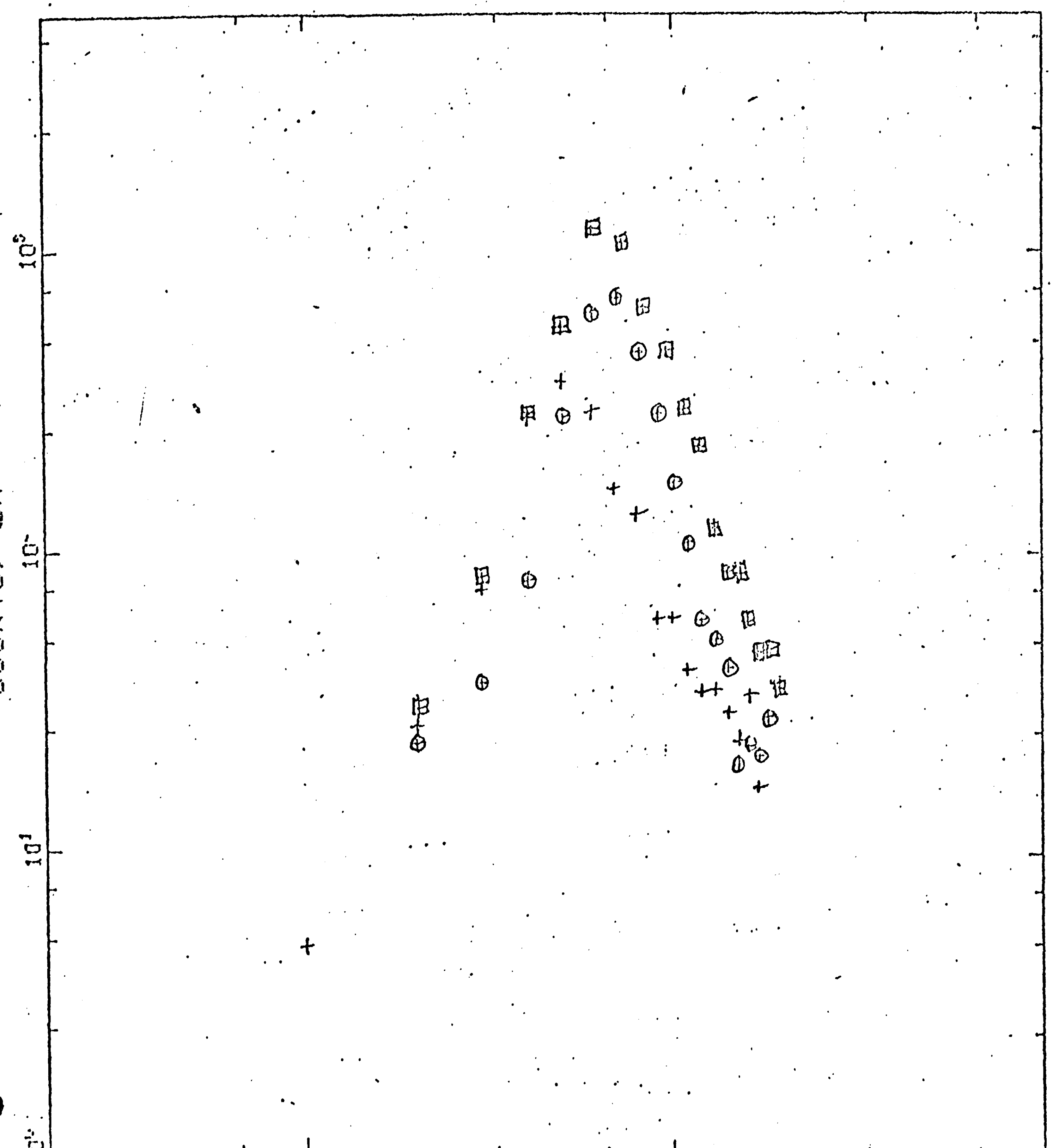

#9

P QUADS [264+265+274+275]

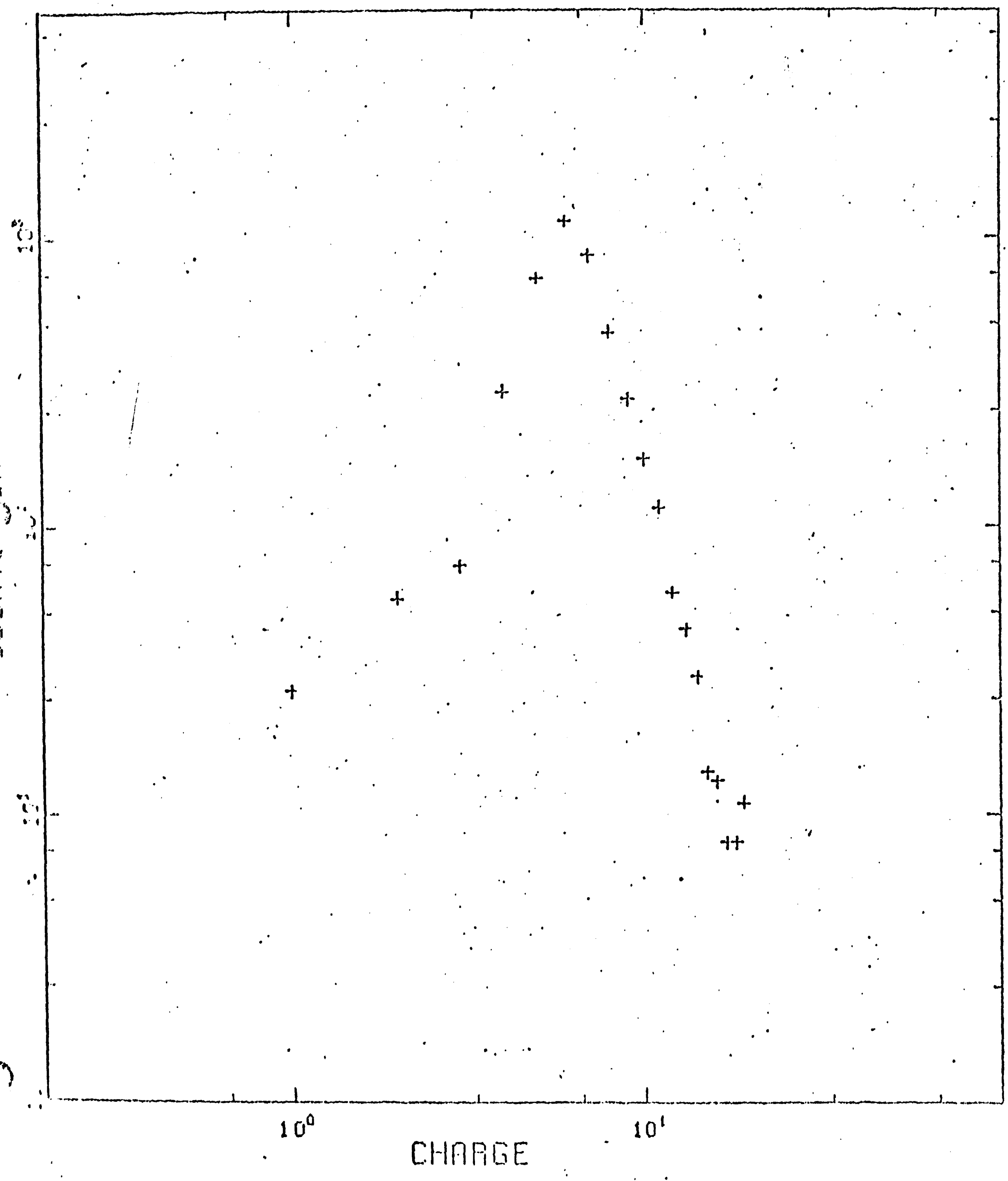

#10

π QUADS [264+265+274+275]

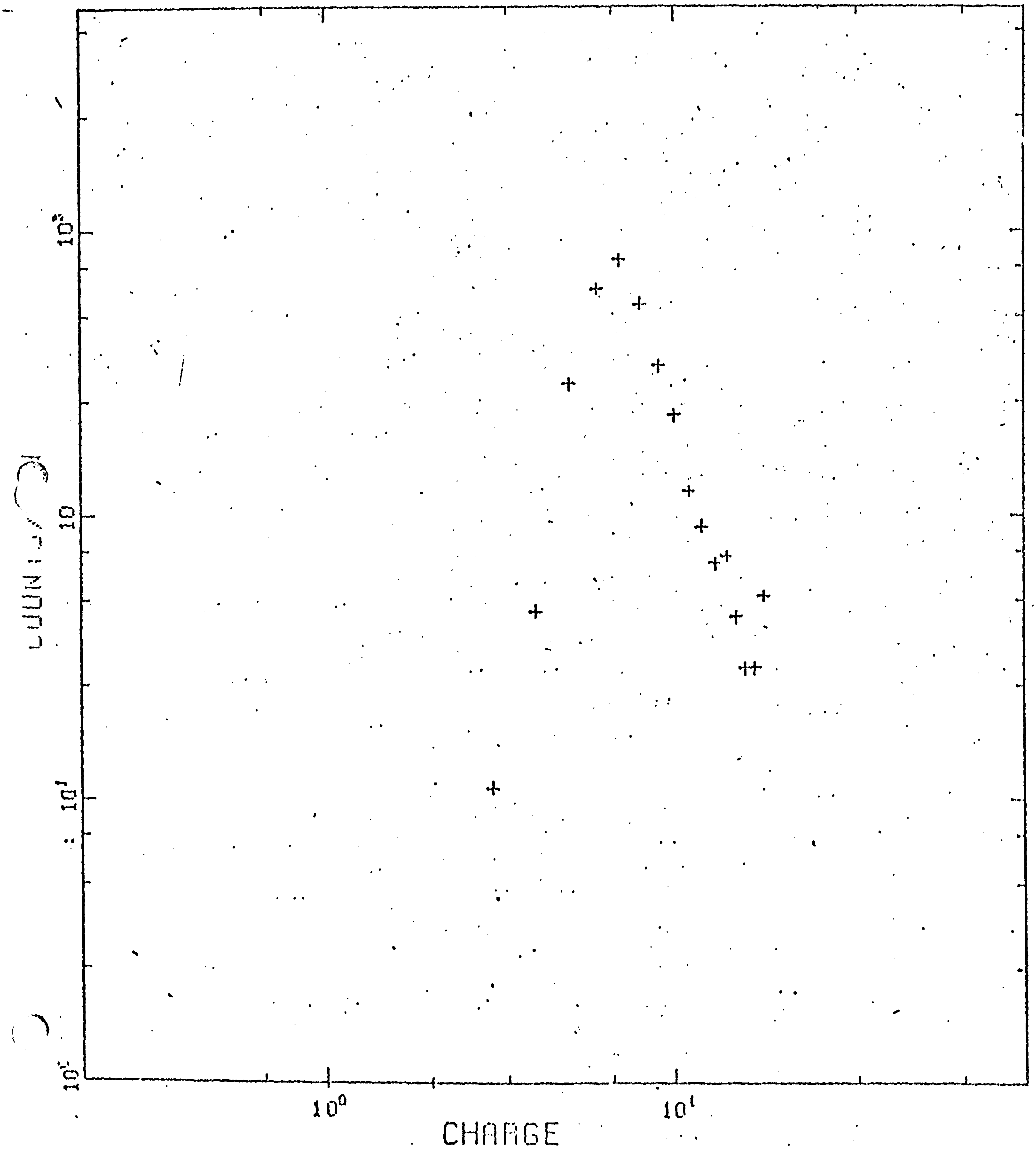

Protons 10σ Quads - - + -

650 MeV/C Protons (noise = .19 fc) ———

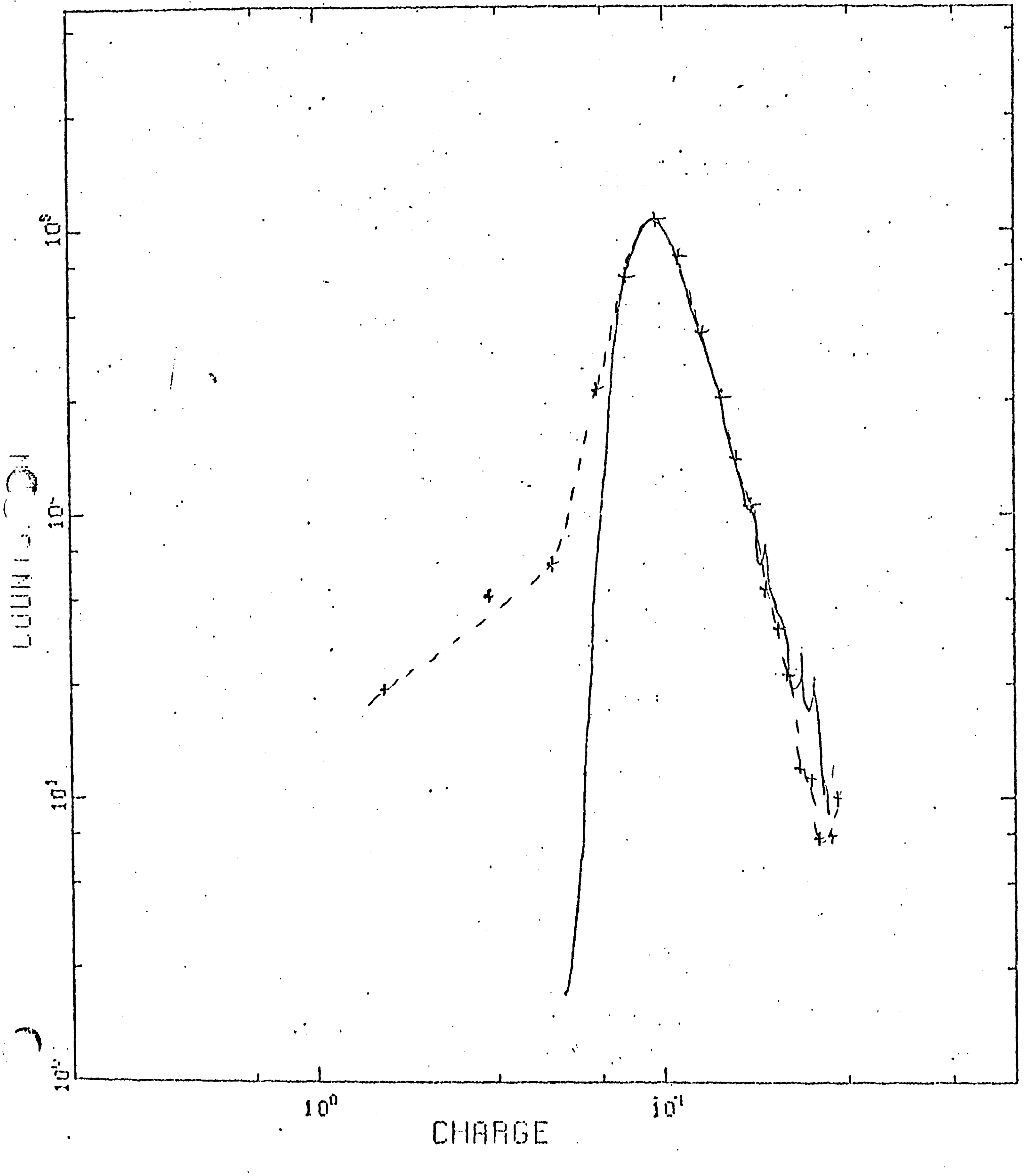

Pion 50 Quads – +

600 MeV/c Pions (noise = .19 fc
.30 fc
.39 fc)

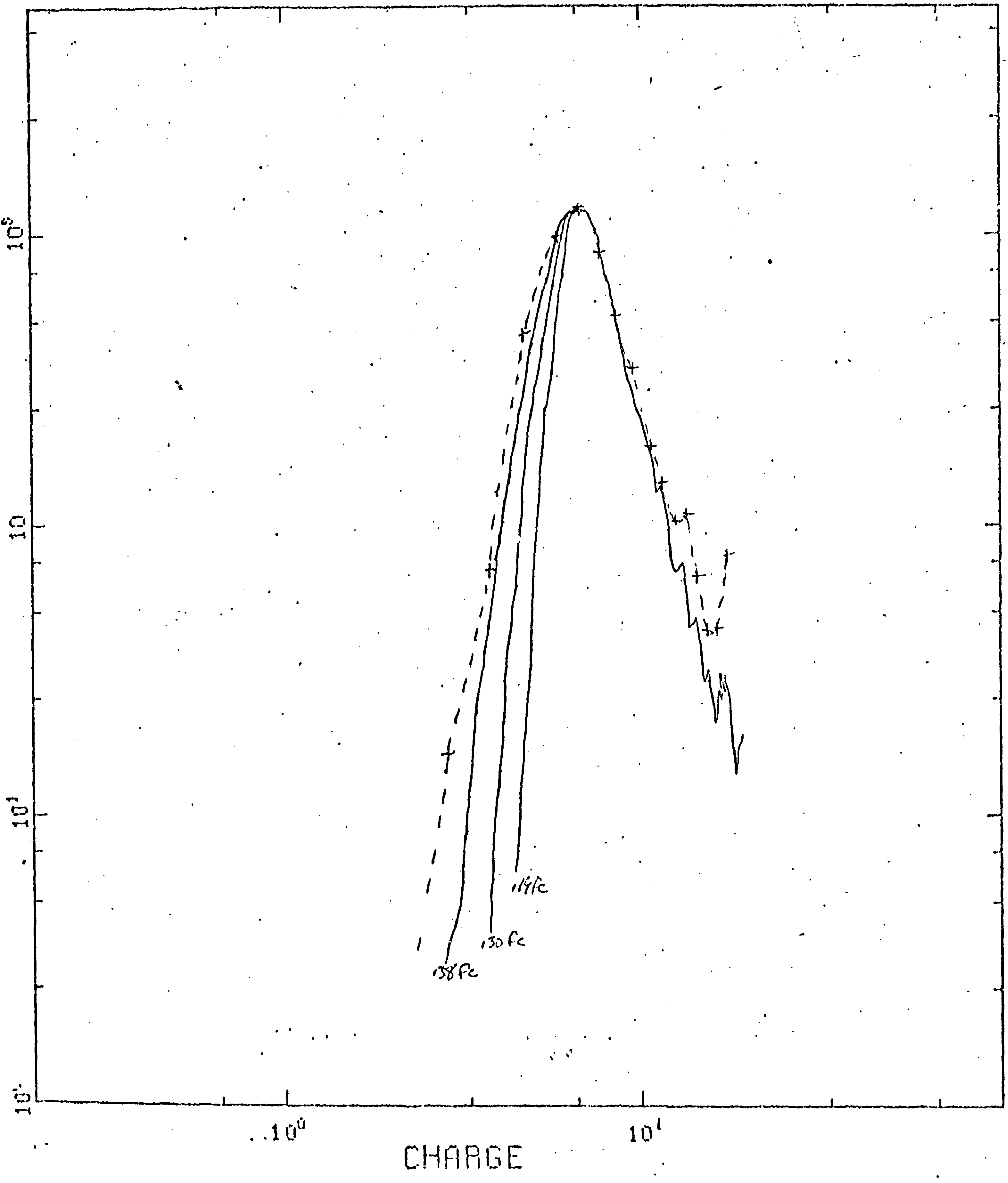

#13

Centronics #1

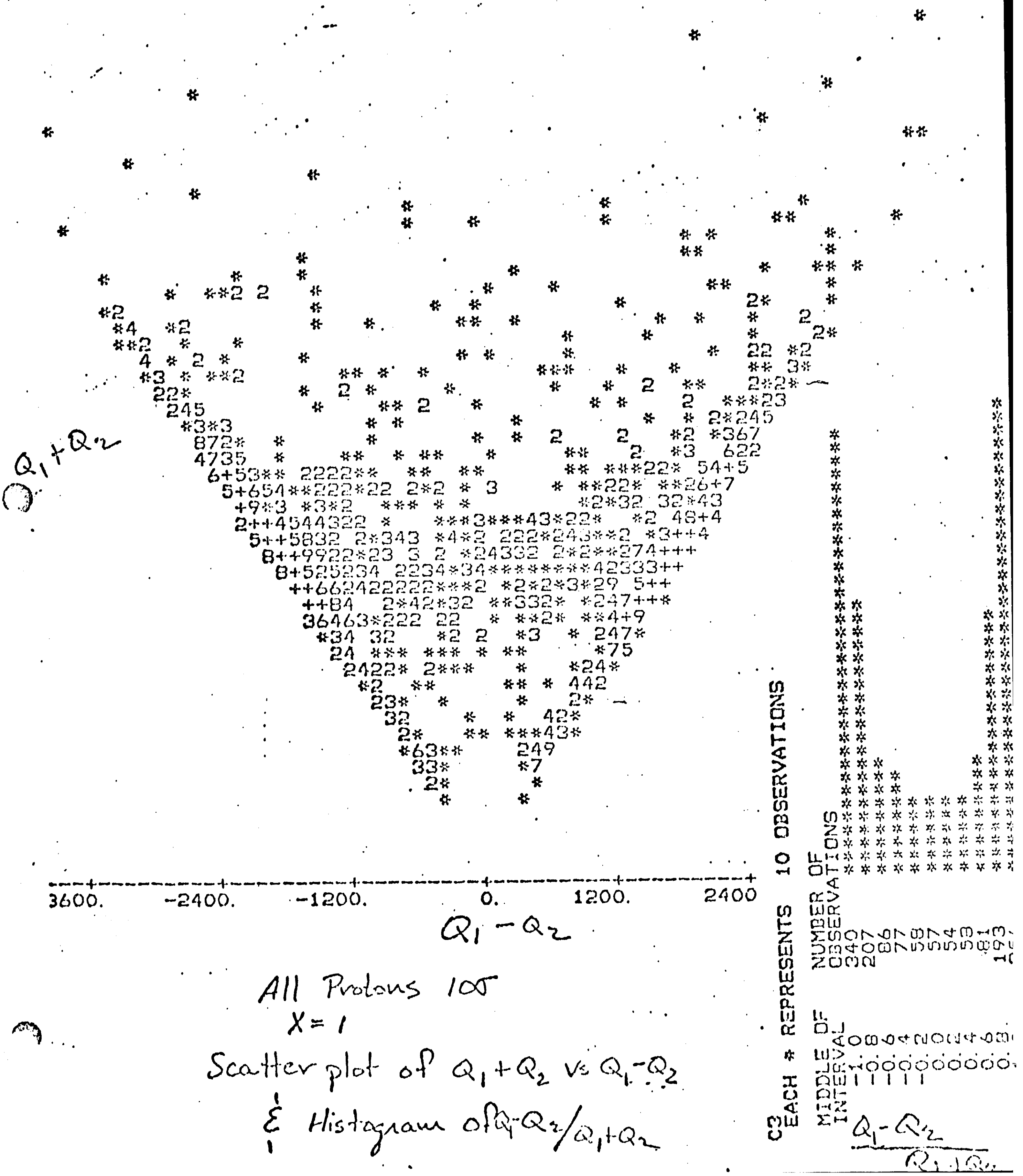

All Protons 100

X = 1

Scatter plot of Q_1+Q_2 vs Q_1-Q_2

& Histogram of Q_1-Q_2/Q_1+Q_2

#14

Centronics #1

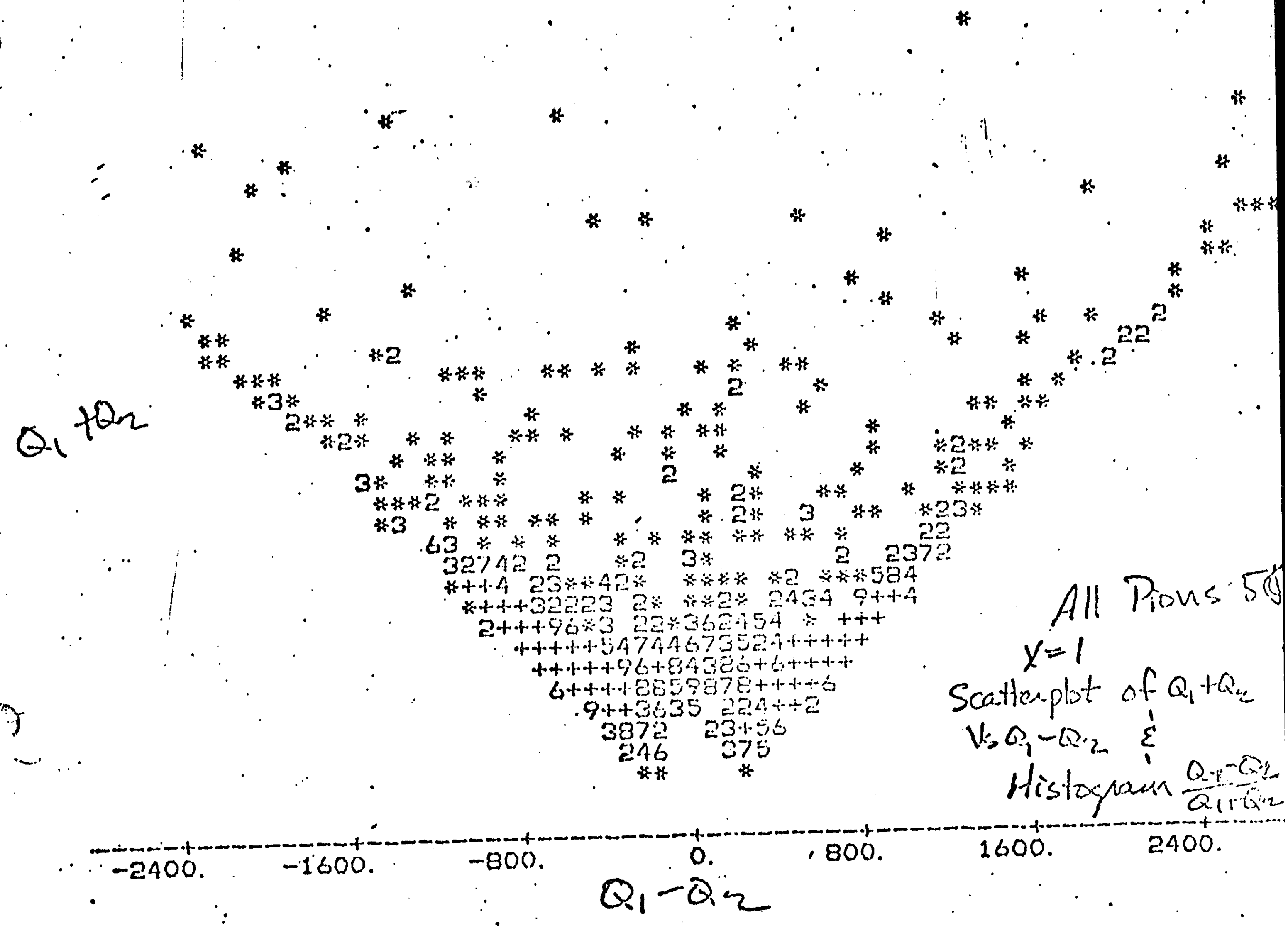

All Pions 50
x=1
Scatterplot of Q_1+Q_2 Vs Q_1-Q_2 &
Histogram $\frac{Q_1-Q_2}{Q_1+Q_2}$

$\frac{Q_1-Q_2}{Q_1+Q_2}$

```
MIDDLE OF    NUMBER OF
INTERVAL     OBSERVATIONS
 -1.000       102        *********************
 -0.900       240        ************************************************
 -0.800       136        ****************************
 -0.700        86        ******************
 -0.600        72        ***************
 -0.500        46        **********
 -0.400        33        *******
 -0.300        42        *********
 -0.200        32        *******
 -0.100        25        *****
  0.000        38        ********
  0.100        36        ********
  0.200        32        *******
  0.300        29        ******
  0.400        40        ********
  0.500        37        ********
  0.600        50        **********
  0.700        67        **************
  0.800       114        ***********************
  0.900       248        **************************************************
  1.000       115        ***********************
```

#1D

Centronics #1

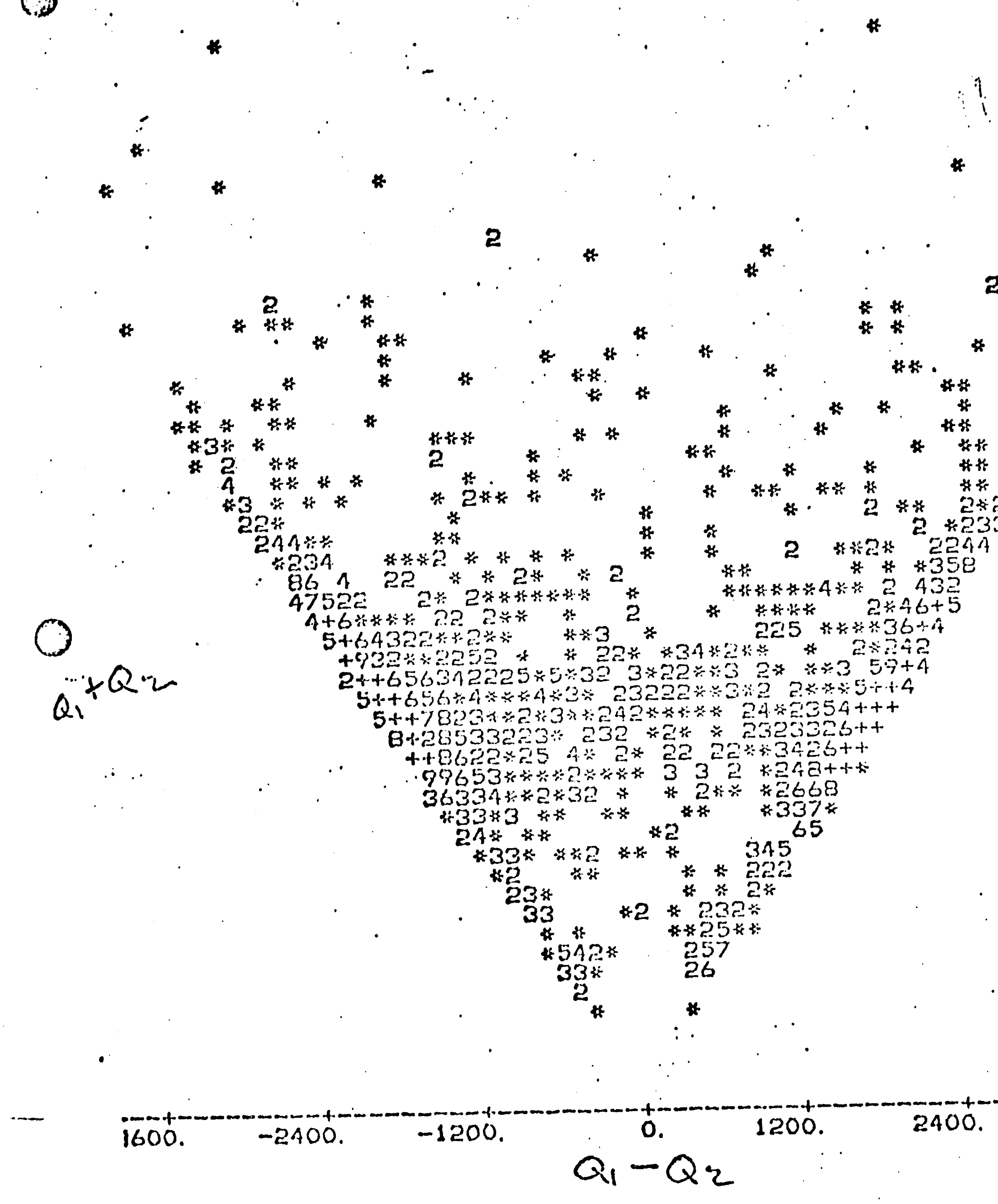

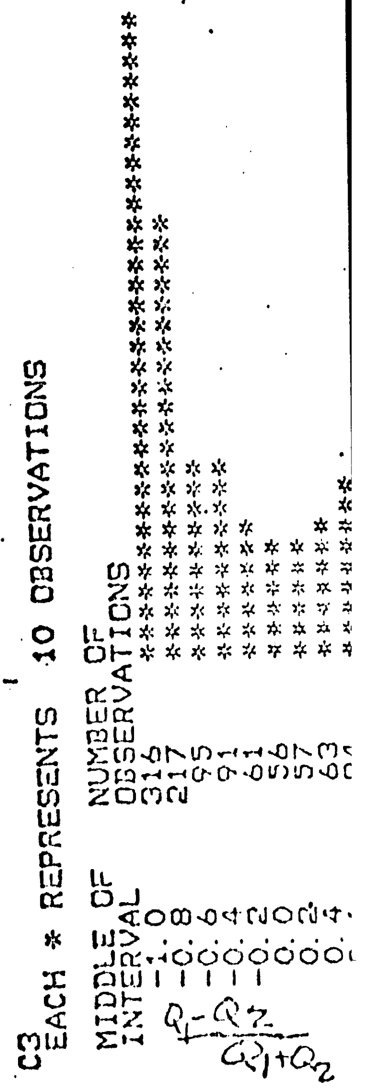

All Protons 10σ

$\chi = \sqrt{2}$

Scatterplot of Q_1+Q_2 Vs Q_1-Q_2

& Histogram of Q_1Q_2/Q_1+Q_2

#F16

Centronics #1

$Q_1 - Q_2$

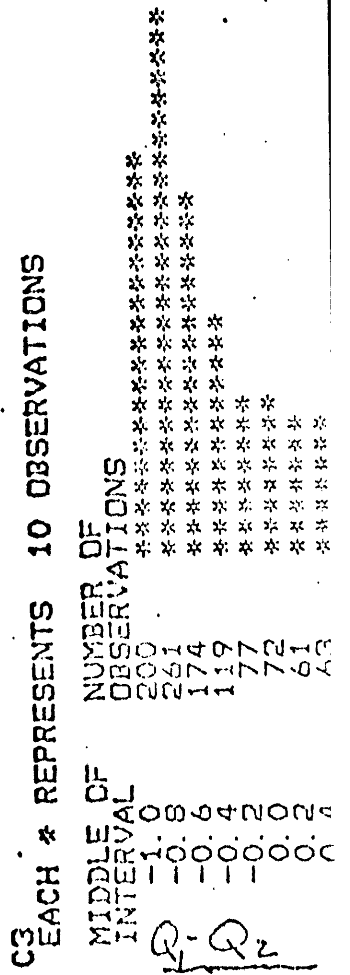

$\frac{Q_1-Q_2}{Q_1+Q_2}$

All Protons 105

X=2

Scatterplot of Q_1+Q_2 vs Q_1-Q_2

& Histogram of Q_1-Q_2/Q_1+Q_2

#11

Centronics #1

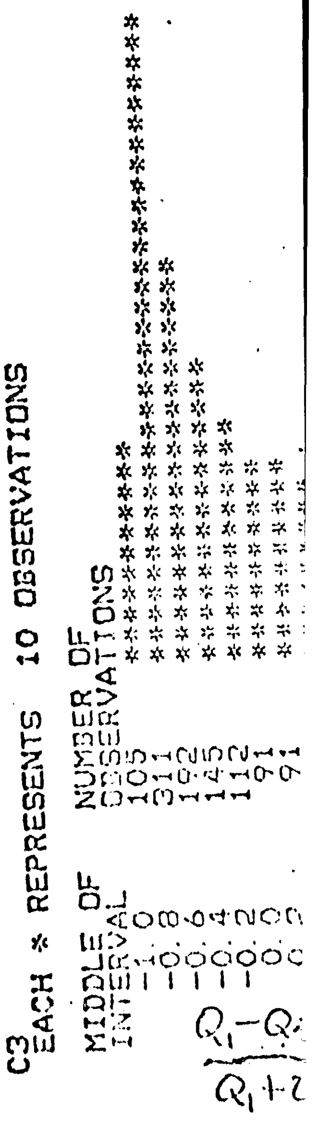

All Rotors 105
X=4

Scatterplot of Q_1+Q_2 vs Q_1-Q_2

& histogram of Q_1-Q_2/Q_1+Q_2

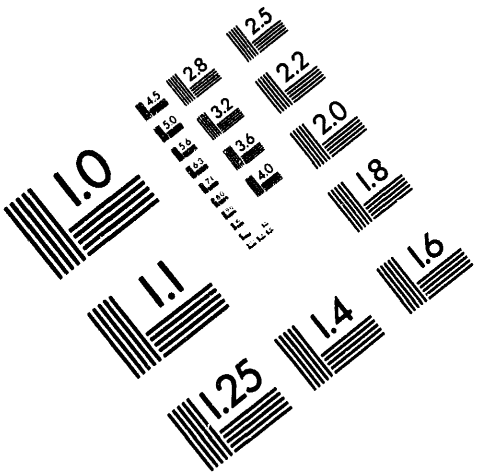

AIIM

Association for Information and Image Management

1100 Wayne Avenue, Suite 1100
Silver Spring, Maryland 20910
301/587-8202

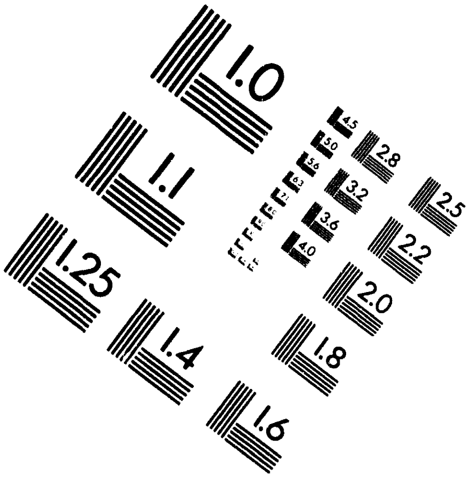

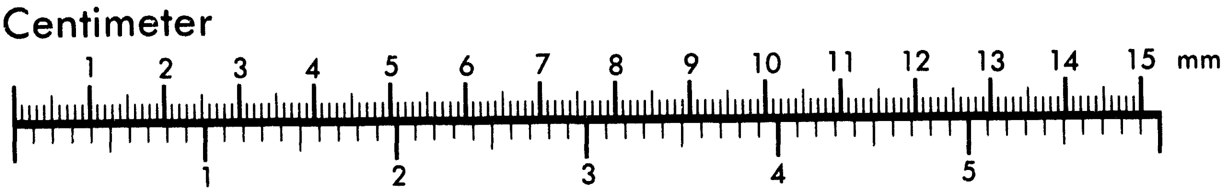

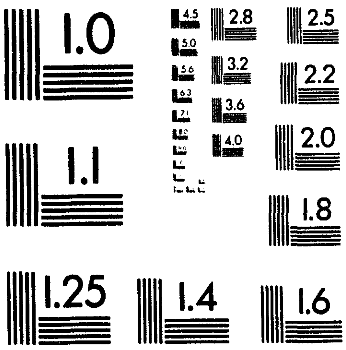

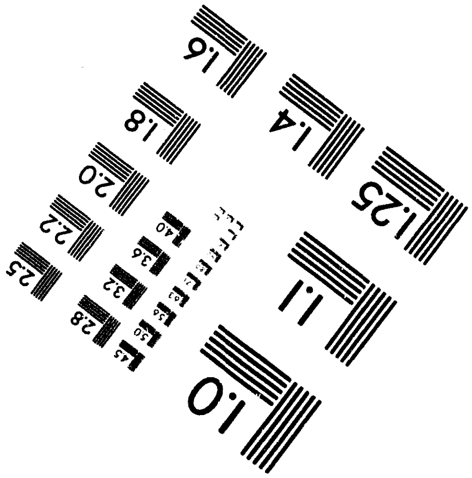

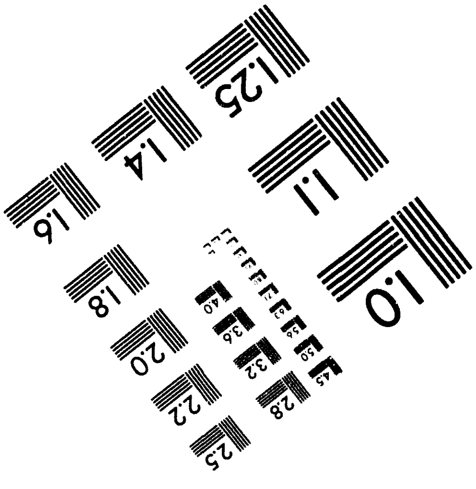

MANUFACTURED TO AIIM STANDARDS
BY APPLIED IMAGE, INC.

2 of 2

#16

Centronics #1

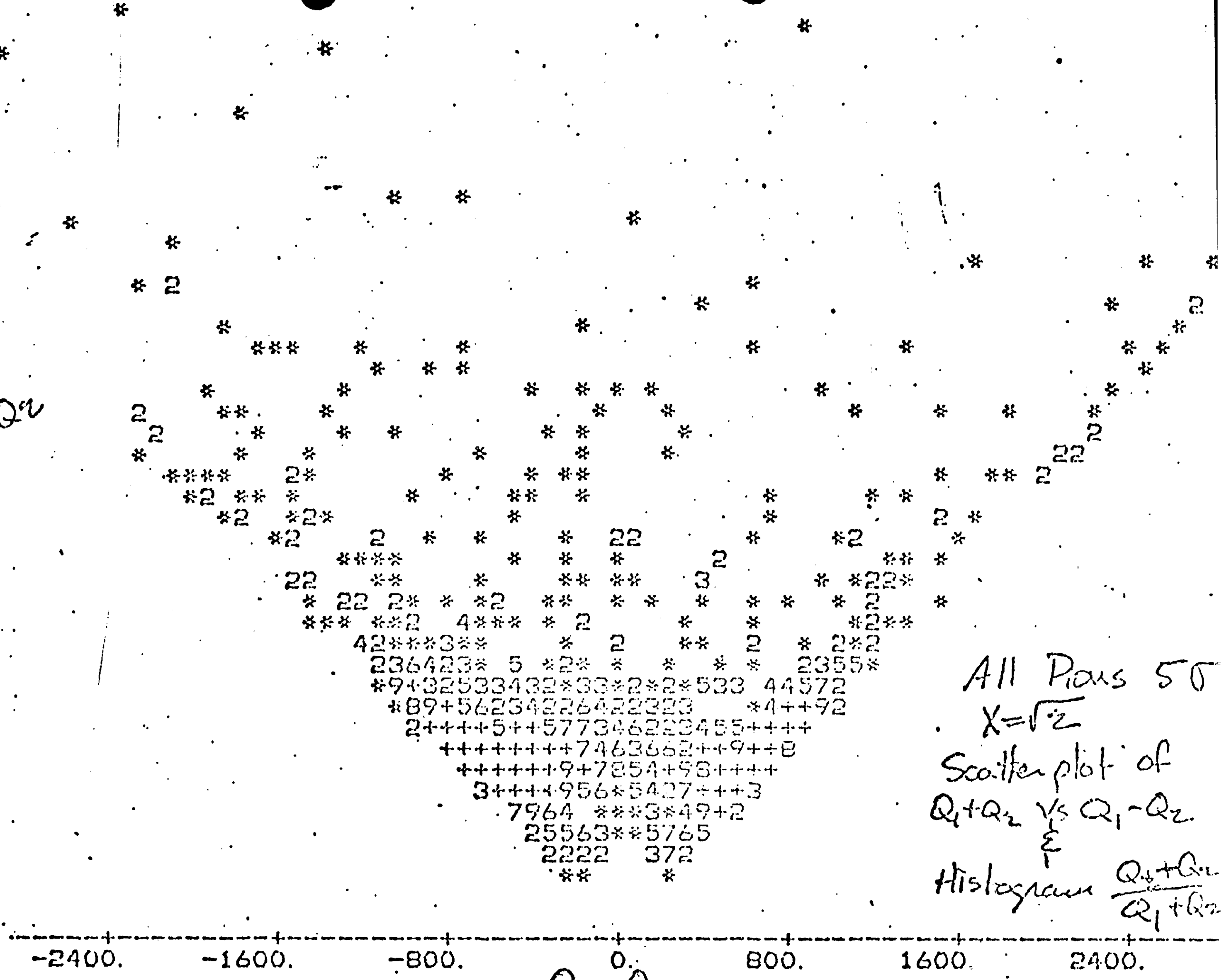

All Pions 5σ

$X=\sqrt{2}$

Scatter plot of Q_1+Q_2 vs Q_1-Q_2 & Histogram $\frac{Q_1+Q_2}{Q_1+Q_2}$

```
MIDDLE OF    NUMBER OF
INTERVAL     OBSERVATIONS
 -1.000        57     ************
 -0.900       200     ****************************************
 -0.800       139     ****************************
 -0.700       118     ************************
 -0.600        73     ***************
 -0.500        70     **************
 -0.400        82     *****************
 -0.300        38     ********
 -0.200        53     ***********
 -0.100        43     *********
  0.000        36     ********
  0.100        30     ******
  0.200        30     ******
  0.300        30     ******
  0.400        36     ********
  0.500        47     **********
  0.600        47     **********
  0.700        75     ***************
  0.800       145     *****************************
  0.900       194     ***************************************
  1.000        77     ****************
```

$\frac{Q_1-Q_2}{Q_1+Q_2}$

#A

Centronics #1

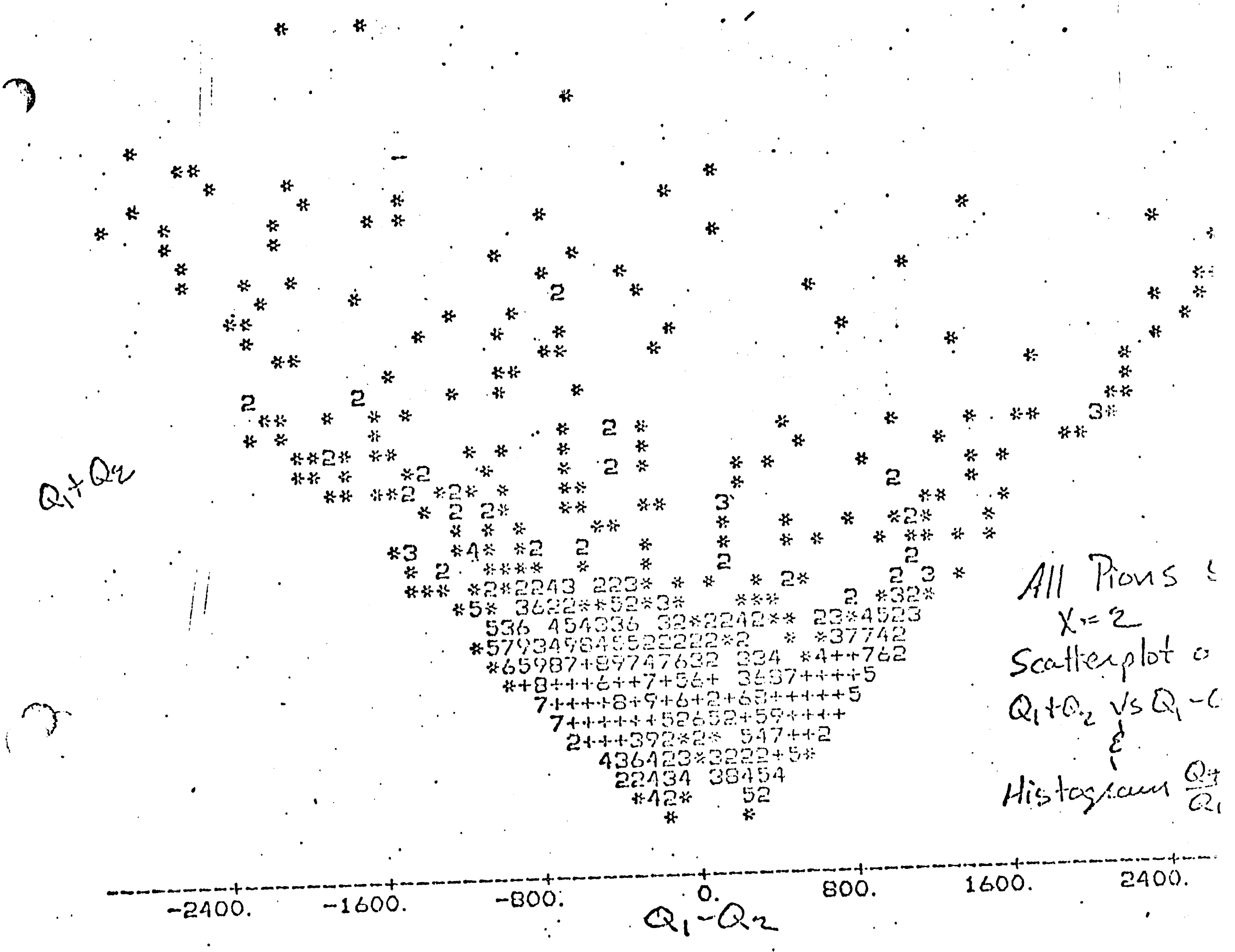

All Pions
X = 2
Scatterplot o
Q_1+Q_2 vs Q_1-
&
Histogram $\frac{Q_1-}{Q_1}$

$$\frac{Q_1-Q_2}{Q_1+Q_2}$$

```
MIDDLE OF    NUMBER OF
INTERVAL     OBSERVATIONS
 -1.000        39    ********
 -0.900       152    *******************************
 -0.800       142    *****************************
 -0.700       119    ************************
 -0.600       103    *********************
 -0.500        87    ******************
 -0.400        81    *****************
 -0.300        76    ****************
 -0.200        59    ************
 -0.100        51    ***********
  0.000        37    ********
  0.100        37    ********
  0.200        34    *******
  0.300        33    *******
  0.400        45    *********
  0.500        42    *********
  0.600        58    ************
  0.700        98    ********************
  0.800       125    *************************
  0.900       152    *******************************
  1.000        50    **********
```

#I-ω Centronics #

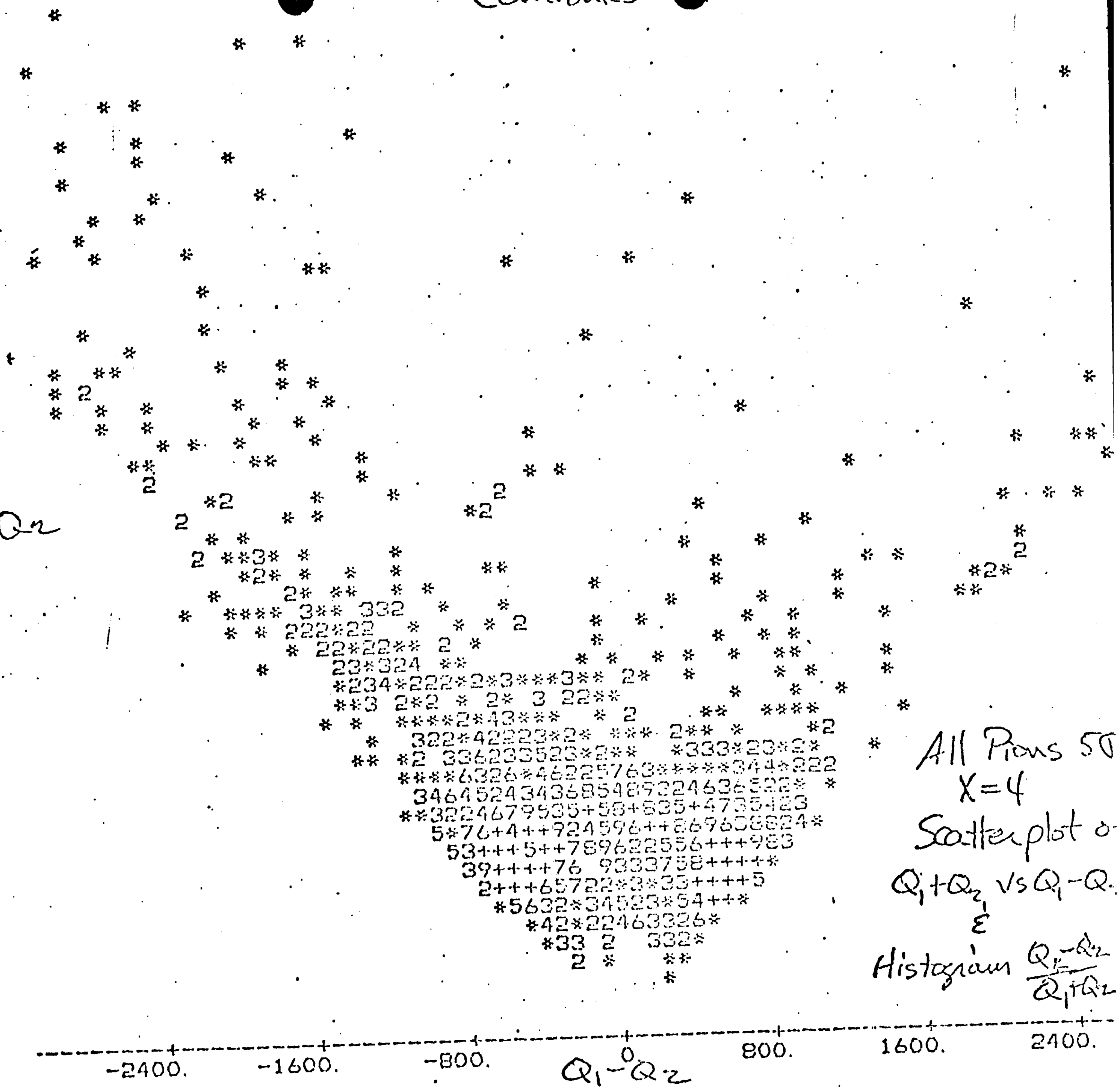

All Pions 50
X=4
Scatterplot of Q_1+Q_2 vs Q_1-Q_2
ε
Histogram $\frac{Q_1-Q_2}{Q_1+Q_2}$

```
MIDDLE OF     NUMBER OF
INTERVAL      OBSERVATIONS
 -1.000          21       *****
 -0.900          79       ****************
 -0.800         136       ****************************
 -0.700         128       **************************
 -0.600         127       **************************
 -0.500         108       **********************
 -0.400         101       *********************
 -0.300          76       ****************
 -0.200          68       **************
 -0.100          71       ***************
  0.000          68       **************
  0.100          68       **************
  0.200          45       *********
  0.300          55       ***********
  0.400          61       *************
  0.500          75       ***************
  0.600          79       ****************
  0.700          79       ****************
  0.800          88       ******************
```

$\frac{Q_1-Q_2}{Q_1+Q_2}$

#21 All Protons 120

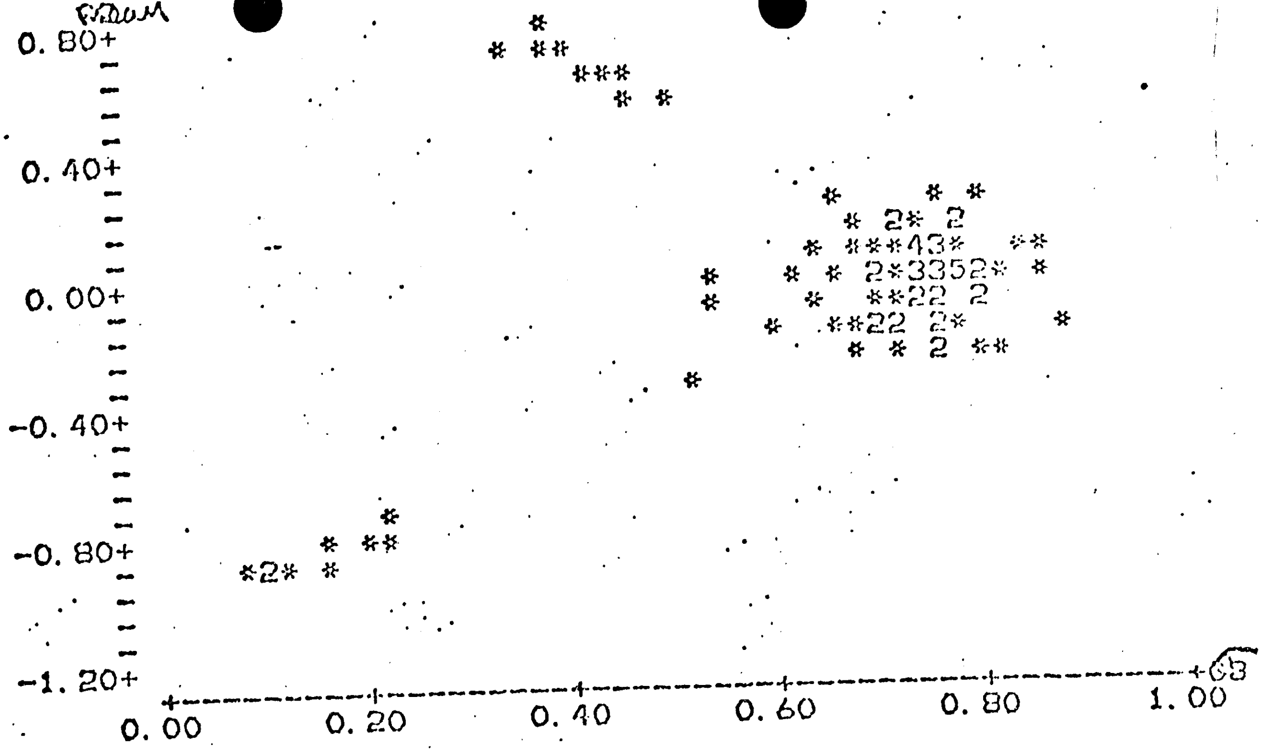

Plot of mean $\left(\frac{Q_1-Q_2}{Q_1+Q_2}\right)$ Vs $\sigma\left(\frac{Q_1-Q_2}{Q_1+Q_2}\right)$ by channel
for X = 1

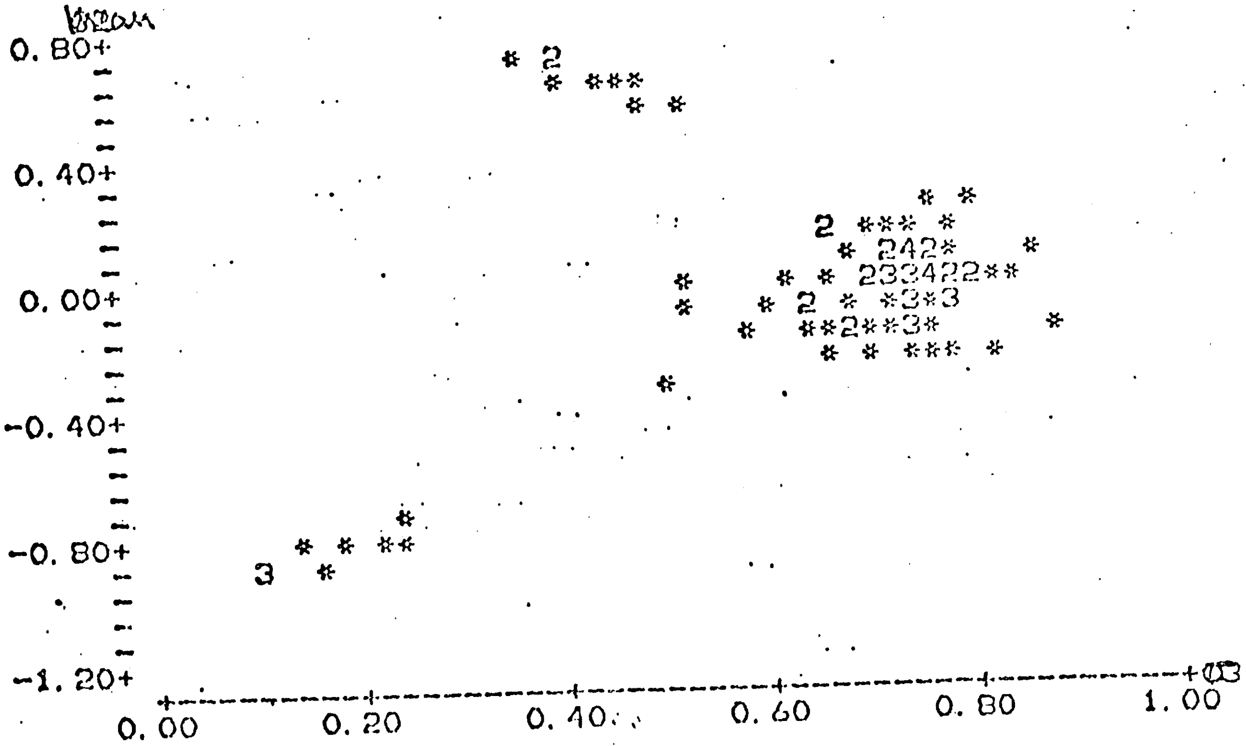

Plot of mean $\left(\frac{Q_1-Q_2}{Q_1+Q_2}\right)$ Vs $\sigma\left(\frac{Q_1-Q_2}{Q_1+Q_2}\right)$ by channel
for $X=\sqrt{2}$

#22

All Protons 10σ

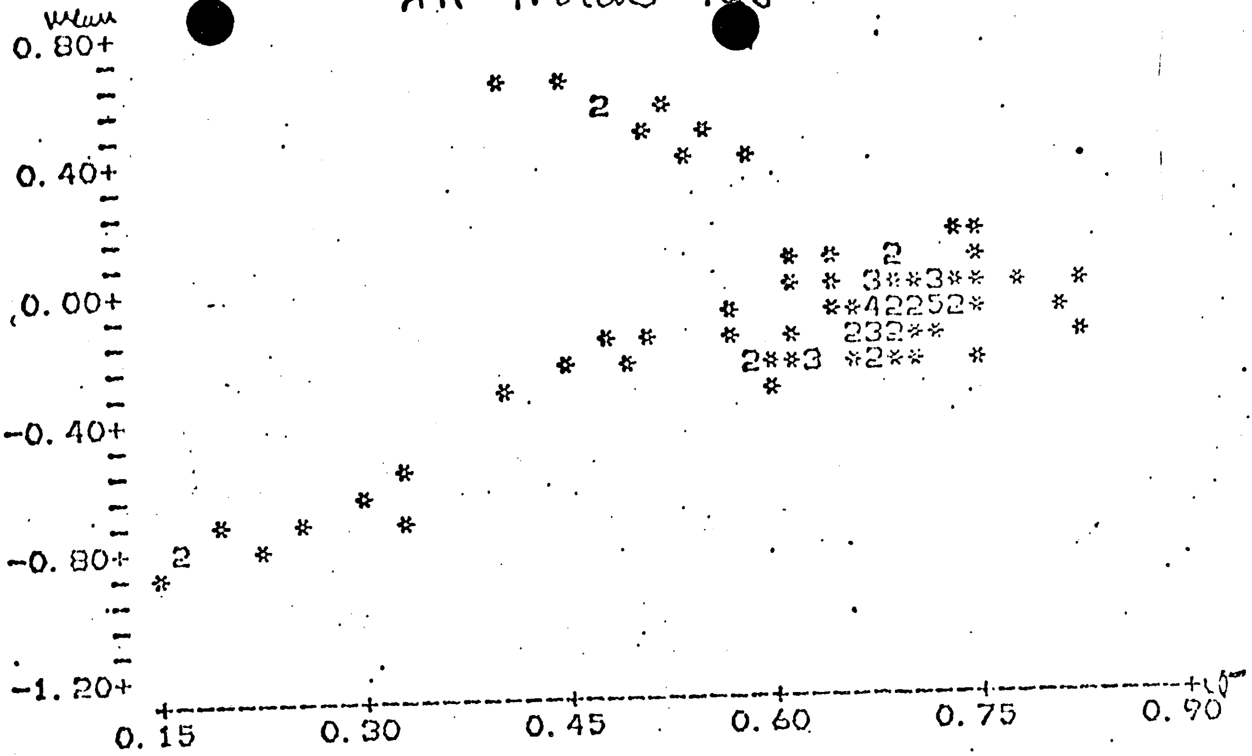

Plot of mean$\left(\frac{Q_1-Q_2}{Q_1+Q_2}\right)$ vs $\sigma\left(\frac{Q_1-Q_2}{Q_1+Q_2}\right)$ by channel for X = 2

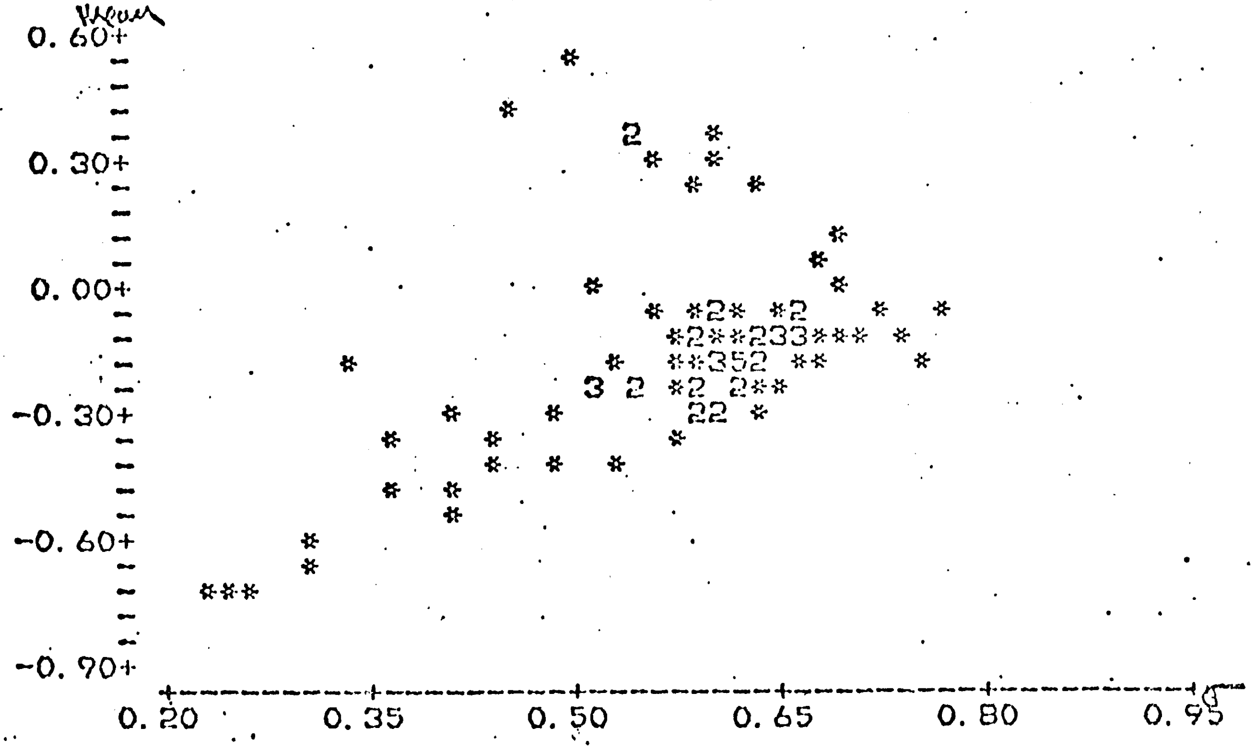

Plot of mean$\left(\frac{Q_1-Q_2}{Q_1+Q_2}\right)$ vs $\sigma\left(\frac{Q_1-Q_2}{Q_1+Q_2}\right)$ by channe

for X = 4

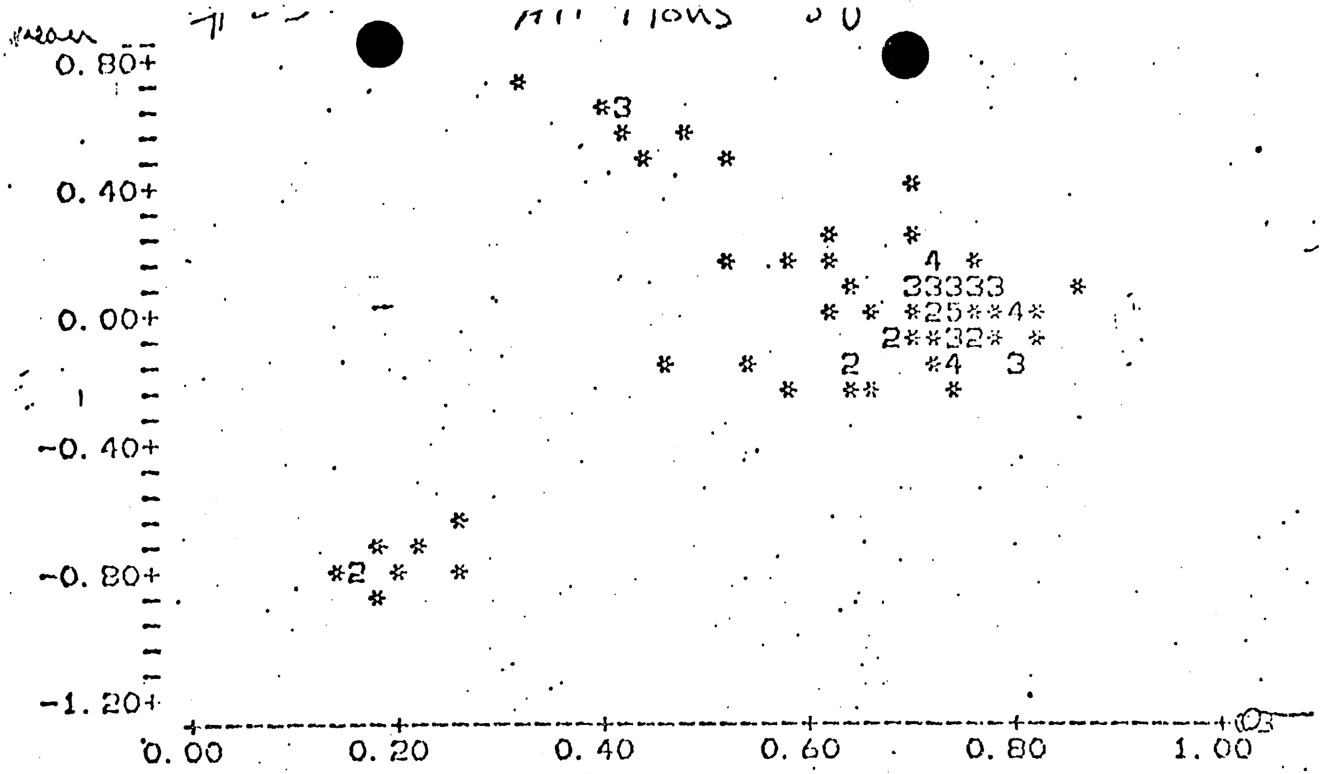

Plot of mean$\left(\frac{Q_1-Q_2}{Q_1+Q_2}\right)$ Vs $\sigma\left(\frac{Q_1-Q_2}{Q_1+Q_2}\right)$ by chann
for $X=1$

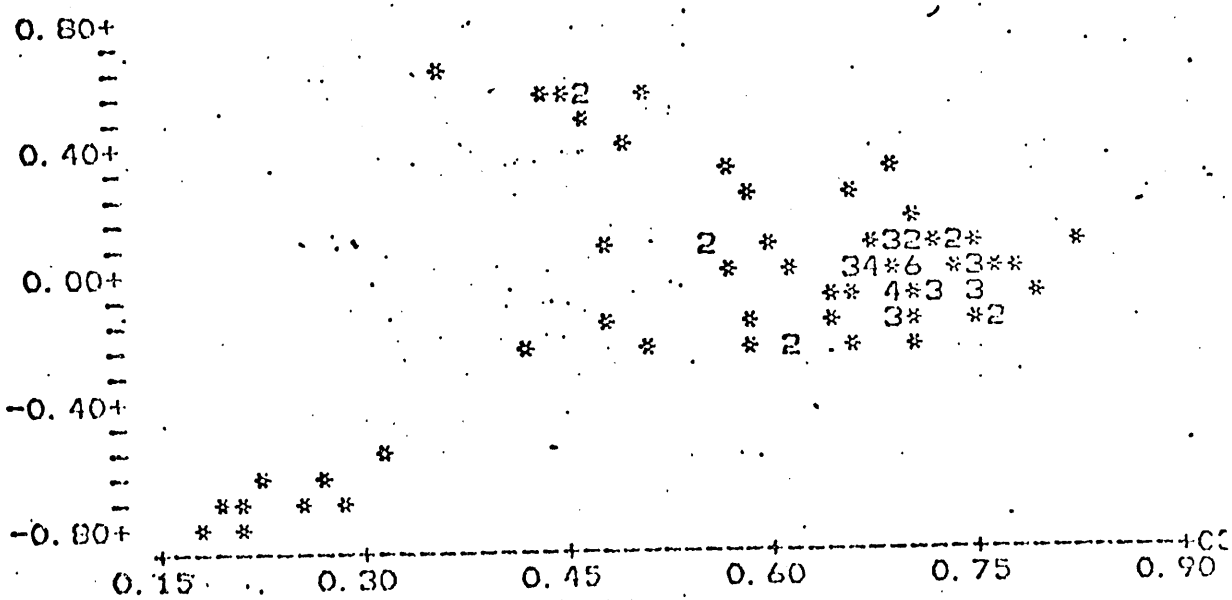

Plot of mean$\left(\frac{Q_1-Q_2}{Q_1+Q_2}\right)$ Vs $\sigma\left(\frac{Q_1+Q_2}{Q_1+Q_2}\right)$ by channel
for $X=\sqrt{2}$

All Ions 50

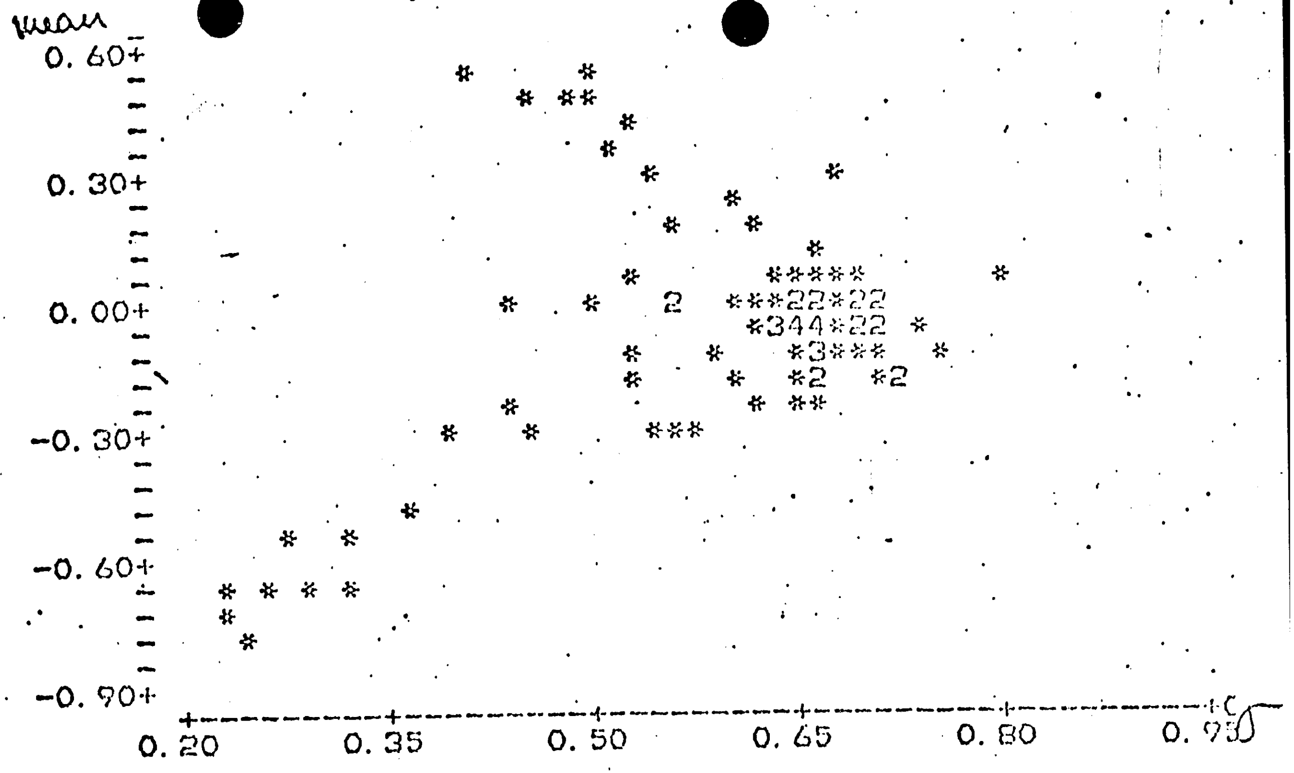

Plot of mean$\left(\frac{Q_1-Q_2}{Q_1+Q_2}\right)$ vs $\sigma\left(\frac{Q_1-Q_2}{Q_1+Q_2}\right)$ by channel for $x=2$

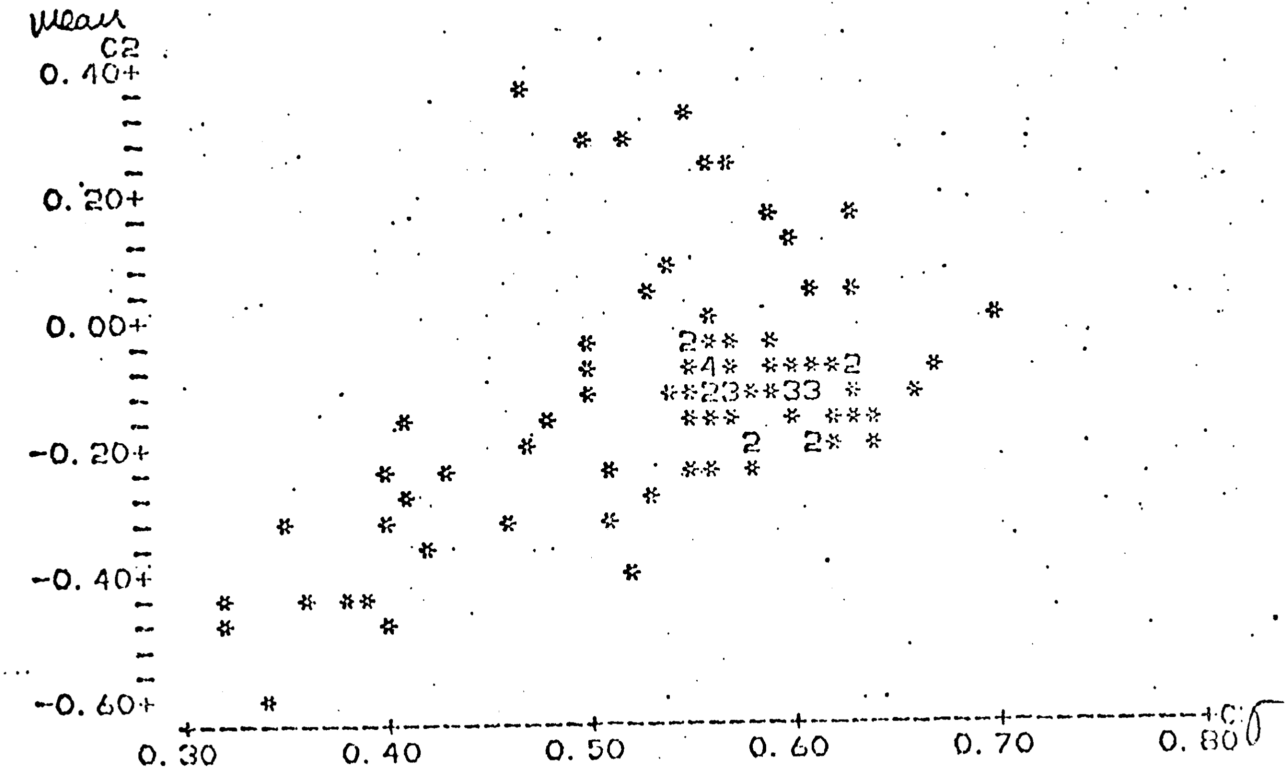

Plot of mean$\left(\frac{Q_1-Q_2}{Q_1+Q_2}\right)$ vs $\sigma\left(\frac{Q_1-Q_2}{Q_1+Q_2}\right)$ by channel for $x=4$

on

100 Protons over interval 1200 - 2500 for Q_1+Q_2

Centronics #1

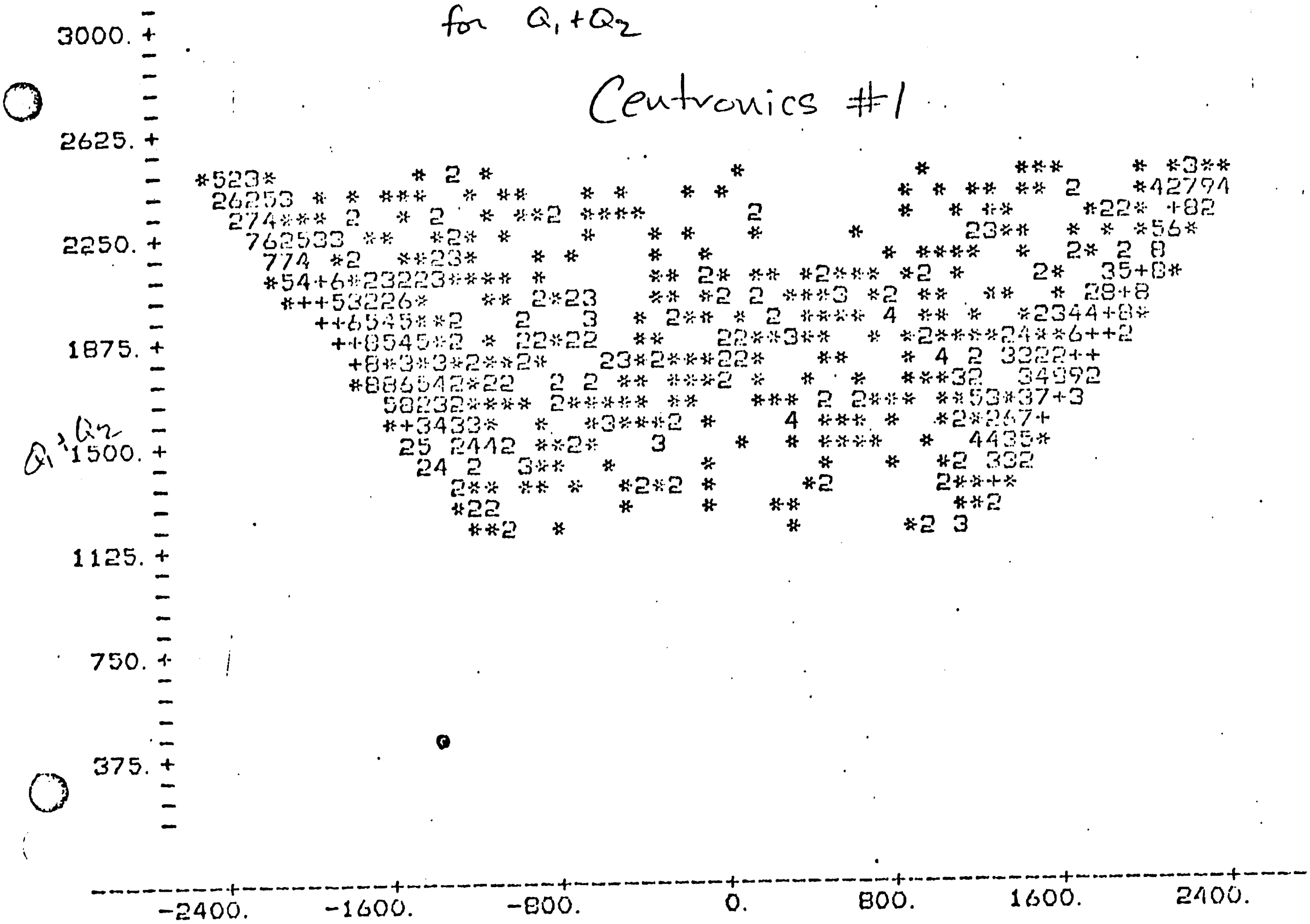

$Q_1 - Q_2$

Scatterplot of Protons Q_1-Q_2 vs Q_1+Q_2

```
EACH * REPRESENTS  10 OBSERVATIONS

MIDDLE OF    NUMBER OF
INTERVAL     OBSERVATIONS
 -1.000      255     **************************
 -0.800      157     ****************
 -0.600       68     *******
 -0.400       55     ******
 -0.200       43     *****
  0.000       43     *****
  0.200       40     ****
  0.400       43     *****
  0.600       52     ******
  0.800      119     ************
  1.000      284     *****************************
```

Histogram of $\left(\frac{Q_1-Q_2}{Q_1+Q_2}\right)$ for Interval 1200 - 2500 for Q_1+Q_2

#26

10[illegible] Protons with $\sigma\left(\frac{[illegible]-Q_2}{Q_1+Q_2}\right) > .55$
(for Centronics #2)

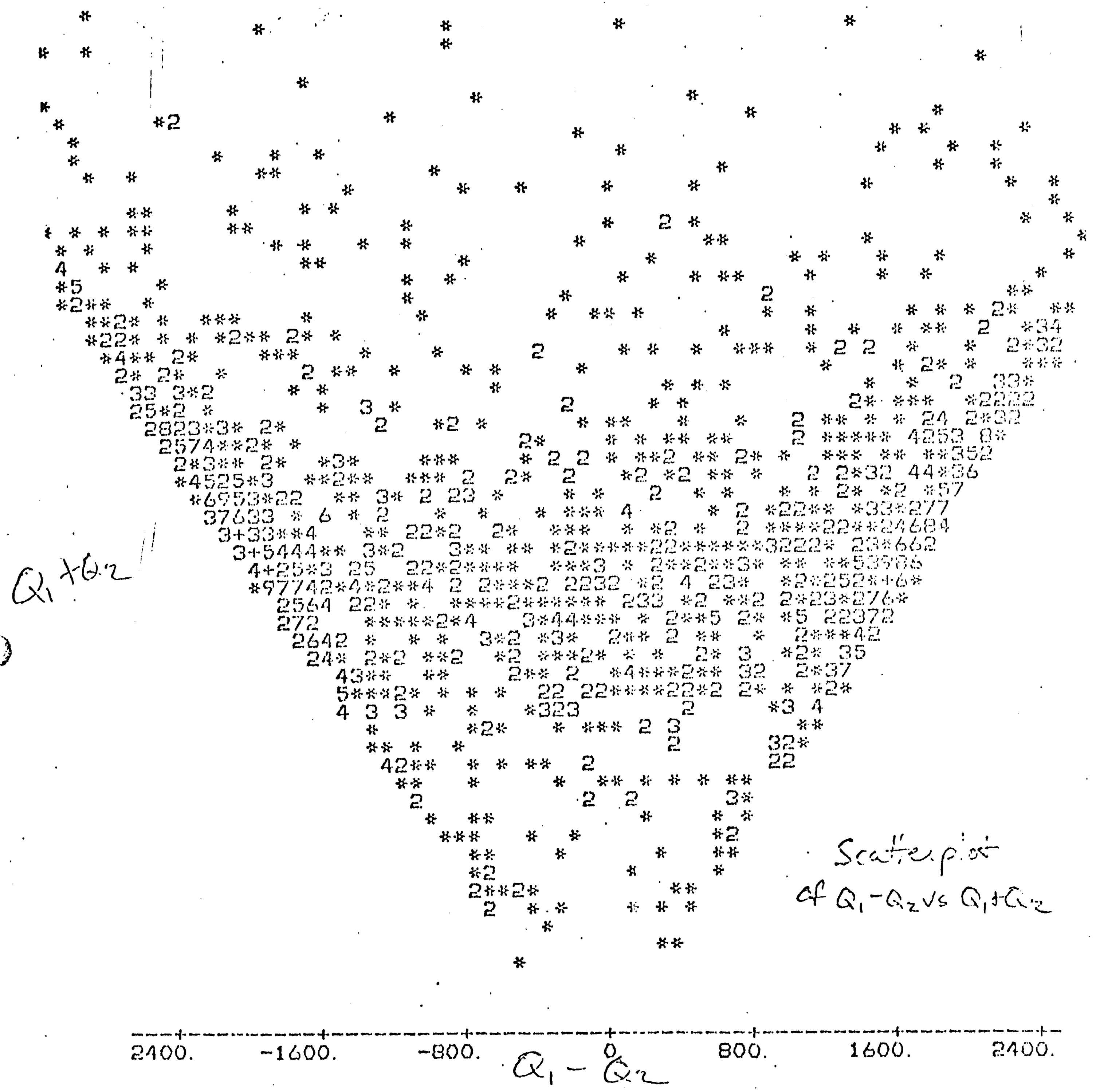

Scatterplot of Q_1-Q_2 vs Q_1+Q_2

Histogram of $\frac{(Q_1-Q_2)}{Q_1+Q_2}$

```
EACH * REPRESENTS  10 OBSERVATIONS

MIDDLE OF   NUMBER OF
INTERVAL    OBSERVATIONS
 -1.000     287      *****************************
 -0.800     189      *******************
 -0.600     109      ***********
 -0.400      94      **********
 -0.200      84      *********
  0.000      94      **********
  0.200      96      **********
  0.400     105      ***********
  0.600     102      ***********
  0.800     188      *******************
```

#27

5σ Pions with Sigma$\left(\frac{Q_1-Q_2}{Q_1+Q_2}\right)$ > .55

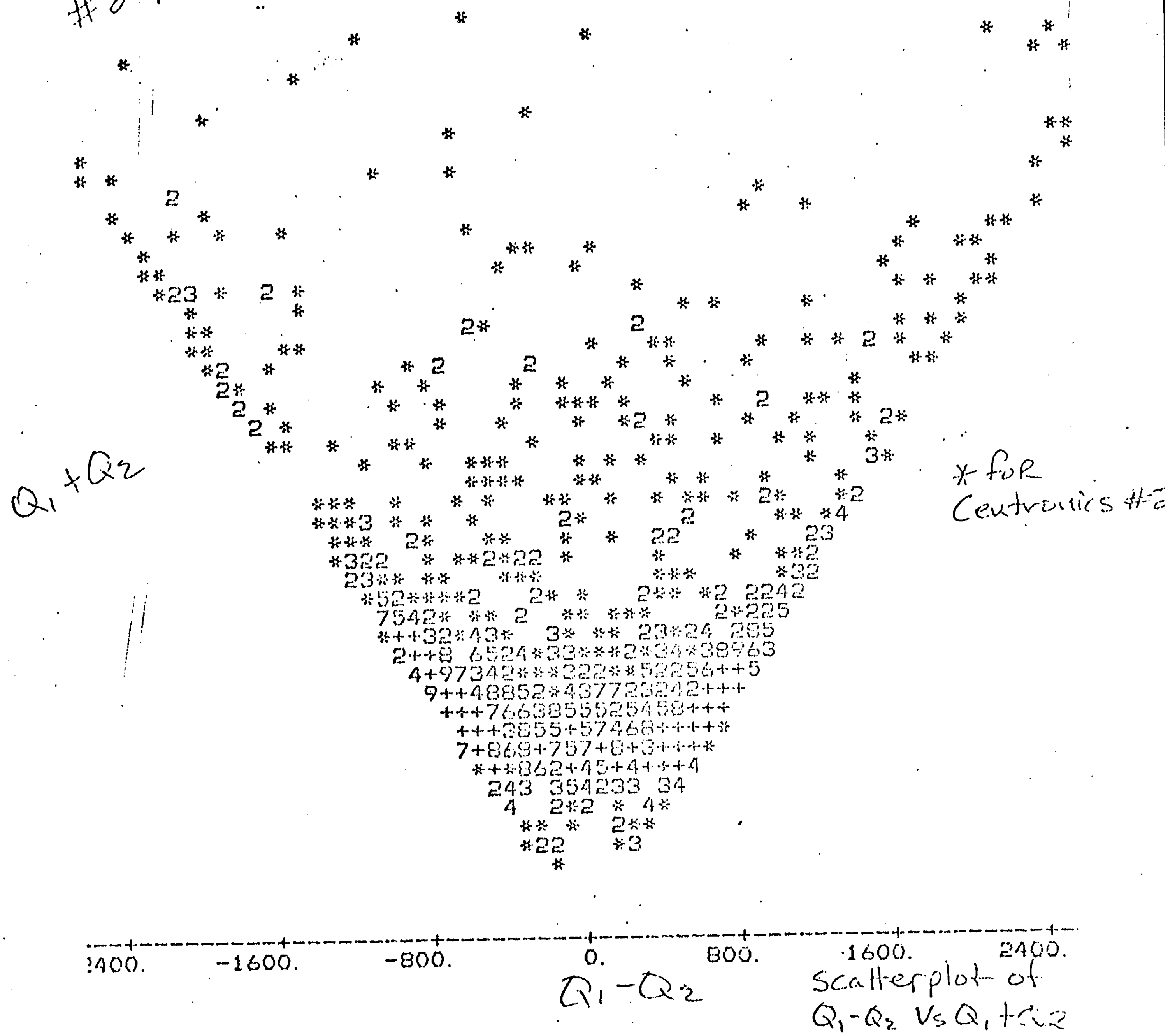

Scatterplot of Q_1-Q_2 Vs Q_1+Q_2

Histogram of $\left(\frac{Q_1-Q_2}{Q_1+Q_2}\right)$

```
EACH * REPRESENTS    5 OBSERVATIONS

MIDDLE OF    NUMBER OF
INTERVAL     OBSERVATIONS
  -1.000      120       ************************
  -0.900      190       **************************************
  -0,800      118       ************************
  -0.700       43       *********
  -0.600       60       ************
  -0.500       53       ***********
  -0.400       44       *********
  -0.300       43       *********
  -0.200       54       ***********
  -0.100       49       **********
   0.000       46       **********
   0.100       46       **********
   0.200       38       ********
   0.300       40       ********
   0.400       58       ************
   0.500       41       *********
   0.600       50       **********
   0.700       72       ***************
   0.800      123       *************************
   0.900      181       *************************************
   1.000      101       *********************
```

#28

Centronics #1, #[illegible] #3

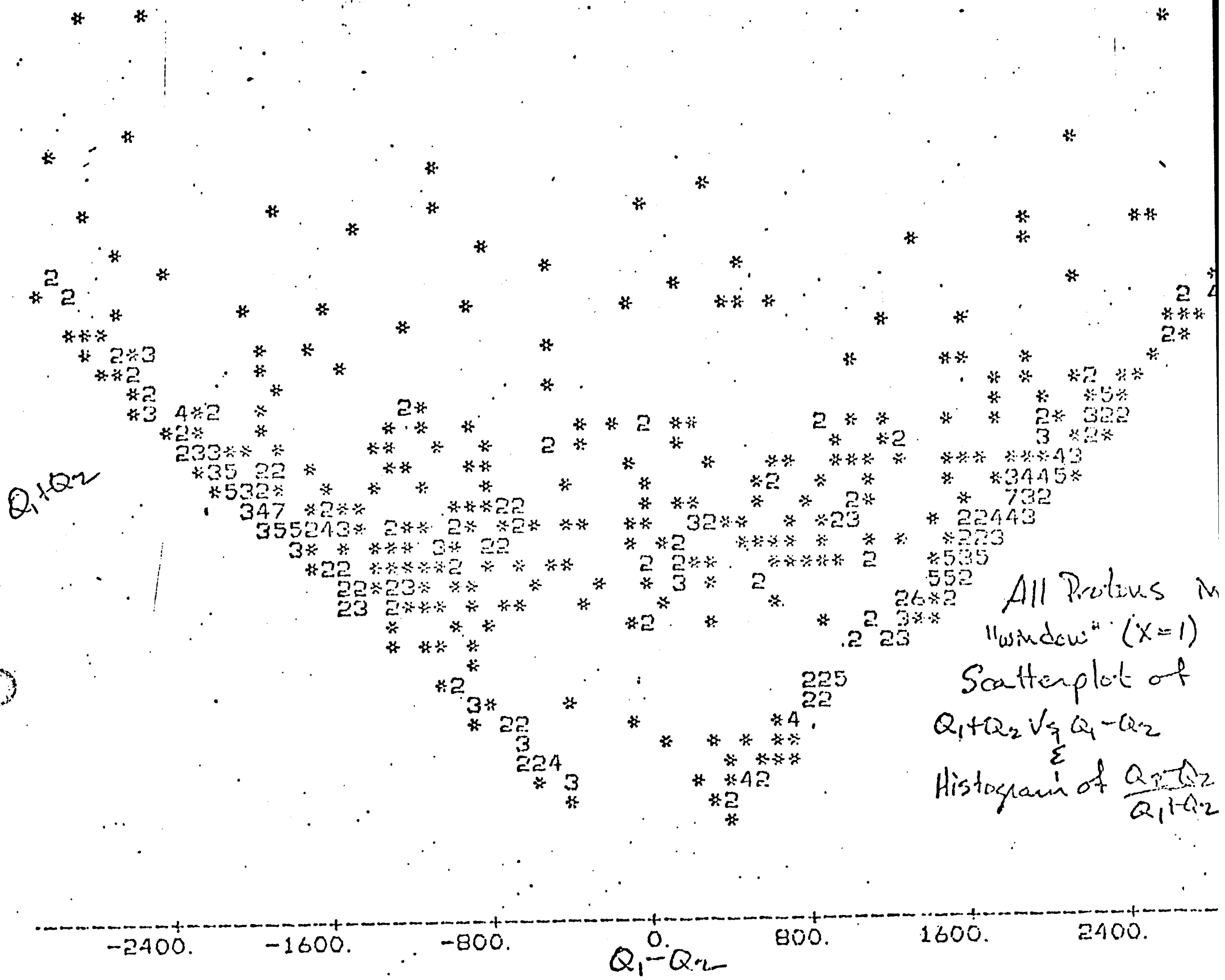

All Protons
"window" (X=1)
Scatterplot of
Q1+Q2 Vs Q1-Q2
&
Histogram of $\frac{Q_1-Q_2}{Q_1+Q_2}$

$\frac{Q_1-Q_2}{Q_1+Q_2}$

```
MIDDLE OF     NUMBER OF
INTERVAL      OBSERVATIONS
 -1.000         72    ***************
 -0.900         67    **************
 -0.800         41    *********
 -0.700         27    ******
 -0.600         20    ****
 -0.500         21    *****
 -0.400         16    ****
 -0.300         12    ***
 -0.200         11    ***
 -0.100          6    **
  0.000         16    ****
  0.100         20    ****
  0.200         11    ***
  0.300         13    ***
  0.400         15    ***
  0.500         18    ****
  0.600         16    ****
  0.700         20    ****
  0.800         32    *******
  0.900        102    *********************
  1.000         70    **************
```

#29

Centronics #1, #2, #3

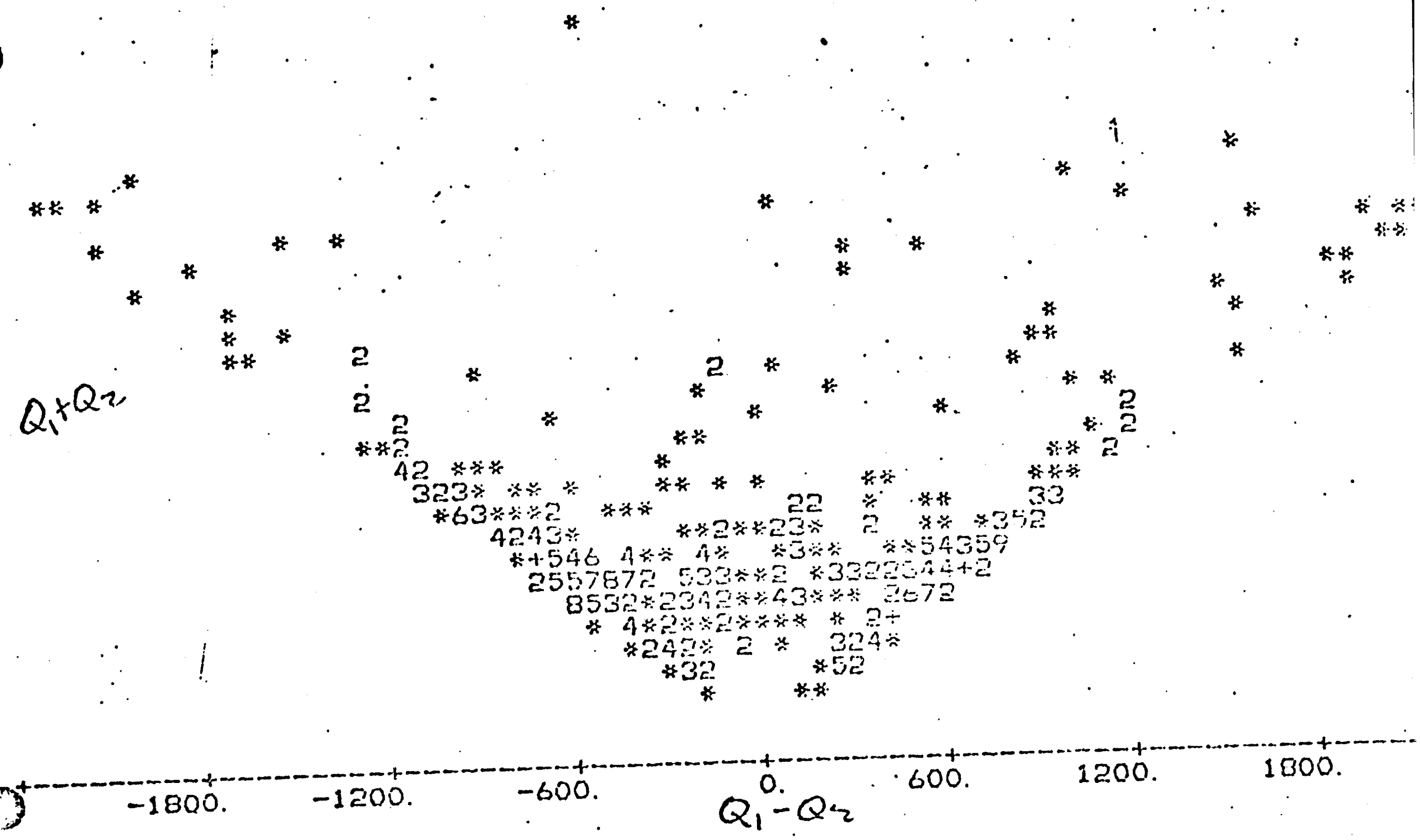

All Pions 5σ in "window" (x=1)

Scatterplot of Q1+Q2 Vs Q1-Q2

&

Histogram of Q1-Q2/Q1+Q2

$\frac{Q_1-Q_2}{Q_1+Q_2}$

```
MIDDLE OF    NUMBER OF
INTERVAL     OBSERVATIONS
 -1.000       30    ***************
 -0.900       65    *********************************
 -0.800       36    ******************
 -0.700       32    ****************
 -0.600       20    **********
 -0.500        9    *****
 -0.400       10    *****
 -0.300       13    *******
 -0.200       17    *********
 -0.100       11    ******
  0.000       11    ******
  0.100       16    ********
  0.200       12    ******
  0.300        7    ****
  0.400        9    *****
  0.500       11    ******
  0.600       13    *******
  0.700       21    ***********
  0.800       35    ******************
  0.900       57    *****************************
  1.000       36    ******************
```

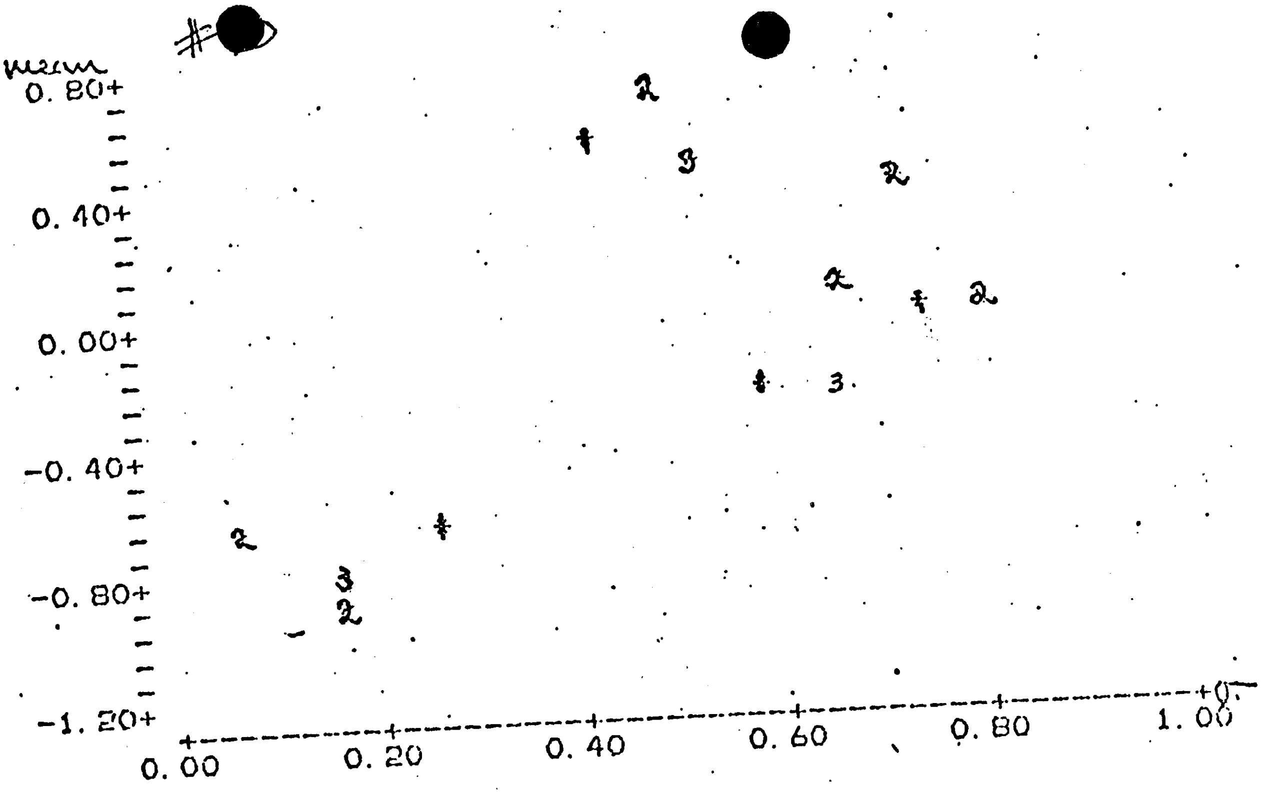

Ⓐ All Pions 5σ in "window" (x=1)
(over Centronics #1, #2, #3)
scatterplot of mean$\left(\frac{Q_1-Q_2}{Q_1+Q_2}\right)$ vs $\sigma\left(\frac{Q_1-Q_2}{Q_1+Q_2}\right)$

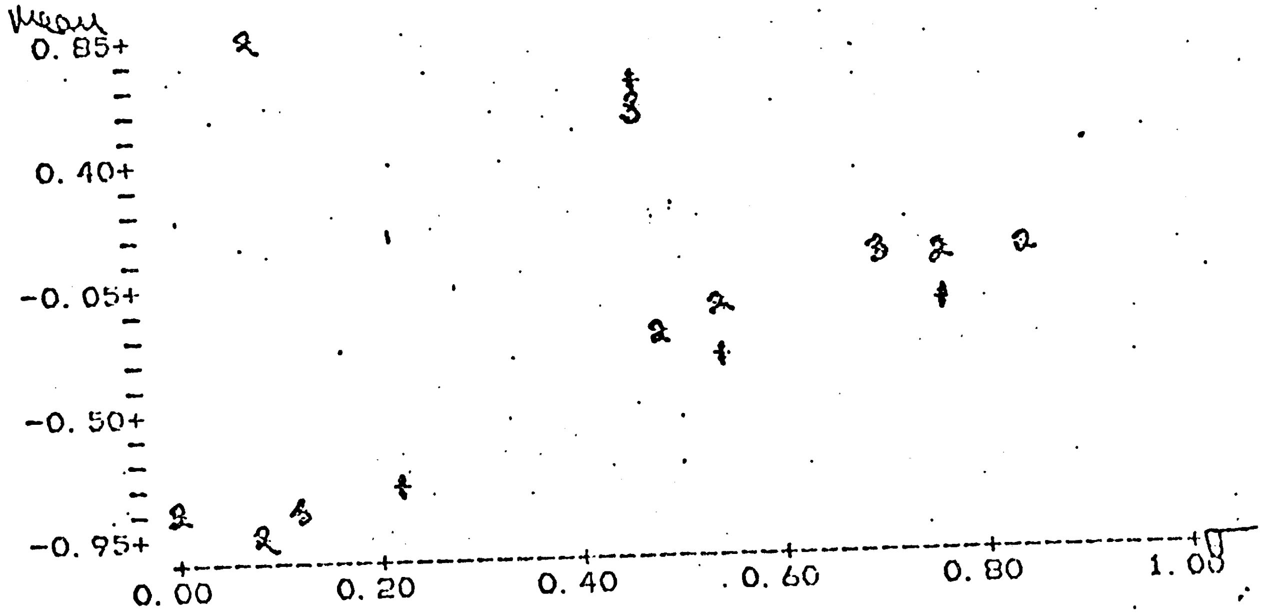

Ⓑ All Protons 10σ in "window" (x=1)
(over centronics #1, #2, #3)
scatterplot of mean$\left(\frac{Q_1-Q_2}{Q_1+Q_2}\right)$ vs $\sigma\left(\frac{Q_1-Q_2}{Q_1+Q_2}\right)$

Sample event in "Window" on Centronics #3.

* Denotes a Dead Channel, 1-Z denotes a hit.

(Note: weak channels Also shown as *).

```
EVENT # =      596.000
ON CHANNELS
 16   56 102 213 253
```

10σ Pr event

```
     874.
    1568.
    2378.
      25.
    2046.
     600.
 NN(1-8)=       0       0       1       1       1       1       1
```

```
      + * * + + I + * + + + + + + + + + * * + + + + * * * + + * * * * + +
         + * + K + * * + + + + + + + + * + + + + + * * + + + * * * * + +

  + + + + + + + M * + + * * + + + + + + + + + + + + + + + + + + + + + +
             + * 2 + * + + * + + + + + + + + + + + + + + + + + + + + + + +

  * * * * * * * M * * * * * * * + + + + + + + + + + + + + + + + + + + +
    * * * * * * + G * * * * * * * * + + + + + + + + + + + + + + + + + +
          1     2     3  4    5     6     7     8     9     10    11
```

not dead but are neighbors to dead (ie weak)

③ Window

```
*BLOW-UP* REGION =
QSHR--M, I, J, KK, JJ, JA& QA=   3   1  19   1   6  19    873.5
QSHR--M, I, J, KK, JJ, JA& QA=   4   1  13   2   4  13   1567.9
QSHR--M, I, J, KK, JJ, JA& QA=   5   1  19   1   8  19   2377.9
QSHR--M, I, J, KK, JJ, JA& QA=   6   1  13   2   3  13     24.5
QSHR--M, I, J, KK, JJ, JA& QA=   7   1  19   1  35  19   2046.2
QSHR--M, I, J, KK, JJ, JA& QA=   8   1  25   2  33  25    600.0
FROM QSHR
                               3    1.185188        1.116194        2.054127
  596.0000
  2.267975                                                          239.0000
 0.3162498      -3.5585403E-02   210.0000          219.0000
  500.0000        263.0000       252.0000          228.0000
            - - - - - + - - - - - + - - - - - + - - - - - + - - - - - + -
      - - - - - + - - - - - + - - - - - + - - - - - + - - - - - + - - - -

DELTAX=2ND-AVG1ST3RD=       1.19 AND LOSS-CORR. =       1.12

            - - - Q - X - - - - - + - - - - - * - - - - - + - - - - - + -
      - - - - - X Q - - - - + - - - - - * - - - - - * - - - - - + - - - -

            - - - - - Q - - - - - * - - - - - + - - - - - + - - - - - * -
      - - - - - X - - Q - - + - - - - - * - - - - - + - - - - - + - - - -

            * - - - - - - XQ- - - - - - * - - - - - * - - - - - * - - - - - * -
      * - - - - - + - - -Q- - X - - - - - * - - - - - * - - - - - * - - - -
```

Blow up Showing Charge Sharing Position (Q).

A typical "window" event (5σ run)

```
EVENT # =       333.000
ON CHANNELS
 16   57 102 213 252

      476.       707.       624.
      605.       204.       387.
      642.
       51.
      256.
      403.
NN(1-8)=      0         0         3         3         1         1         1         1
```

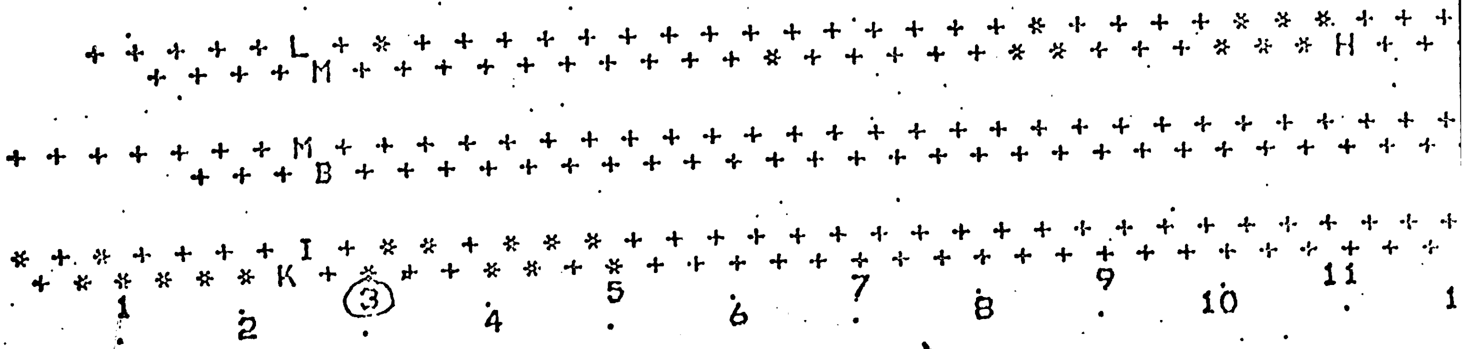

A sample event (Run34 evt 333) showing the 3 centronic dectectors with hits (A-Z) and dead channels (*). Notice the "window" where three point tracks can be found is limited to a small region (around region 2-3).

A Blowup of Region ③ Above Showing a 3 point track with charge sharing occuring on centronics #1 & centronic

```
DELTAX=2ND-AVG1ST3RD=     0.59 AND LOSS-CORR.=     1.52
```

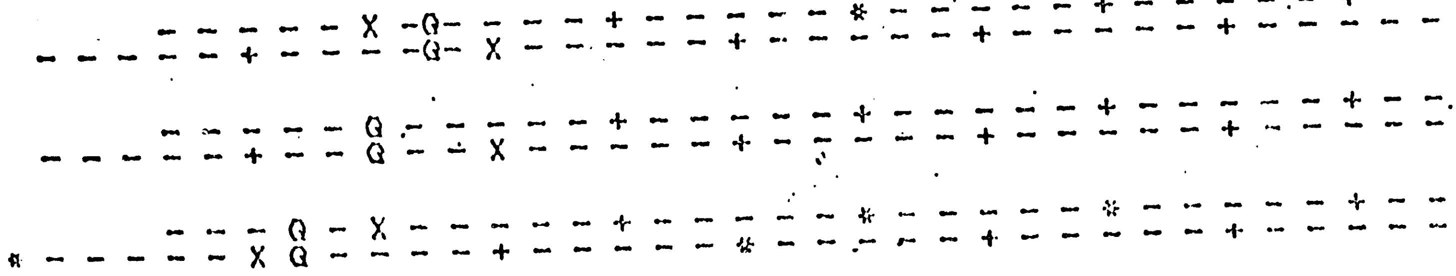

H-31

Plot of Scint#vs delta (x=1)

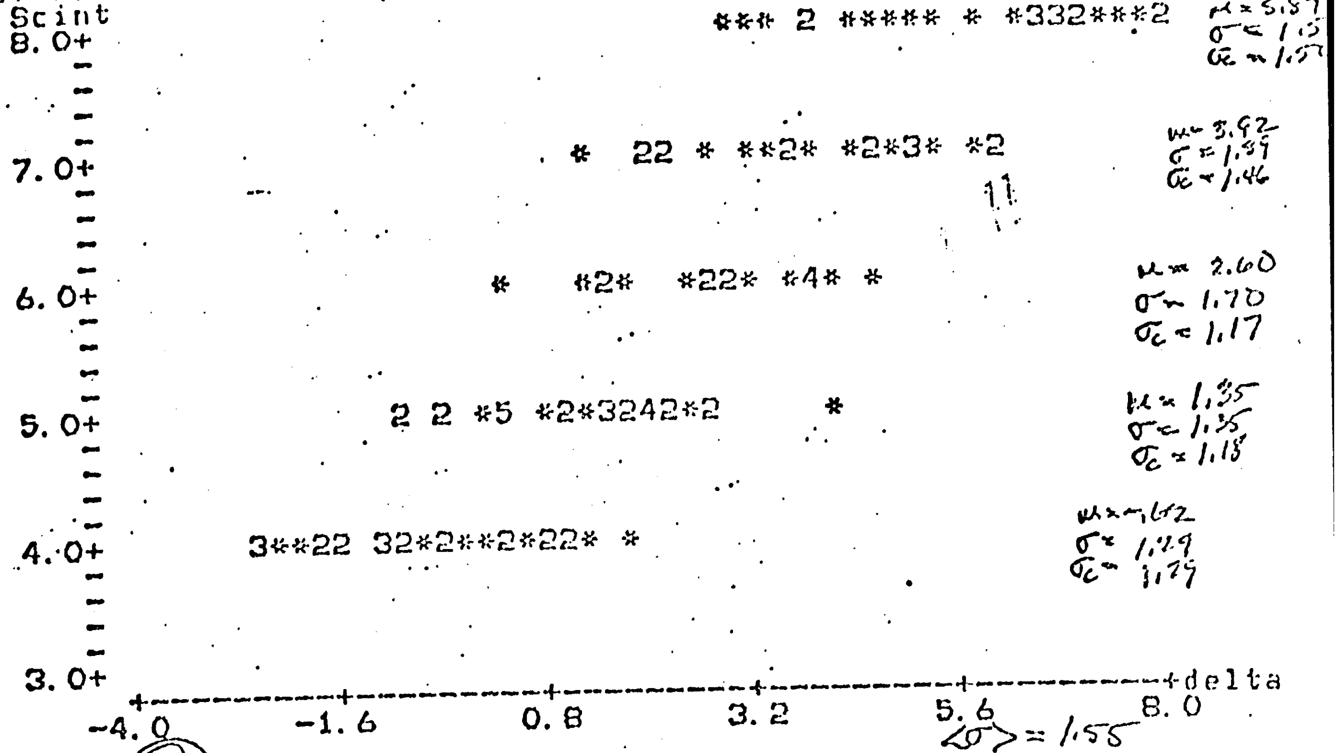

$\langle\sigma\rangle = 1.55$

$\langle\sigma\rangle_c = 1.33 \times 10\mu$

(A)

X = 1

Resolution Plots (All Protons 10σ)

Plot of Scint#vs delta (x=2)

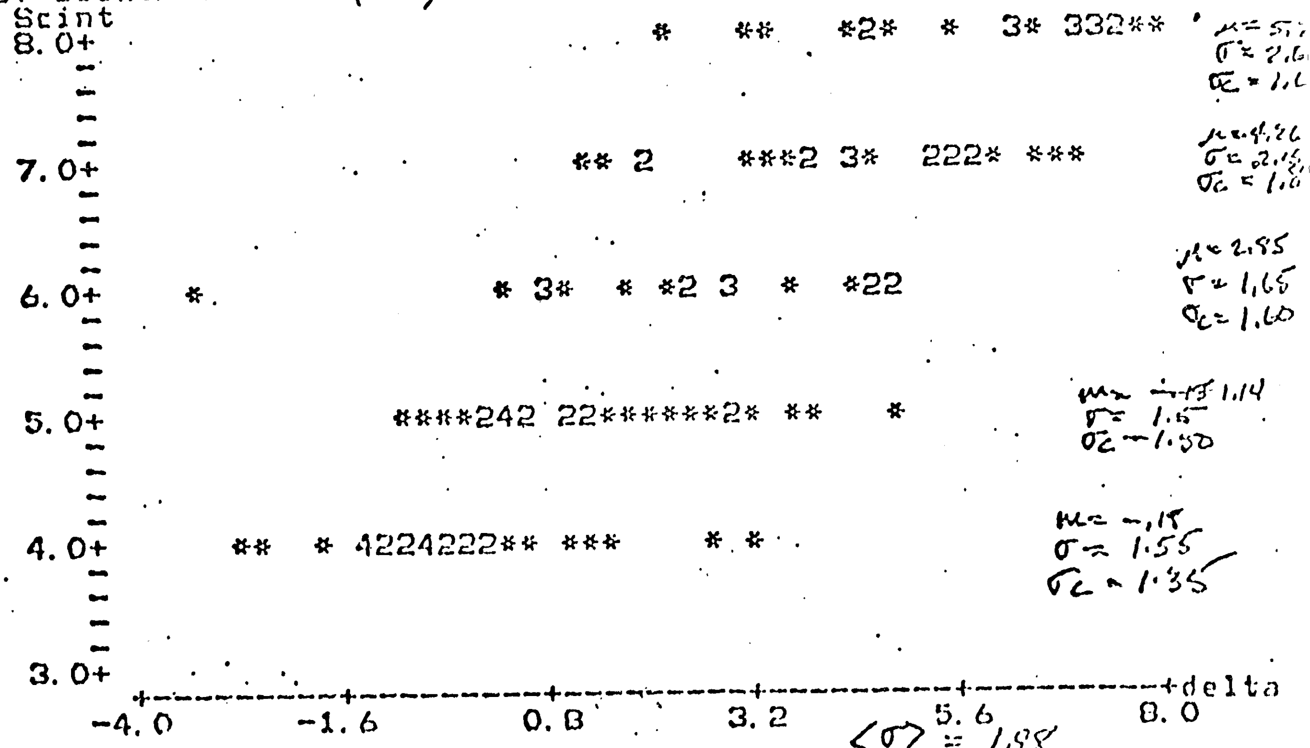

$\langle\sigma\rangle = 1.98$

$\langle\sigma\rangle_c = 1.68 \times 10\mu$

(B)

X = 2

#120

Plot of Scint#vs delta (for x=1)

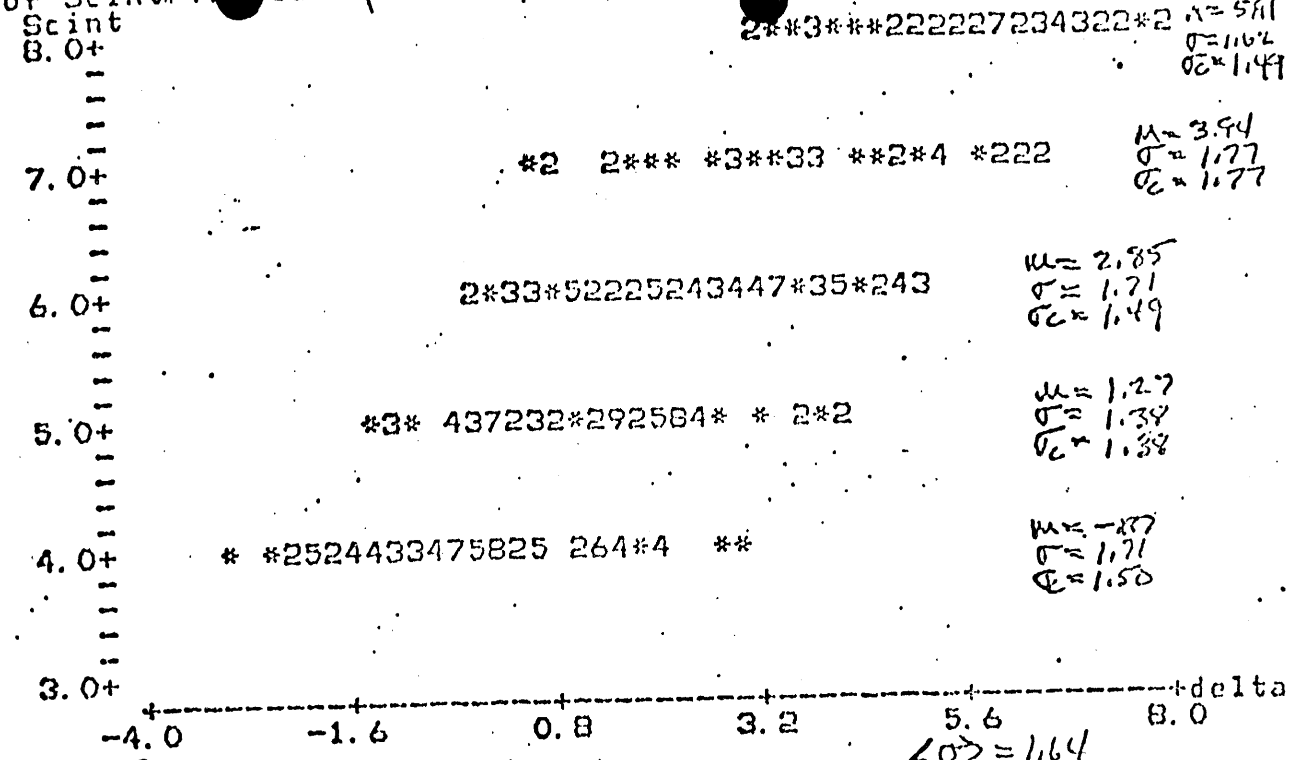

$\mu = 5.81$
$\sigma = 1.62$
$\sigma_c = 1.49$

$\mu = 3.94$
$\sigma = 1.77$
$\sigma_c = 1.77$

$\mu = 2.85$
$\sigma = 1.71$
$\sigma_c = 1.49$

$\mu = 1.27$
$\sigma = 1.38$
$\sigma_c = 1.38$

$\mu = -.187$
$\sigma = 1.71$
$\sigma_c = 1.50$

X=1

$\langle\sigma\rangle = 1.64$
$\langle\sigma\rangle_c = 1.49$ *10/^

Ⓐ

Resolution Plots (All Pions 5σ)

Plot of Scint#vs delta (x=sqrt(2))

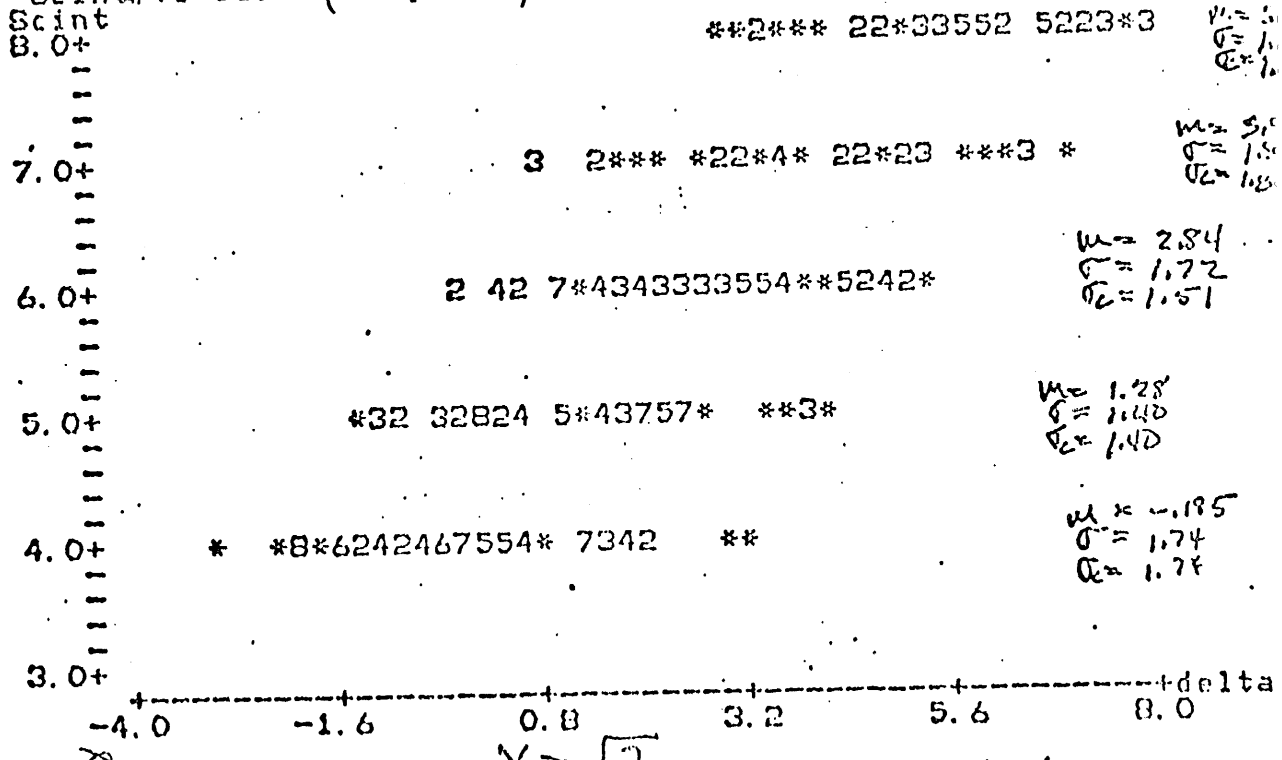

$\mu =$
$\sigma =$
$\sigma_c =$

$\mu =$
$\sigma =$
$\sigma_c =$

$\mu = 2.84$
$\sigma = 1.72$
$\sigma_c = 1.51$

$\mu = 1.28$
$\sigma = 1.40$
$\sigma_c = 1.40$

$\mu = -.185$
$\sigma = 1.74$
$\sigma_c = 1.74$

$X = \sqrt{2}$

$\langle\sigma\rangle = 1.67$
$\langle\sigma\rangle_c = 1.52$ *10/^

Ⓑ

Plot of Scint#vs delta (for x=1)

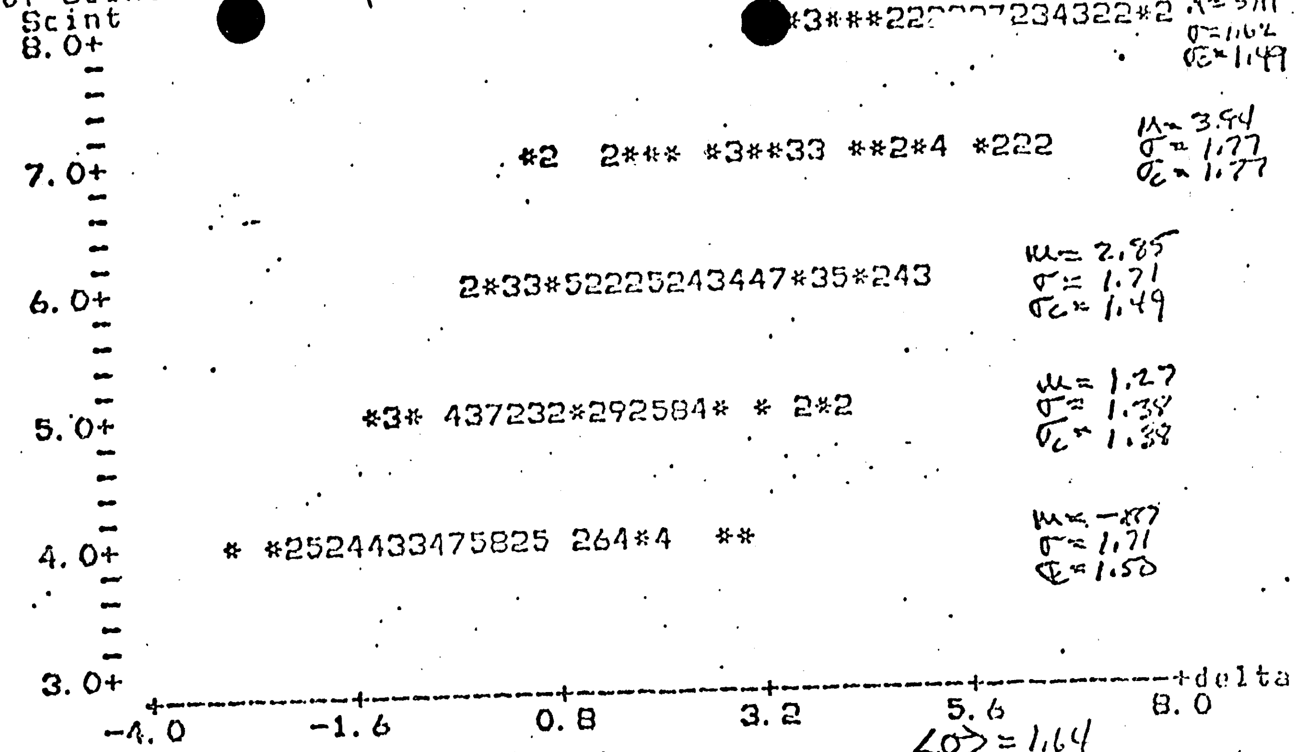

$\mu = 5.11$
$\sigma = 1.62$
$\sigma_c = 1.49$

$\mu = 3.94$
$\sigma = 1.77$
$\sigma_c = 1.77$

$\mu = 2.85$
$\sigma = 1.71$
$\sigma_c = 1.49$

$\mu = 1.27$
$\sigma = 1.38$
$\sigma_c = 1.38$

$\mu = -.87$
$\sigma = 1.71$
$\sigma_c = 1.50$

$x = 1$

$\langle\sigma\rangle = 1.64$
$\langle\sigma_c\rangle = 1.49 \pm 10\%$

Ⓐ

Resolution Plots (All Pions 5σ)

Plot of Scint#vs delta (x=sqrt(2))

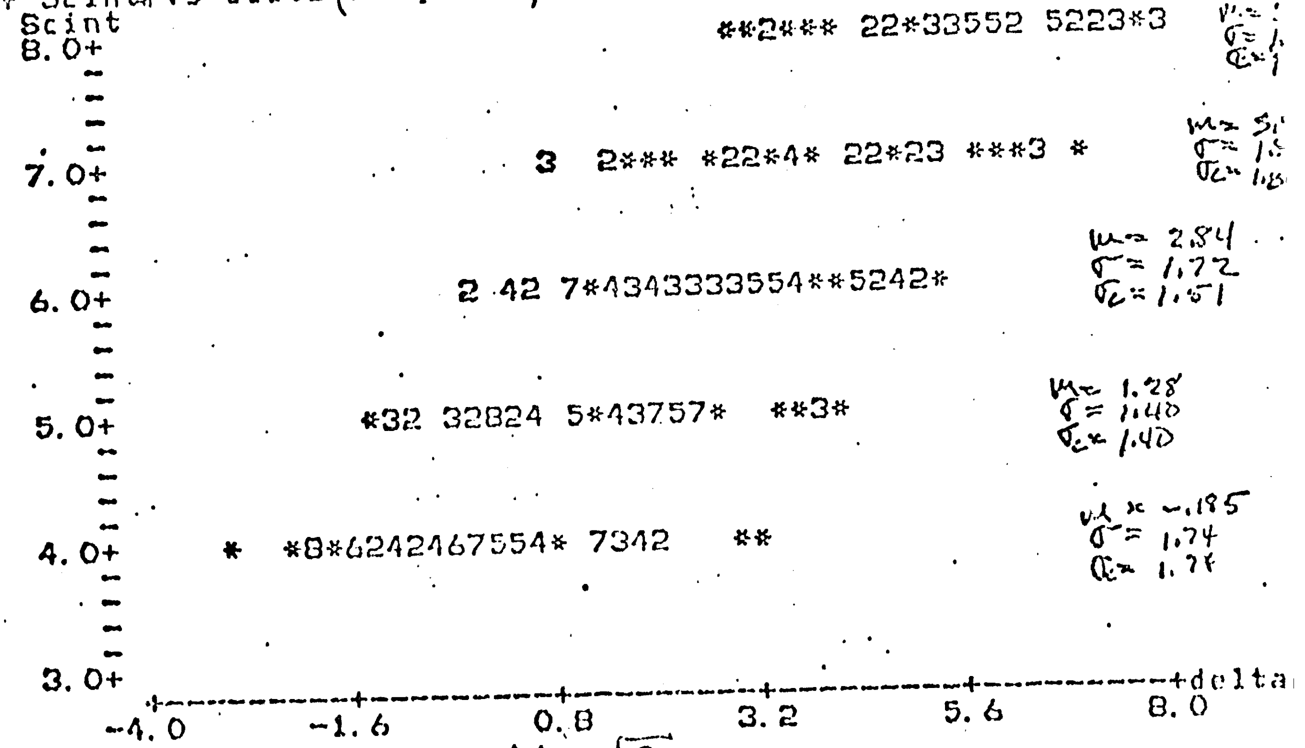

$\mu =$
$\sigma = 1.$
$\sigma_c = 1$

$\mu = 5.$
$\sigma = 1.$
$\sigma_c = 1.$

$\mu = 2.84$
$\sigma = 1.72$
$\sigma_c = 1.51$

$\mu = 1.28$
$\sigma = 1.40$
$\sigma_c = 1.40$

$\mu = -.185$
$\sigma = 1.74$
$\sigma_c = 1.74$

$x = \sqrt{2}$

$\langle\sigma\rangle = 1.67$
$\langle\sigma_c\rangle = 1.52 \pm 10\%$

Ⓑ

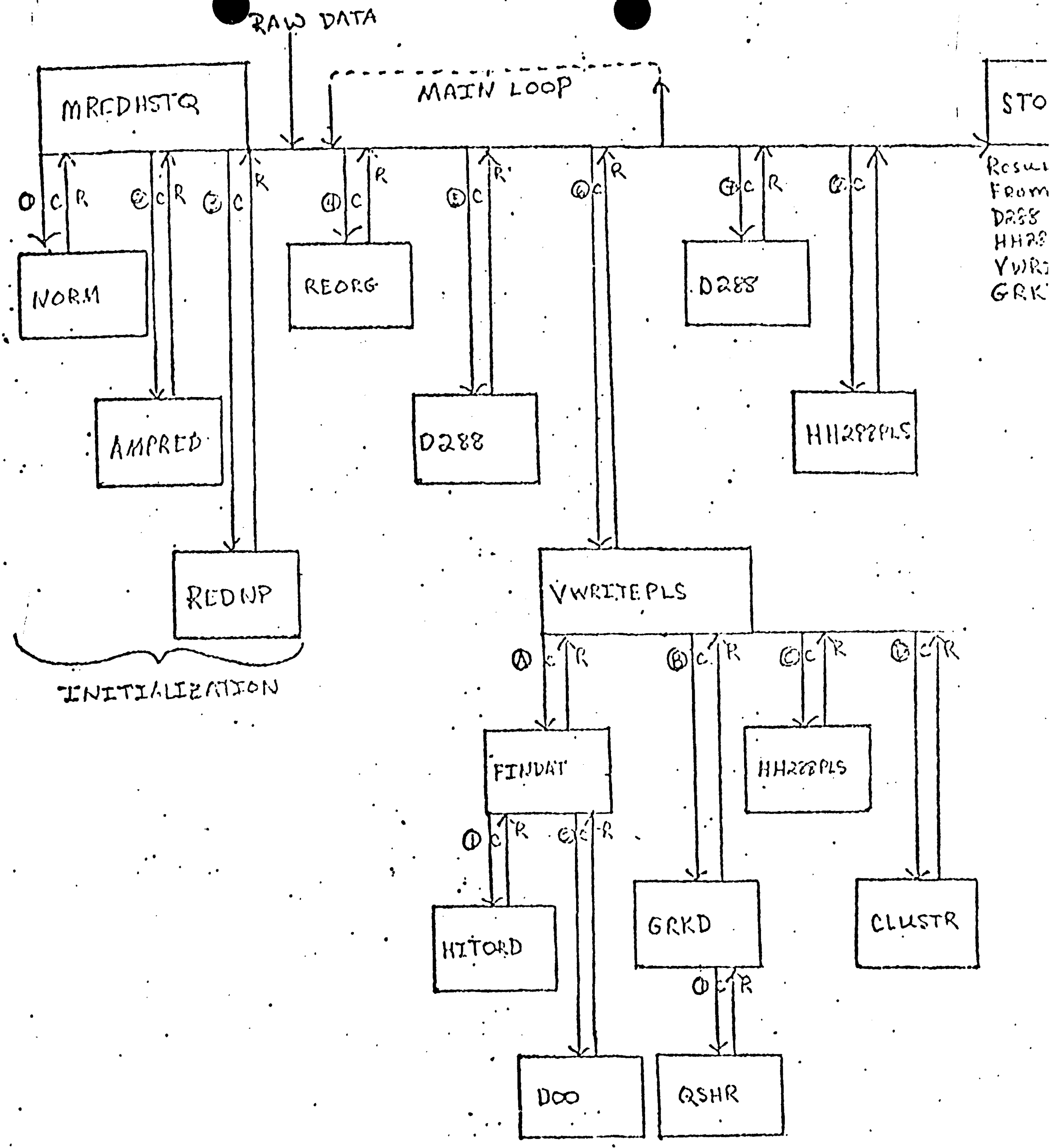

FLOW CONTROL OF DATA ANALYSIS PRGM.

MREDHSTQ4

Diagram 3

OU-HEP MEMO #13

HADRON CALORIMETER

By

Patrick Skubic
Anthony Aldrich
Tariq Jaffry

September 16, 1983

OU HEP MEMO #13

9/16/83

HADRON CALORIMETER

DETECTOR DIMENSIONS

The full size detector will be 91" x 91" in active area. Each gap will contain one layer of plastic tubes interleaved between two layers of copper clad G-10. Alternate layers will be rotated 90 degrees. Each layer will consist of 3 chamber modules each 30.2" x 91" in active area. Pads will be etched into the G-10 boards to provide correlated X-Y position and energy measurements with a tower geometry.

Fig.1 shows the layout for one single-gap layer including a possible pad arrangement. Each layer will require twelve 30" x 45" G-10 boards. Fig.2 shows a blow-up of the pad pattern in the central 30"x 30" region.

P.C. BOARD FABRICATION

We have designed a system which makes it necessary for us to make giant p.c. boards. Each layer requires 12 p.c. boards of size 30" x 45". Sample tests were run using different methods, but the use of screen printng guarantees the reproducibility of pattern. Our present prototype test chamber is a combination of routed boards and screen printed boards. P.C. board fabrication is a process which will involve these steps:

i) screen printing
ii) etching

PREPARATION FOR SCREEN PRINTING

Pattern Drawing: It was made on IBM 3081 computer system on NorthBase

(size 30" x 45")

Art Work: Precision slit tapes were used to make the art work, later a master negative was made which can be used to make the desired size print.

Screen Printing: It is a stencil printing process which uses a precision woven fabric stretched tightly over a frame. Onto this frame,or screen, is adhered a stencil which dictates the image to be printed via blocked or open areas of the screen. The image is transferred to the G-10 sheet by forcing resist-ink through the open areas using a squeegee. On fully automatic printing 10mil lines with 10mil spaces can be imaged, whereas our screen printer can go only down to 20 mil line with 30mil space.

Ink: Initilly we used "Dexter Hysol plating resist PR-3011-black", but this being viscous creates problem in forcing the ink through the screen. So later we decided to mix a thinner made by the same company called, "50-916 Retarder (AD 2003).

Distributers:

i)	Earnest W. Dorn CO. INC. Denver, Colo.	303-791-2511
ii)	Oliver Sales Co. Dallas, Tx.	214-231-1522

ETCHING:

Ferric Chloride: cheap chemical, but waste treatment is expensive, copper can not be extracted easily from used solution, need polypropylene containers.

amount of solution required

to etch all G-10 sheets ■ 170 gal
■ at 31.47% ferric chloride
■ and 68.531% water by vol

operating temperature room temperature

Ferric chloride is available in powder form.

Hydrogen Peroxide Based Etchant: Designed by shipley company of Dallas

person to contact: Bill Roach

Tele: 1-800-527-3730

100 gallon bath make up requires:

D.I. water	68 gal
hydro-etch 371M	25 gal
50% hydrogen peroxide	7 gal

operating temperature 115 F but less than 120 F

Dangers: Above 120 F hyrogen peroxide may decompose.
Its a corrosive acid solution.

Waste Treatment: Need to be studied.

Osco-Super-Etch: Designed by "Lou Griffin" of Oliver Sales Co. Dallas.

Tele: 214-231-1522

contact Lou Griffin

100 gallon bath make up requires:

Osco-Super- Etch make up	84% by vol
Osco-Super- Etch replenisher	10% by vol
Osco-Super- Etch stablizer	6% by vol

operating temperature 126 F_ 130 F

Waste Treatment: If solution is cooled down from the normal operating temperature, etched copper is recovered as metallic copper or copper sulfate pentahydrate crystals. Amount of solution required approx. 200 gal

EXPERIMENTAL TESTS OF PROTOTYPE DETECTOR

The experimental detector consisted of 22 1.2cm x 183cm plastic tubes glued sandwiched in between 1oz, 1/16" G-10. The outputs of 8 central tubes and the pads etched in the G-10 directly above the tubes were read out. The outputs from the tubes were ganged together and the resulting signal was amplified 40x by channel one of a Lecroy 612 amplifier. One output was attenuated 6 db and then feed into channel one of a Lecroy 2285A ADC. The other output went into input A of a Chronetics 151 dual discriminator. The threshold was 50mv and the gate width was 50ns. The outputs of one or more pads were ganged together and amplified 40x by channel two of the 612 and the amplifier output went into channel two of the 2285A.

A gas mixture of 50% Argon - 50% Ethane bubbled through ethyl alcohol at room temperature was used. Fig.3 shows typical pictures of the qvt pulse height distribution for tube proportional signals at an operating voltage of 2.5Kv. Fig. 4 shows the integrated charge for minimum ionizing electrons from a Ruthenium (Ru 106) beta source versus high voltage before amplification for a typical tube. Due to the finite resistivity of the tubes (approx. 20 kilo ohms/sq.) charge will flow from one pad to an adjacent one along the tubes. Fig 5(a) shows the charge flow versus position for limited streamer signals measured with the smallest pads (see Fig 5(b)).

A 1/32" thick piece of scintillator mounted on a phototube was placed in front of the beta source positioned over the center of a pad. The phototube output went into input B of the 151. The threshold was 220mv and the gate was 50ns. The discriminator outputs for the proportional tube and the phototube went into a majority coincidence set at level two. The coincidence output went into a 151 to shape the pulse to 400ns and the 400ns pulse was the gate for the 2285A ADC. Thus we required the 2285 to read only signals generated by a particle causing a coincidence pulse between the scintillator and proportional tube. This is what is refered to as a double trigger on tube and scint. in the tables.

The largest pad is 8 x 8cm, next to largest pad is 4 x 4cm, next to smallest pad is 2 x 2cm, and smallest pad is 1 x 1cm. The output of the pads and tubes were timed with the gate pulse so that the gate pulse enveloped all of the signal from the tube and pad. Each test run consisted of reading the amplified signal of one or more pads ganged together and the outputs of the eight tubes ganged together. To find the noise of each test run set up, the coincidence was set to level 1 so that only the phototube output generated the gate pulse and the voltage of the phototube was raised 200 volts. In this way the gate was generated by noise which let the 2285A read only noise pulses.

During all of the test runs the wire in the proportional tubes was kept at a voltage of +2.5kv and the tube walls were grounded. The eight tubes generaly drew .8 microamperes with the source on and .3 to .4 microamps with the source off. The peak integrated charge for various pad combinations is summarized in tables I and II. The table labeled Horizontal assembly is the data taken with the detector on its edge and the table labeled Vertical assembly includes the data taken with the detector hanging from one end. Note that the peak signal is ~4 times minimum ionizing because of scattering caused by the G-10 boards. Charge collection improves as the size of the pad increases. For the largest pads, the pad signal approaches 50% of the tube signal.

NEW TUBES

We have recently recieved shipment of full sized tubes which will be used in the final detector. One tube has been tested. Fig.6 shows the current vs high voltage curve for the new 11mm x 16mm x 2.4m tube. Space charge build-up causes discharge at lower voltages with the source on the tube. The integrated charge distribution for minimum ionizing electrons is shown in Fig. 7 for the new tube at 2.5 Kv where a 612 amplifier was used with a gain of x47.

THE DRAWING SHO[illegible]S THE OVEALL SIZE OF La[illegible]n
AND THE DESIGN/SIZE OF SEGMENTATION IN EACH REGION
DOTTED LINE SHOWS SEPARATION OF SMALL BOARDS

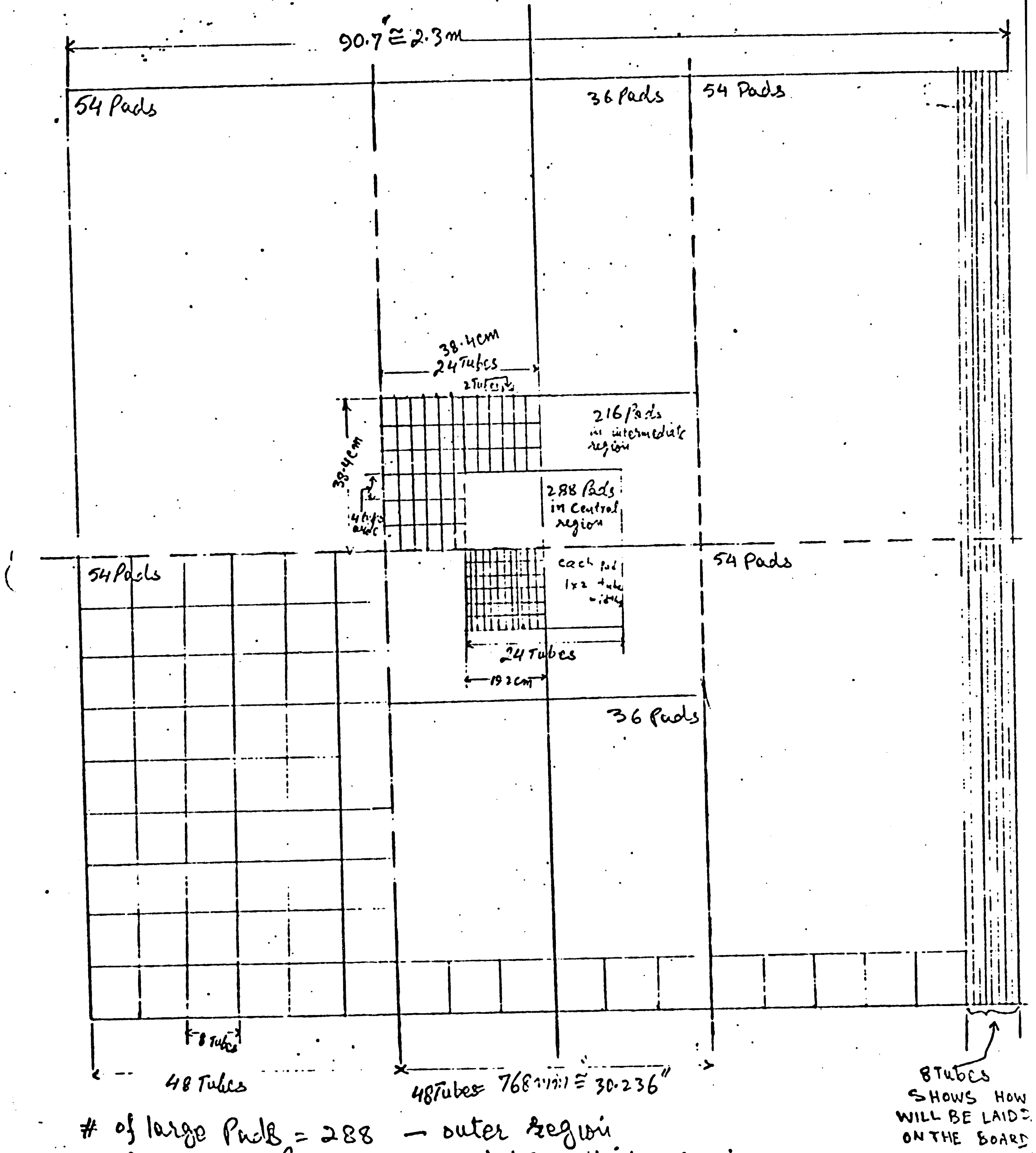

# of large Pads = 288 — outer region
# of intermediate Pads = 216 — intermediate region
# of smalle Pads = 288 — central region

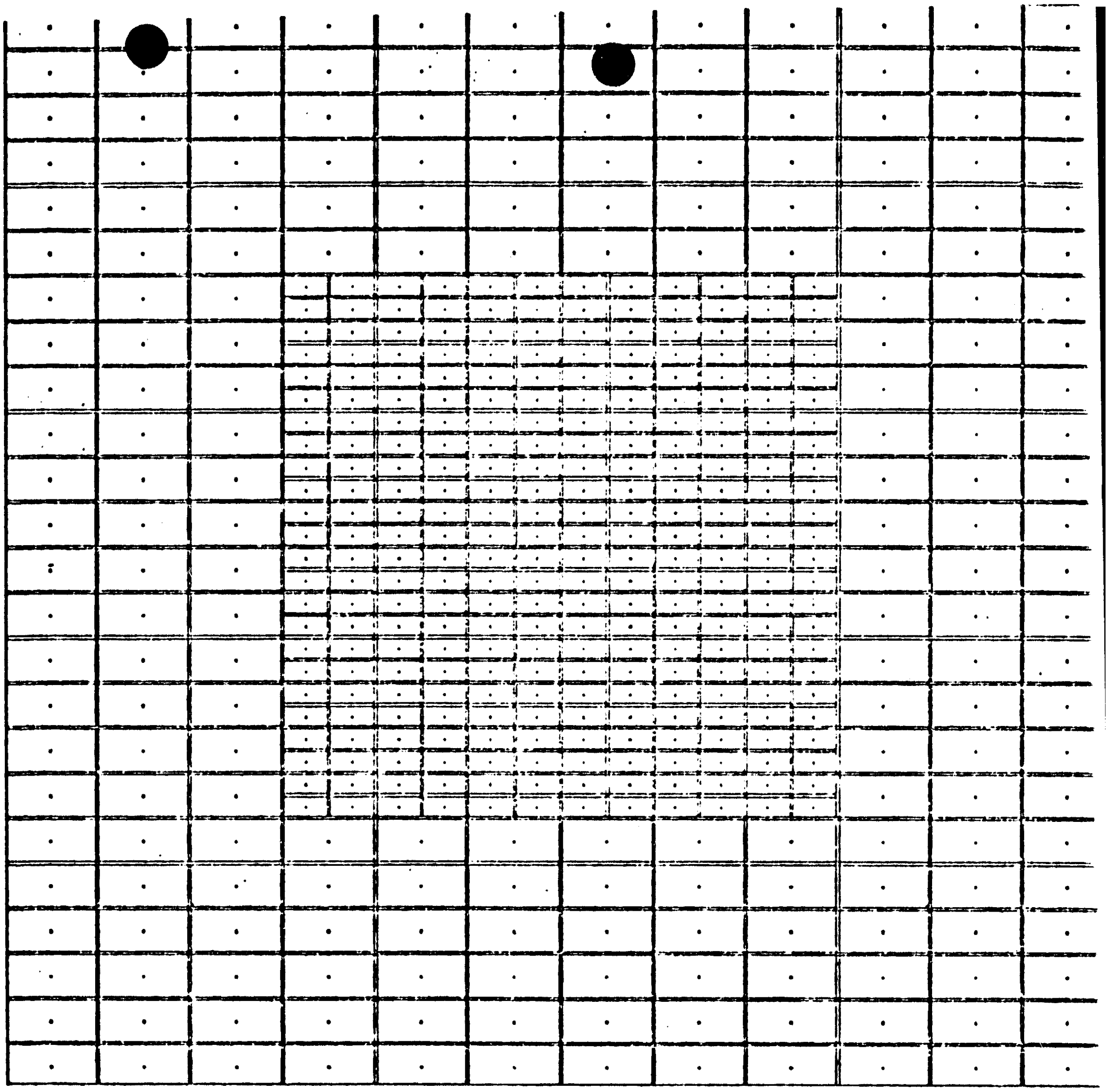

Fig. 2

[illegible]

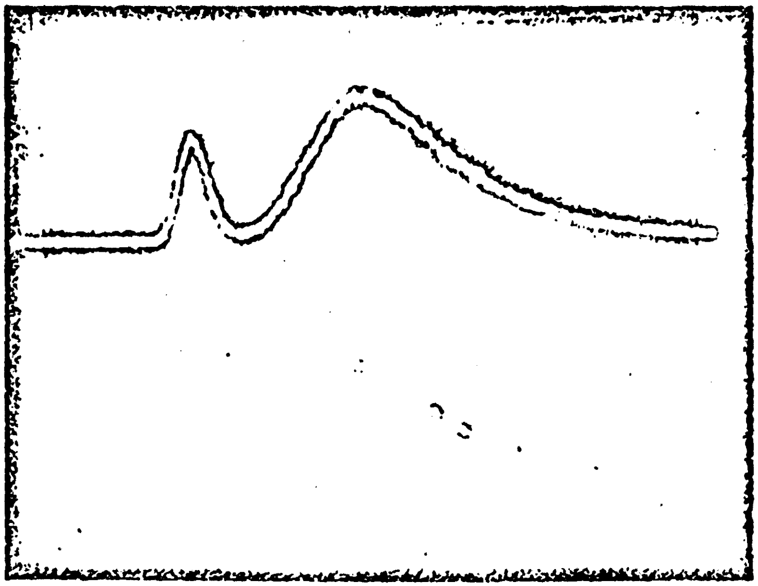

position 7

ped 137
δ ped 126, 147
peak 243
δ peak 205, 317
valley 167
position 8
ped 140
δ ped 129, 148
peak 219
δ peak 190, 269
valley 163

cont run on position 9 voltage 2,5 kV

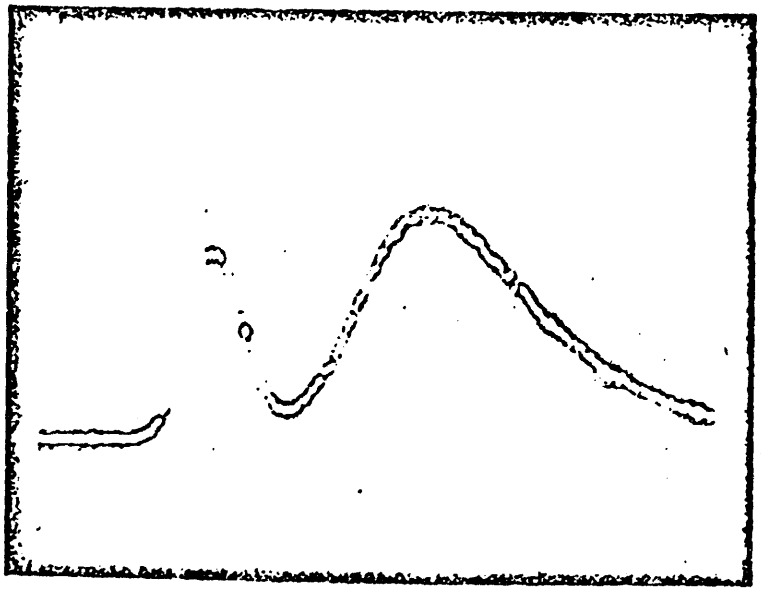

ped 140
δ ped 130, 150
peak 210
δ peak 186, 247
valley 164

Fig. 3

Tube # 3 (see page 151)
Proportional Signal

Fig. 4

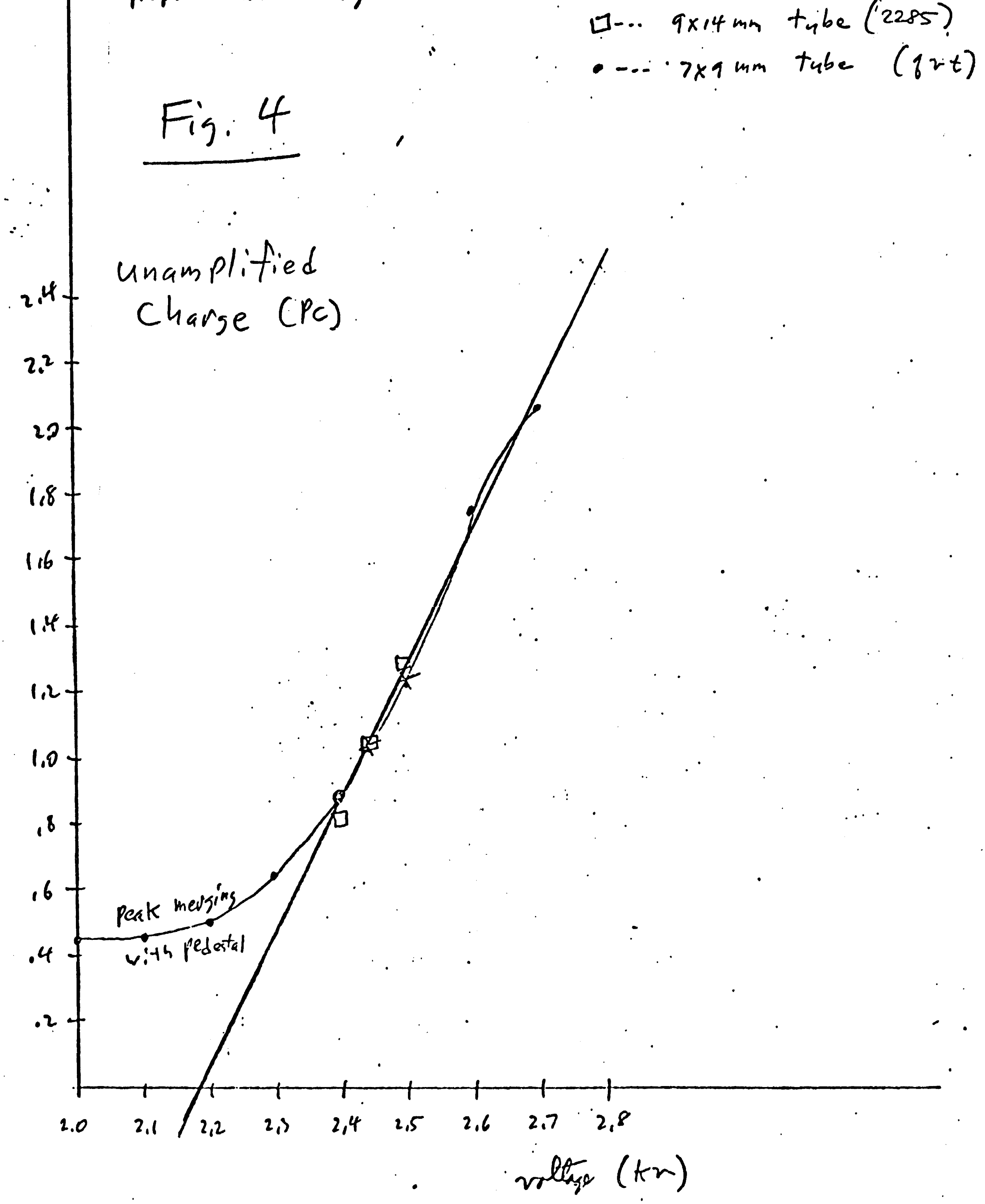

Fig. 5 (a)

7 X 10 mm ID tube

10 X 10 mm pads with 3 mm gap

150 ns gate

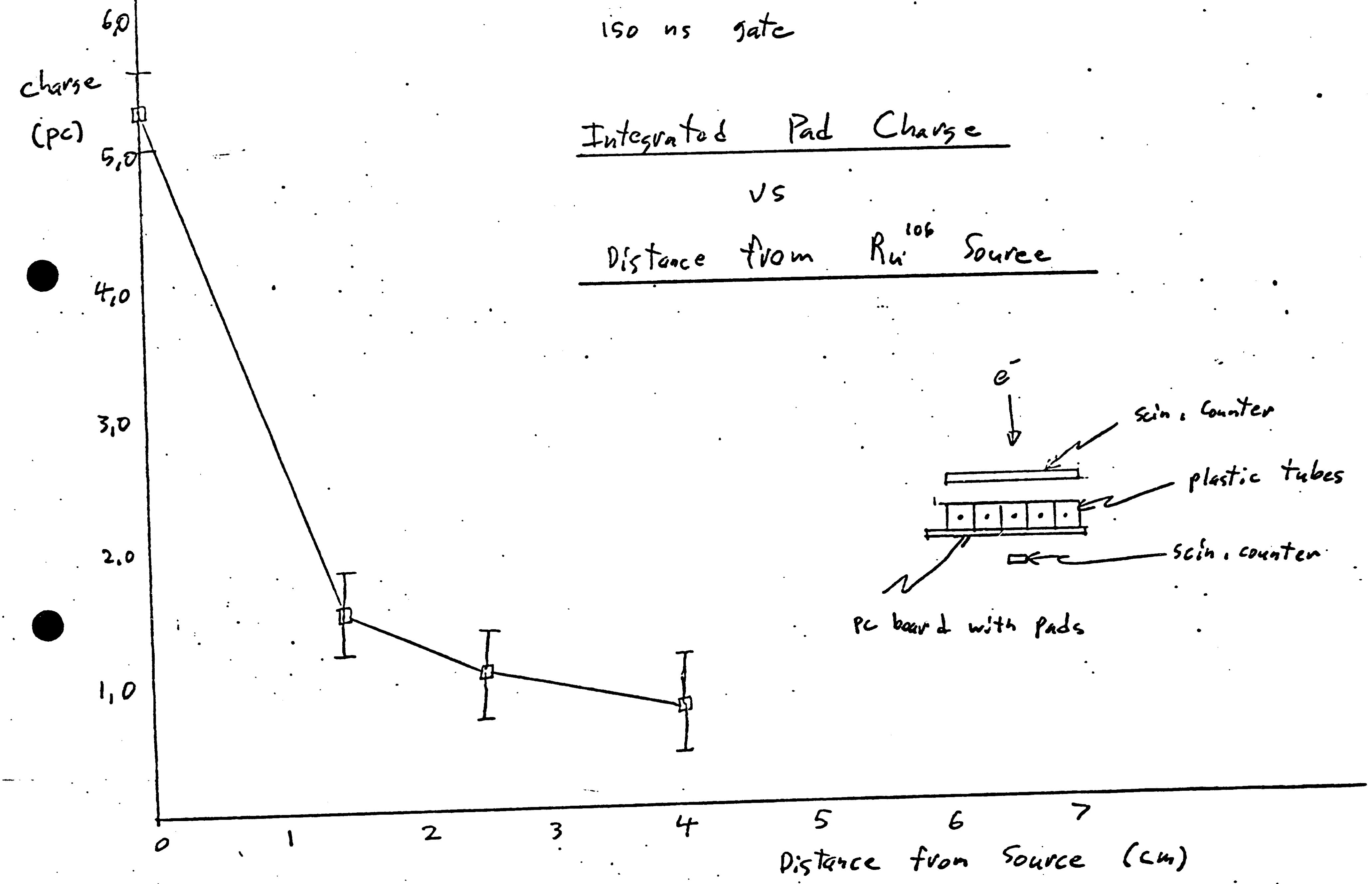

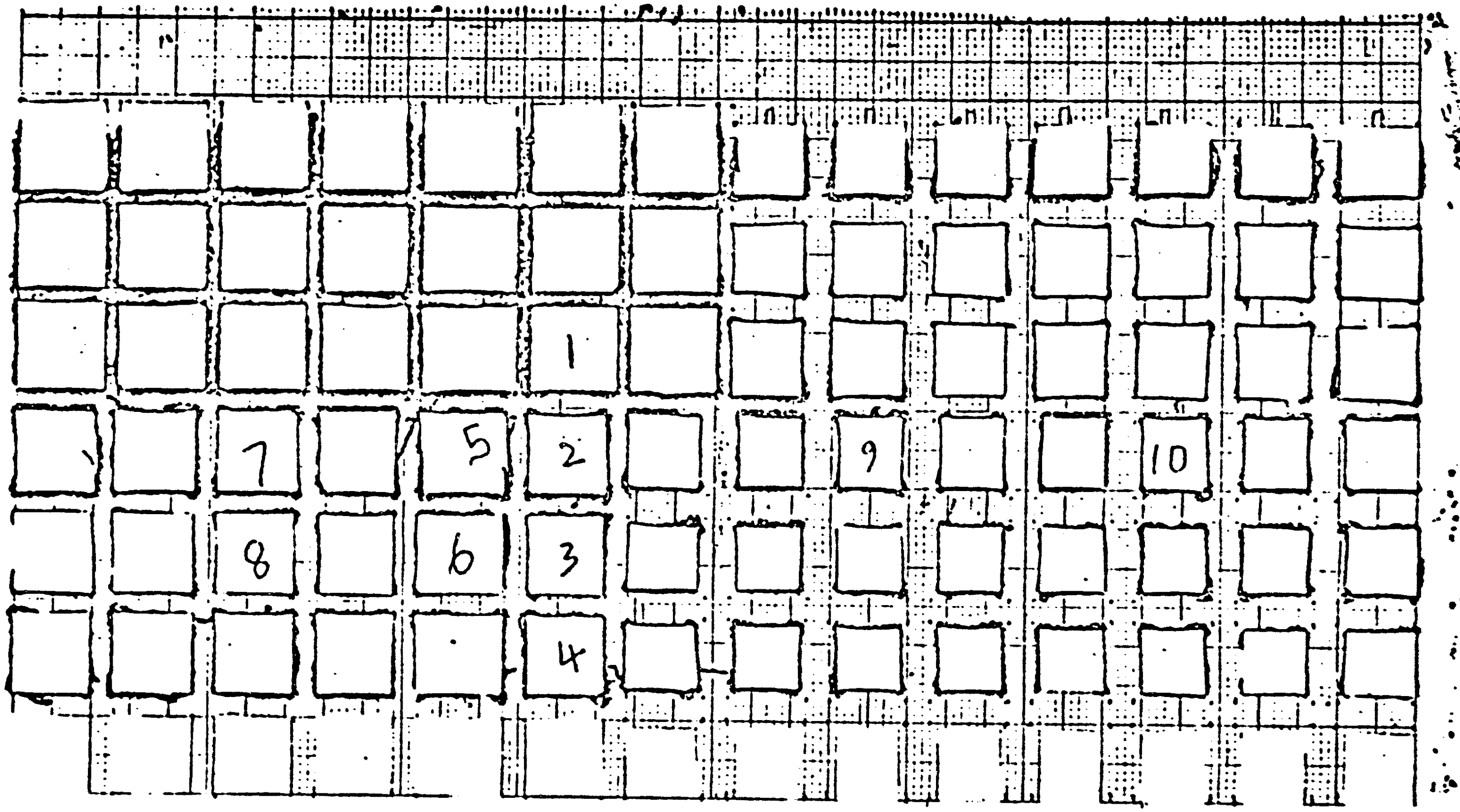

Fig. 5(b)

Current vs. Voltage Plot 50/50 [illegible]
For [illegible]arge new tubes

[illegible]

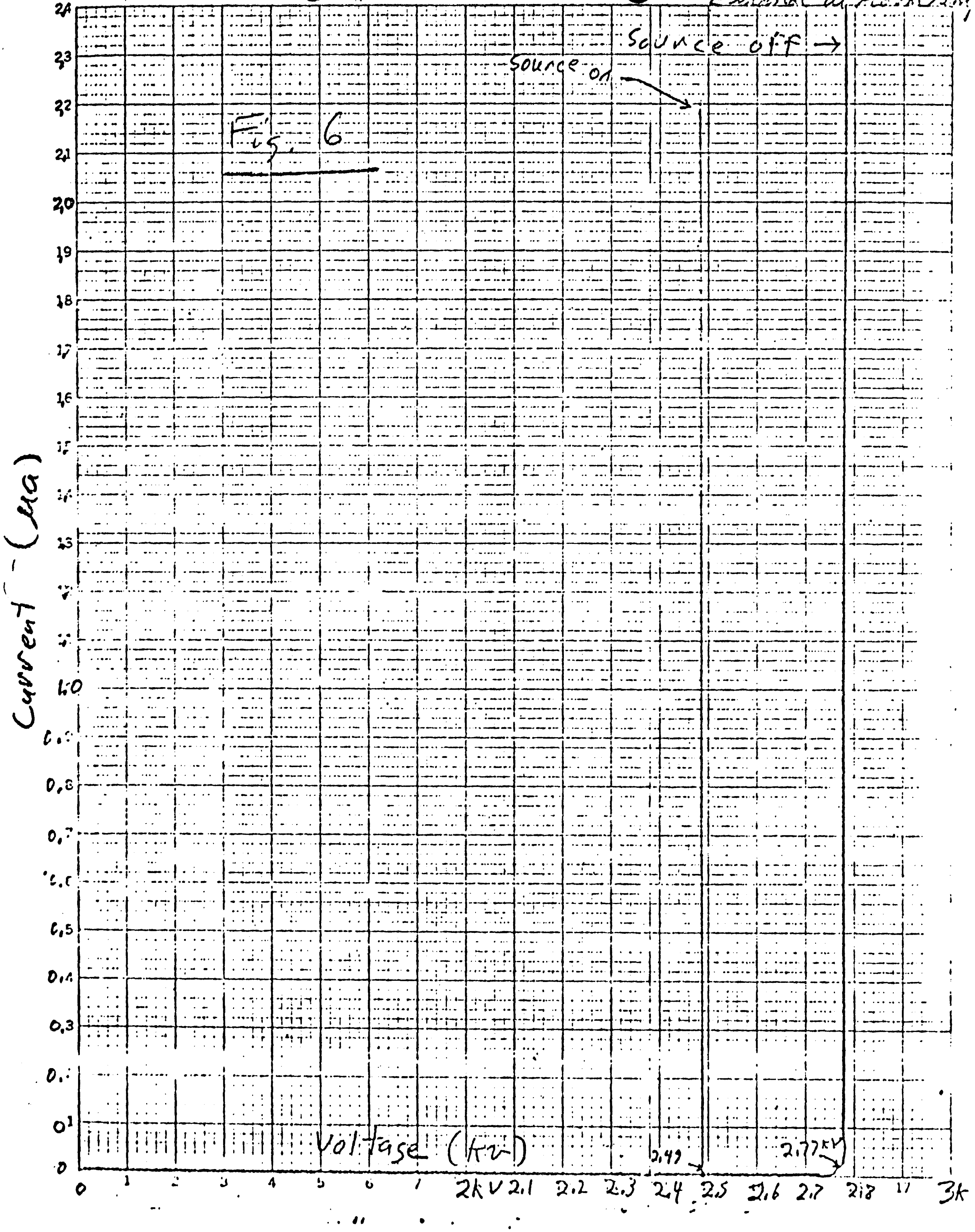

Fig. 6

Horizontal Assembly

current .4 MA voltage 2.5 KV 600ns gate

pad signal

ube real peak	pad real peak	tube signal width	pad signal width	peak tube signal	pad signal peak	tube signal	pad signal	σ	signal/noise	Situati
3.5	3.5	5	5	8.5	9.5	4.5 p.c.	2.7 p.c.	2.17	2.76	3 long
3,5	3.5	5	8	8.5	9.5	4.5 p.c.	2.7 p.c.	3.48	1.72	2 "
3,5	3.5	5	7	8.5	9.5	4.5 p.c.	2.7 p.c.	3.04	1.97	1 "
3,5	3.5	5	5	9	8	4.95 p.c.	2.025 p.c.	2.17	2.074	1. next to
.5	3.5	5	5	8.5	8.5	4.5 p.c.	2.25 p.c.	2.17	2,304	2 " "
3.5	3.5	6	6	8.5	9.5	4.5 p.c.	2.7 p.c.	2.61	2.30	3 " "
3.5	3.5	5	4	8.5	8.5	4.5 p.c.	2.25 p.c.	1.74	2,22	4 " "
.5	4	5	5	8.5	6	4.5 p.c.	0.9 p.c.	2.17	0.922	1 " "
.5	7.5	6	6	5.5	11.5	4.5 p.c.	1.8 p.c.	2.11	1.53	2 next to
.5	7.5	5	4	5.5	10.5	4.5 p.c.	1.35 p.c.	1.74	1.72	1 " "
.5	7.5	4	5	5.5	11.5	4.5 p.c.	1.8 p.c.	2.17	1.84	3 " "
.5	7.5	5	6	5.5	12	4.5 p.c.	2.025 p.c.	2.61	1.72	4 " "

peak 16

gain 40 6.0 db on tube

Vertical Assembly

double [illegible] with tube and [illegible]. gate 400ns
2.5 kV [illegible]

Run	tube Ped	Pad Ped	tube Signal width	Pad Signal width	tube peaks	Pad Peak	tube Signal	Pad signal	Pad σ	Pad sig width	Situation
1	.5	10.5	8	8	5.5	16.5	4.5 pc.	2.7 p.c.	3.48	1.73	1 largest pad.
2	.5	9.5	7	9	6.5	18.5	5.4 pc	4.05 pc	3.913	2.3	2 largest pads
3	.5	9.5	7	8	6.5	18.5	5.4 pc	4.05 pc.	3.48	2.59	3 largest pads
4	.5	10	5	7	5.5	15.5	4.5 pc.	2.48 pc	3.04	1.64	1 next to largest pad
5	.5	9.5	7	9	6.5	16.5	5.4 p.c.	3.15 pc	3.915	1.79	2 " " "
6	.5	9.5	6	9	6.5	17	5.4 p.c	3.38 pc	3.913	1.92	3 " " " "
7	.5	9.5	7	10	6.5	18.5	5.4 pc	4.05 pc.	4.38	2.07	4 " " " "
8	.5	9.5	6	5	6.5	12.5	5.4 pc.	1.35 pc.	2.17	1.38	1 next to smallest pad
9	.5	9	5	5	5.5	13.5	4.5 pc.	2.025 pc	2.17	2.07	2 " " " "
10	.5	9	7	6	6.5	14	5.4 pc.	2.25 pc	2.61	1.92	3 " " " "
11	.5	9.5	6	6	6.	15	4.95 pc.	2.7 pc.	2.61	2.11	4 " " " "

```
6       400.77          .77          .02
.7      519.92          .25          .01
 8      450:95         1.31          .04
HAT CHANNEL(1-8,REG.,9-11,LEFT,MID,RIGHT)? 2

 0.5>       0
 1.5>       0
 2.5>       0
 3.5>       0
 4.5>       0
 5.5>       0
 6.5>       0
 7.5>       0
 8.5>       0
 9.5>       0
10.5>       0
11.5>       0
12.5>       0
13.5>      12******
14.5>      34*****************
15.5>      16********
16.5>       2*
17.5>       0
18.5>       1
19.5>       2*
20.5>      14*******
21.5>      22***********
22.5>      60******************************
23.5>      66*********************************
24.5>      53**************************
25.5>      75*************************************
26.5>      77**************************************
27.5>      62*******************************
28.5>      79***************************************
29.5>      58*****************************
30.5>      58*****************************
31.5>      45**********************
32.5>      37******************
33.5>      33****************
34.5>      32****************
35.5>      20**********
36.5>      17********
37.5>      15*******
38.5>      13******
39.5>      13******
10.5>      14*******
:1.5>      11*****
12.5>       7***
13.5>       7***
14.5>       2*
15.5>       1
i6.5>       2*
:7.5>       5**
i8.5>       0
i9.5>      34*****************
:E HISTOGRAMS(Y/N)? N
                     Y
' AGAIN..?..(Y/N)...
D** at address 2DB8 **

uPer8
```

612 amp gain = x 47

HV = 2.5 kv

(50 ADC ch./BIN)

~ 0.1 pc/ADC ch.

← pedastal

← min. ion. proportio Peak ≈ 60 pc

Fig. 7

(new tube)

Ru^{106} Source

OU-HEP MEMO #14

OU-HEP's AMP with LRS Hybrid

By

Tom Thiel
John A. White
G. R. Kalbfleisch

November 10, 1983

OU-HEP MEMO #14

OU-HEP's AMP with LRS Hybrid

Tom Thiel, John A. White and G. R. Kalbfleisch
11-10-83

A. We are using LRS HQV-810-3 (OSU's hybrid H8) preamp and our own design 10115-delay line shape-10115 mid-stage amp. Various choices and tested values of components have been made. We expect to use 400 ns shaping and 350 ns gating times in final version. These tests have all been made with 300 ns shaping and 200 ns gate. The theoretical improvement of SQRT(200/350) is not expected; our measurements indicate will get only a factor of 0.9 improvement over the data given here.

We were concerned that calibrations with TEST PULSING only would not necessarily agree with an absolute calibration with a source (or other beam) on a detector. We report here results with test pulsing on crossing board trace test capacitor (0.18 pf average) with inline input with 1.1pf external test pulse capacitor and with a 20 mm2 300 micron thick fully depleted (at 100 volts) N-type Enertec detector, with and without a Ru-106 beta source. The peak value of charge for this detector is expected to be 3.4 fc.

a) with amplifier only, 0.18 pf TP, sigma(noise)= 0.10 to 0.14 for 8 channels
= 0.125 fc average
b) with detector connected " " = 0.16 to 0.22 fc
0.195 fc average
(implies detector equivalent noise=0.15 fc,
reverse bias current is supposedly very low, na's)

c) calibration (amp ch #10= hybrid ch #3)
496 ch/fc amp. only using 0.18 pf TP cap
486 " + detector conn. "
466 " only using 1.1 pf TP cap
412 " via 3.4 fc Ru-106 absolute

d) 2 channels--comparison .18TP, 1.1TP and Ru-106. NOISE SIGMA's

	0.18 pf(no det) /	+detect /		Ru-106
amp ch #10, hybrid ch#3---	0.12 fc	(0.20 fc	vs	0.22 fc)
" #11, " #2---	0.12	(0.19		0.21)

Thus, TP and source calibrations agree within 10-20 percent.

B. We have not had any trouble with blowing out channels on H8 hybrid, without using any special precautions. Long term failure modes, heating problems, etc. are of course unknown yet to us. We have crudely looked at some "cross-talk" numbers, easily 10 percent or more in our present test board. We don't know yet if its hybrid, or PCB layout or both. We will address this in detail when we get our first true proto-type PCB layout made (in a few weeks at most we hope). We expect to place order for hybrids with LRS next week since it appears that we can manage with them (?is revision? for protection diode inside hybrid package?). Will start getting all components on order, stand included, for amplifier boards. No news yet back from Colin Willburn on production of 10 beam SSD's.

DATE
FILMED
9/14/94

END